Dissertation zum Erwerb des Doktorgrades der Medizin an der Medizinischen Fakultät der Ludwig-Maximilians-Universität München

Structure and function of the PLK1-EBNA2 protein complex in B-lymphocytes

Viktoria Vladimirova Tsoneva

2021

Aus der Abteilung Research Unit Gene Vectors
Helmholtz Zentrum München,
Deutsches Forschungszentrum für
Gesundheit und Umwelt (GmbH)
Leitung: Prof. Dr. Wolfgang Hammerschmidt
Arbeitsgruppe: EBV Latenz
Leitung: Prof. Dr. Bettina Kempkes

Structure and function of the PLK1-EBNA2 protein complex in B-lymphocytes

Dissertation
zum Erwerb des Doktorgrades der Medizin an der
Medizinischen Fakultät der
Ludwig-Maximilians-Universität zu München

vorgelegt von

Viktoria Vladimirova Tsoneva aus Sofia

2021

Mit Genehmigung der Medizinischen Fakultät der
Universität München

Berichterstatter: Prof. Dr. med. K. Spiekermann

Mitberichterstatter: Prof. Dr. med. Ralf Schmidmaier

Prof. Dr. med. Tobias Feuchtinger

Dekan: Prof. Dr. med. Thomas Gudermann

Tag der mündlichen Prüfung: 28.10.2021

Eidesstattliche Versicherung

Tsoneva, Viktoria Vladimirova

Ich erkläre hiermit an Eides statt,
dass ich die vorliegende Dissertation mit dem Titel
“Structure and function of the PLK1-EBNA2 protein complex in the transformation of B-lymphocytes”
selbständig verfasst, mich außer der angegebenen keiner weiteren Hilfsmittel bedient und alle Erkenntnisse, die aus dem Schrifttum ganz oder annähernd übernommen sind, als solche kenntlich gemacht und nach ihrer Herkunft unter Bezeichnung der Fundstelle einzeln nachgewiesen habe.

Ich erkläre des Weiteren, dass die hier vorgelegte Dissertation nicht in gleicher oder in ähnlicher Form bei einer anderen Stelle zur Erlangung eines akademischen Grades eingereicht wurde.

München, 28.10.2021 *Viktoria Tsoneva*

(Ort, Datum) (Unterschrift Doktorandin)

Table of Contents

Registers

List of figures

List of tables

List of abbreviations

°C degree Celsius
α alpha/ anti
β-ME ß-Mercaptoethanol
Δ Delta / deletion
µl microliter
µM micromolar
aa amino acid
AIDS acquired immunodeficiency syndrome
APC/C anaphase-promoting complex/cyclosome
APS Ammonium persulfate
BL Burkitt's lymphoma
bp Base pair(s)
BSA Bovine Serum Albumin Cysteine/2'-
CBF1 C-promoter binding factor 1
CD Cluster of differentiation
CDK Cyclin-dependent kinase
cDNA complementary DANN
CIP calf intestinal phosphatase
cm centimeter
CMV Cytomegalovirus
Co-IP Co-Immunoprecipitation
D day(s)
DIM Dimerisation domain
DMSO Dimethyl sulfoxide
DNA 2'-deoxyribonucleic acid
dNTP 3'-deoxyribonucleotide-5'-phosphate
Dox Doxycycline
DTT Dithiothreitol
e exon
E1 EBNA1
E2 EBNA2
E3A EBNA3A
E3B EBNA3B
EBNA EBV Nuclear Antigen
EBV Epstein-Barr virus
E. coli Escherichia coli
EDTA Ethylenediaminetetraacetic acid
EtBr Ethidium bromide
FACS Fluorescence-activated cell sorting
FCS Fetal Calf Serum
Fig. figure
GAPDH Glyceraldehyde 3-phosphate
GFP Green florescent protein
gp Glycoprotein
GST Glutathione S-transferase
H Histidine
h hour(s)
HA Hemagglutinin
HDAC Histone deacetylase
HIV Human immunodeficiency virus
HL Hodgkin lymphoma
HRP Horseradish peroxidase
Hyg Hygromycine
IC_{50} half-maximal inhibitory concentration
IP Immunoprecipitation
kb Kilobasepairs
KD kinase domain
kDa Kilodalton
ko Knock out
L Leucine
LCL Lymphoblastoid cell line
M molar
mA Milliampere
min Minute
MHC Major histocompatibility complex
ml Milliliter
mM Millimolar
mRNA messenger RNA
MTT (3-(4, 5-dimethylthiazolyl-2)-2, 5-diphenyltetrazolium bromide) assay
myc / c-myc cellular Myc
NaCl Sodium chloride
NaOH Sodium hydroxide
ng Nanogram
NK cell Natural killer-cell
nm Nanometer
ori Origin of replication
P Proline
PBD polo box domain
PCR Polymerase chain reaction
PI Proteinase inhibitor
PLK Polo-like Kinase
PLK1 Polo-like Kinase 1
PLK2 Polo-like kinase 2
PLK3 Polo-like kinase 3

PLK4 Polo-like kinase 4
PLK5 Polo-like kinase 5
PP1 protein phosphatase 1
RNA Ribonucleic acid
RNase Ribonuclease
rpm Rounds per minute
rRNA ribosomal RNA
RT Reverse transcription
S Serine
s second(s)
SD Standard deviation
SDS Sodium dodecyl sulfate
SDS-PAGE SDS-polyacrylamide gel electrophoresis
T Threonine
TAD Transactivation domain
TAE Tris-acetate EDTA
TE Tris EDTA buffer
TEMED Tetramethylethylenediamine
Temp. temperature
Tris Tris(hydroxymethyl)aminomethane
UV Ultraviolet
V Volt
Vol Volasertib/ BI 6727
vs. versus
WB western blot
wt wild type

Acknowledgements

I would like to thank Prof. Bettina Kempkes and Prof. Karsten Spiekermann for the possibility to work on this exciting subject and for all their support and patience during my lab experience in the previously unknown to me field of microbiology during my medical studies. Thank you for all the understanding and trust in my credibility. The immense amount of devotion, time consumption and constructive criticism during the whole process of writing this dissertation from Prof. Bettina Kempkes is highly appreciated. It has been a knowledgeable challenge and hopefully lucrative endeavor to make a difference in both worlds of biology and medicine.

I am grateful to Conny Kuklik-Roos for her continuous support, for being a mentor, exceptional technician, who generously shared techniques, reagents and words of wisdom to become a friend in recent years.

I would like to thank Simone Rieger for her support and many helpful discussions, but even more for the permanent warm atmosphere and welcoming setup of the lab. Thanks to my predecessor on the project, Elena Fiestas for all the data and knowledge she provided, and thanks to Xiang Zhang for continuing with the project.

I would also like to acknowledge the generous support of the whole laboratory team of Monika Raab and Prof. Klaus Strebhardt who contributed to conducting the experiments, which we could not have performed technically.

My deepest gratitude goes to my parents for all their support, for believing in me and for their patience over the years. Last but not least, I am truly blessed to have such friends who withstood the process of laboratory work and writing with much compassion and tolerance for my scientific venture.

Zusammenfassung

Das Epstein-Barr Virus (EBV) ist mit der Entstehung von zahlreichen Tumorerkrankungen und lymphoproliferativen Krankheiten assoziiert. Aufgrund der hohen Durchseuchungsrate des Viruses in allen menschlichen Bevölkerungsgruppen weltweit, der lebenslangen Latenzzeiten, sowie der rezidivierenden Symptomatik, wird intensiv geforscht, um den Pathomechanismus und die Folgen einer EBV-Infektion im Hinblick auf die Diagnostik und Behandlung von assoziierten Karzinomen zu etablieren. In der Zellkultur kann EBV B-Lymphozyten immortalisieren und deren unbegrenzte Proliferation ermöglichen. Das Epstein-Barr-Virus nukleäre Antigen 2 (EBNA2) ist ein virales Transaktivatorprotein. Es ist essentiell für die Immortalisierung von B-Zellen und hat bei der Regulation viraler und zellulärer Gene eine tragende Funktion. EBNA-2 initiiert den Eintritt in den Zellzyklus und die Aufrechterhaltung der Proliferation.

PLK1 ist ein Enzym aus der Familie der Serin-Threonin Kinasen, das eine entscheidende Rolle in der Mitose spielt. Bekannt sind jedoch auch nichtmitotische Rollen von PLK1, einschließlich abnormer Schutz gegen Apoptose und Regulation von Krebszelleninvasivität. Eine Überexpression von PLK1 wurde in einer Reihe solider Tumoren sowie bei akuter myeloischer Leukämie beobachtet und korreliert mit schlechter Prognose, fortgeschrittenem Krankheitsstadium, undifferenzierten histologischem Grad, hohem Metastasenpotenzial und niedrigen Überlebenschancen, deshalb sind PLK1-Inhibitoren vielversprechende Kandidaten für neue therapeutische Ansätze in der Krebstherapie.

Unsere Forschungsgruppe hat entdeckt, dass EBNA2 mit der Polo-like Kinase (PLK1) einen Protein Komplex ausbilden kann. Die nächste Herausforderung besteht darin, die strukturelle und funktionale Bedeutung dieser Interaktion zu erforschen, um die Biologie der EBV-Infektion besser zu verstehen. In diesem Dissertationsprojekt wird die Interaktion von PLK1 mit EBNA2 biochemisch detailliert beschrieben und untersucht, ob der EBNA2/PLK1 Protein Komplex die Transformation von B-Lymphozyten unterstützt.

Anhand der durchgeführten Experimente wurde bestätigt, dass EBNA2 und PLK1 einen stabilen Proteinkomplex ausbilden. Der PLK1-ATP-kompetitive Kinaseinhibitor Volasertib verhindert die Bildung des EBNA2-PLK1-Komplexes

nicht. Wir verglichen die Toxizität und Wirksamkeit der PLK1-Hemmung in EBNA2-positiven und negativen Zelllinien. Wir haben festgestellt, dass EBV-infizierte B-Zellen empfindlich auf die Behandlung mit Volasertib reagieren und dass EBNA2 exprimierende EBV-negative B-Zelllinien für die Volasertib-Behandlung sensibilisiert sind. Um die Rolle von PLK1 und den Einfluss von EBNA2 auf seine Funktion in verschiedenen Zellzyklusphasen zu analysieren, wurden in einer Pilotstudie experimentelle Bedingungen für den G2 / M Arrest von DG75-Zellen als Voraussetzung für die biochemische Analyse in Kooperation mit anderen Forschungsgruppen festgelegt. Schließlich konnten wir zeigen, dass eine konservierte Region von EBNA2 (CR7) essenziell ist, jedoch nicht allein für die Bindung von EBNA2 an PLK1 zuständig ist. Im Gegenteil, scheint PLK1 auch mehr als eine Bindungsstelle für die Interaktion mit EBNA2 zu haben. Möglicherweise können sowohl die Polo-Box-Domäne als auch die Kinase-Domäne effizient an EBNA2 binden. Die hier vorgestellte Studie ist ein Ausgangspunkt für weitere Arbeit.

Die Identifizierung von PLK1 als Interaktionspartner von EBNA2 erfordert die Charakterisierung der regulatorischen Einzelvorgängen, um die genaue Bedeutung dieses Proteinkomplexes für die Kausalkette bei der Tumorgenese aufzulösen und dadurch bei der zukünftigen Entwicklung von onkologischen Behandlungen beizutragen.

Summary

The Epstein-Barr virus (EBV) is associated with the development of numerous tumour and lymphoproliferative diseases. The virus has become ubiquitous in all human populations worldwide and has the ability to establish lifelong latency and reactivation syndromes after primary infection. Therefore, intensive research is being conducted to elucidate the pathomechanism and consequences of EBV infection in view of potential clinical applications in diagnosis and treatment of associated carcinomas. In cell culture, EBV can immortalise B-lymphocytes and allow their unlimited proliferation. Epstein-Barr virus nuclear antigen 2 (EBNA2) is a central viral transactivator protein. It is essential for the immortalisation of B-cells through regulation of viral and cellular genes. EBNA2 initiates entry into the cell cycle and continuous maintenance of proliferation.

Polo-like kinase 1 (PLK1) is an enzyme in the serine-threonine kinase family that plays a crucial role in mitosis. However, non-mitotic roles of PLK1 are also reported, including enhanced protection against apoptosis and regulation of cancer cell invasiveness. PLK1 is known to be overexpressed in several solid tumours and in acute myeloid leukemia and is correlated with poor prognosis, advanced disease stage, low histological grading, high metastatic potential and limited chances of survival. Therefore, PLK1 inhibitors are promising candidates for novel oncologic therapies.

Our research group has discovered that EBNA2 can form a protein complex with the PLK1. Consequently, the next challenge is to exploit the structural and functional insights of this interaction in order to improve our comprehension of the development of EBV infection. In this dissertation project, the interaction of PLK1 with EBNA2 is confirmed. This interaction is thoroughly examined through the application of various biochemical and molecular approaches with a focus on the question of whether the EBNA2-PLK1 protein complex supports the transformation of B-lymphocytes.

In view of the conducted experiments, it was confirmed that EBNA2 and PLK1 form a stable protein complex. The PLK1 ATP-competitive kinase inhibitor Volasertib does not inhibit EBNA2/PLK1 complex formation. Both active and inactive PLK1 can bind to EBNA2. We also compared the toxicity and efficacy levels of PLK1 inhibition in EBNA2 positive and negative cell lines. EBV infected B-cells are sensitive to Volasertib treatment and more importantly, EBNA2

sensitises EBV-negative B-cell lines to Volasertib treatment. Furthermore, to analyse the role of PLK1 and the influence of EBNA2 on its function during different cell cycle phases, we established the experimental conditions in a pilot study for G2/M arrest of DG75 cells as a prerequisite for the biochemical analysis performed by our collaborators. Finally, we were able to demonstrate that the CR7 domain is essential, but not alone responsible for the binding of EBNA2 to PLK1. On the contrary, PLK1 appears to have more than one binding site for the interaction with EBNA2. Both, the polo-box domain and the kinase domain of PLK1 can bind efficiently to EBNA2.

The study presented here is a foundation for further work. The identification of PLK1 as an EBNA2 interaction partner suggests the characterisation of regulatory correlated pathways to elucidate the exact importance of this protein complex for the pathological molecular mechanisms of tumourigenesis in an attempt to contribute to the future development of oncological treatments.

1 Introduction

1.1 Epstein-Barr Virus

1.1.1 Basics of EBV biology

EBV is a common herpesvirus, the causative agent of infectious mononucleosis, and associated with multiple malignancies (Epstein et al., 1964). Also known as human herpesvirus 4 (HHV-4), EBV is the first human virus identified as having a proven association with the pathogenesis of cancer. From the whole herpesviridae family, which consists of more than 100 different viruses, only nine of them have pathogenic significance for humans: herpes simplex virus 1, herpes simplex virus 2, varicella-zoster virus, EBV, cytomegalovirus , human herpesvirus 6, human herpesvirus 7 and Kaposi sarcoma–associated herpesvirus (Whitley et al., 1996).

EBV consists of an enveloped icosahedral capsid and a double-stranded DNA genome that encodes approximately 100 genes (Kempkes et al., 2015; Karrer et al., 2014). EBV-positive B-cells are better known as lymphoblastoid cell lines (LCLs), which can maintain the genome intact through generations, regardless of the viral genome persisting intracellularly (Thorley-Lawson et al., 2004). Each infected cell of the LCL carries multiple copies of the viral episome and expresses a limited set of six latent viral nuclear antigens (EBNAs 1, 2, 3A, 3B, 3C and LP), as well as three latent membrane proteins (LMPs 1, 2A, 2B). Furthermore, small noncoding RNAs, EBERs 1 and 2 are constitutively expressed in all forms of latent EBV infection (Kieff and Rickinson, 2001). EBNA2 is one of the first genes expressed in the beginning of the transformation of B-cells to lymphoblastoid cell-lines, after EBV infection (Alfieri et al., 1991; Rooney et al., 1989). It plays a major role in the conversion from primary to latent infection by securing the survival of the immortalised lymphocytes. The expression of EBNA2, EBNA3C and LMP1 as key effectors of the immortalisation process induces LCL-like phenotypic changes such as upregulation of antigens and transactivation of the viral C-promoter (Hammerschmidt and Sudgen, 1989). These evasion mechanisms prevent the eradication of EBV transformed cells and benefit the viral oncogenesis (Cohen et al., 1989; Kempkes et al., 1996).

1.1.2 EBNA2 the protein

EBNA-2 is an 86kDa and 487 amino acid protein that has several characteristic regions. Three of the EBNA2 regions have been studied intensely and functions could be assigned as described below. First, an acidic transactivation domain (TAD) near the carboxyl-terminus, secondly a region important for interaction with cellular DNA adapter proteins (adapters) such as CBF1 and finally a region (DIM1 and DIM2) at the amino terminus, which enables the dimerisation of the protein (Friberg et al., 2015).

Furthermore, besides a proline-rich region (polyP), an arginine- and glycine-rich region (polyRG), EBNA2 also has the so-called diversity region (DIV), poorly conserved between the two virus strains (EBV types A and B). Essential for the transcriptional regulation function of EBNA2 are three regions, the self-association domain (aa 101-214), transactivation domain (TAD) (aa 424-468), and nuclear localisation signals (NLS) (aa 284-341 and aa 468-487) (Kempkes et al., 2010).

Nine conserved regions (CR) have been defined within EBNA2 through comparison of the primary structure of human EBNA2 proteins with EBNA2 related proteins of the lymphocryptoviruses of rhesus monkeys and baboons (Kieff and Rickinson, 2007; Friberg et al., 2015).

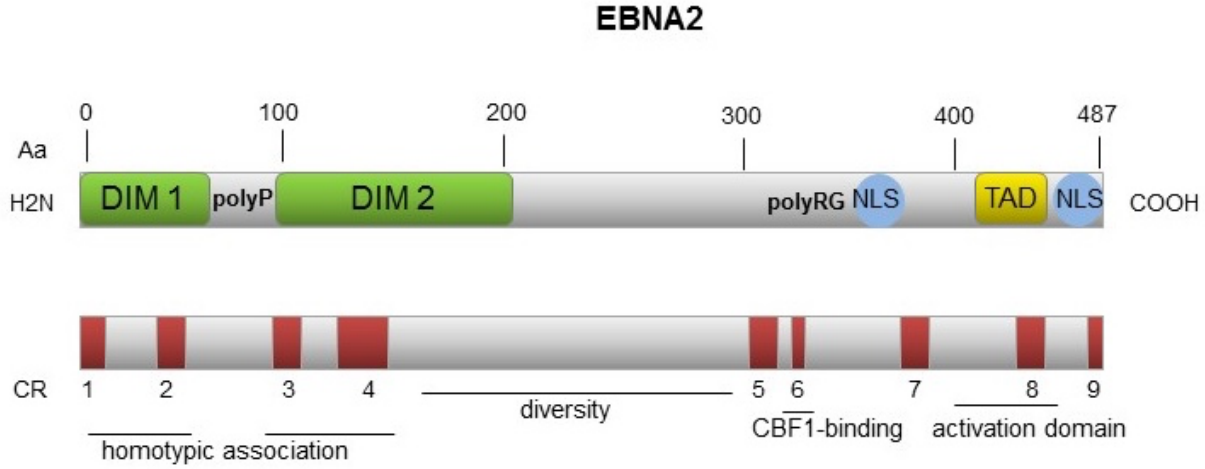

Fig. 1 The structure of the EBNA2 protein
Schematic illustration showing the primary structure of EBNA2.
The EBNA2 protein consists of nine conserved regions (CR1-CR9), a proline repeat (polyP) (aa 59 to 95) and an arginine-glycine repeat (polyRG) (aa 282 to 330). At the N-terminus two separate regions mediate homotypic associations are labelled DIM 1 and 2 as dimerisation motifs. EBNA2 has a diversity region (diversity). The conserved region CR6 mediates the interaction of EBNA2 with CBF1. The homotypic association is characteristic for the self-association domain (aa 101-214). At the C-terminus is localised a transactivation domain (TAD) (aa

424-468) and two nuclear localisation signals (NLS) (aa 284-341 and aa 468-487) (Kempkes et al., 2010).

1.1.3 EBV pathophysiology

Infection with EBV, as with other herpes viruses, involves both a lytic and a latent phase. The establishment of latent infection requires the transformation of the B-cells called immortalisation (Thorley-Lawson et al., 2004). The few infected B-cells can initiate proliferation in immunocompromised hosts with a dysfunctional or limited number of T-cells creating lymphoblastoid cell lines (LCLs) (Rickinson et al., 1997). Primary infection of B-cells results in a rapid expansion of infected lymphocytes congruent to the proliferation rate observed in EBV-immortalised LCLs (Zhao et al., 2011). Following a marked EBV-specific cytotoxic T-cell response by the host, the virus establishes a lifelong latent infection in the B-cells, where it is present in 1 in 10^5–10^6 circulating cells (Zhou et al., 2015). The presence of virions in throat washings of healthy carriers suggests that these latently infected cells can under certain circumstances be urged into a lytic phase. Oropharyngeal epithelial cells were once thought to be the site of primary infection, but it is now believed that EBV initially targets B-cells located in pharyngeal tissues as tonsillar parenchyma (Laichalk et al., 2002)

Various studies using EBNA2 expression in EBV-positive LCL cell lines (Spender et al., 2006; Zhao et al., 2006) or conditional EBNA2 expression in EBV-negative BL cell lines (Maier et al., 2006) confirm numerous EBNA2 target genes, independent of the expression of other viral factors. In the EBV-positive cells, the protooncogene myc and phosphorylated subunits of different kinases were suggested to be direct targets of EBNA2, independent of de novo protein synthesis of the virus. The protooncogene c-myc (myc) can be activated by mitogenic signals and switched off or even induce apoptosis of cells in the absence of proliferation conditions. Its constitutive expression as a common feature of malignant transformation triggers uncontrolled cell cycle progression. Therefore, myc appears to have an important role as an EBNA2 target for the induction of B-cell proliferation (Kaiser et al., 1999). In the absence of EBNA2 activity, the endogenous myc is not expressed in EBV infected B-cells (Kempkes et al., 1995). EBNA2 is known to indirectly access DNA and induce the expression of the LMPS. By binding to the cellular transcription factor, C-promoter binding factor 1 (CBF1), the key downstream effector of Notch

signaling, EBNA2 recruits co-activators of transcription (Hsieh et al., 1995). Furthermore, EBNA2 is reported to control phosphorylation as a result of its interaction with the protein phosphatase 1 (PP1) (Fahraeus et al., 1994). The PP1 is a member of the family of protein serine-threonine phosphatases and is reported to be ubiquitous in all eukaryotic cells (Cohen P., 2002).

The Epstein-Barr virus (EBV) also encodes a serine/threonine protein kinase (PK) that promotes the lytic DNA replication. PK interacts with EBNA2 and phosphorylates it at Ser-243, which results in suppressed transactivation activity for LMP1 (Yue et al., 2005). However, the interaction remains questionable as it was reported only once.

1.1.4 EBV-associated non-malignant diseases

EBV, an orally transmitted virus, infects the majority of the world´s population and can persist as a lifelong asymptomatic infection, which can be detected in oropharyngeal secretions from infectious mononucleosis patients, immunosuppressed patients and healthy EBV seropositive individuals (Gerber et al., 1972; Strauch et al., 1974; Yao et al., 1985). The primary infection occurs in developed populations mostly in adolescence or adulthood. It leads to the manifestation of infectious mononucleosis (IM, glandular fever) in some cases (Cohen JI, 2000). The illness first manifests itself in flu-like symptoms such as fever, headache and fatigue. Swelling of the lymph nodes due to the massive proliferation of B- and T-cells is also characteristic (Young et al., 2003).
Infected B-cells as a primary target of the virus are characterised by limited expression of viral genes. In individuals with an intact immune defense, the infected, proliferating B-cells are largely eliminated by specific T-cells, so that recovery occurs after a few weeks. In rare cases, after infectious mononucleosis, symptoms may persist for months or years, a condition also known as chronic active infection.

A rare complication of primary EBV infection is referred to as X-linked lymphoproliferative syndromes XLP1 and XLP2, both defined as immunodeficiencies with overwhelming and potentially lethal inflammatory reaction to certain infections. XLP1 is caused by hereditary mutations in the gene encoding the signalling lymphocyte activation molecule (SLAM)-associated protein (SAP). It occurs only in males and is correlated with gene defects on the X-chromosome. Such gene aberrations usually do not cause any symptoms.

However, primary EBV-infection in the presence of nonfunctioning SAP protein can result in an excessive immune response (Morra et al., 2001). XLP2 evokes from mutation of the X-linked inhibitor of apoptosis (XIAP). XLP2 has been found to cause relapsing hemophagocytic lymphohistiocytosis with and without exposure to the EBV (Filipovich et al., 2010).

1.1.5 EBV-associated tumours

Due to the still lengthening list of human cancers resulting from EBV infection, EBV was classified by the World Health Organization (WHO) as a tumour virus in 1997. EBV is associated with Burkitt´s lymphoma, non-Hodgkin´s lymphoma, Hodgkin´s disease, nasopharyngeal carcinoma, lymphoepithelioma-lie carcinoma and gastric adenocarcinoma, and in leiomyosarcomas associated with immunosuppression (Young and Murray, 2003; Hsu et al., 2000). EBV-specific antibody titers are known to be elevated months to years prior to the diagnosis of Burkitt's lymphoma, nasopharyngeal carcinoma, Hodgkin's disease, gastric adenocarcinoma (de-Thé et al., 1978; Levine et al., 1995; Mueller et al., 1989). Clinical evidence confirms that primary EBV infection in iatrogenic immunosuppressed patients can lead to EBV-positive lymphomas (Rickinson and Kieff, 1996). The combination of incidence patterns and risk factors to EBV biology and virus-host interaction elucidates factors involved in EBV-related carcinogenesis. A characteristic feature of EBV is the expression of certain distinct viral latent transcription programs called latency I, II, and III (Kempkes, 2010). In LCLs and EBV-positive malignancies the virus is typically latently present and transcriptionally active (Abbot et al., 1990). At this stage, the gene expression pattern is restricted within the pool of 12 gene products. Each latency motif I-III can be identified by the expressed antigens and is a typical feature for distinct tumours associated with EBV (Kempkes and Robertson, 2015; Saha et al., 2011), as shown in Table 1. Hence, the transition from one EBV latency pattern to another is also possible.

latency type	expressed antigens	associated malignancy
I	EBNA-1 EBERs	Burkitt's lymphoma Gastric carcinoma
II	EBNA-1 LMP-1, -2A, -2B EBERs	Nasopharyngeal carcinoma Hodgkin's disease Nasal T/natural killer-cell lymphomas
III	EBNA-1, -2, -3A, -3B,-3C, -LP LMP-1, -2A, -2B EBERs	AIDS-associated non-Hodgkin's lymphoma Post-transplant lymphoma
other	EBNA-1, -2 EBERs	Leiomyosarcoma

Table 1 Patterns of latent gene expression in EBV-related malignancies
The antigens expressed by EBV include six nuclear antigens (EBNA1, 2, 3A, 3B, 3C, and LP), three latent membrane proteins (LMP1, 2A, and 2B), two small noncoding RNAs (EBER1 and 2). Depending on the expressed antigens, there are three possible latency types: type I in Burkitt´s lymphoma: EBNA 1 and two small noncoding RNAs are expressed, latency type II: typical for nasopharyngeal carcinoma, Hodgkin- and T- cell lymphomas, which all express EBNA 1 (EBV nuclear antigen 1), LMP; type III: characterised by the expression of 11 viral genes in lymphoblastic B-cell lymphomas (Data from Saha et al., 2011).

Burkitt's lymphoma

Burkitt's lymphoma is defined as a high-grade, low-differentiated, monoclonal non-Hodgkin's B-cell lymphoma, mostly localised in the abdominal, especially ileocecal area, and the jaw region in pediatric patients, but also affecting brain tissue and ovaries (Ferry at al., 2006; Mondal et al., 2014; Jiang et al., 2011). Burkitt's lymphomas are characterised by specific chromosomal translocations between chromosome 8 and chromosomes 14, 2, or 22, through which the c-myc gene is placed under the control of an immunoglobulin enhancer and, thus, constitutively active. The African endemic form of Burkitt's lymphoma is 100%

associated with EBV, while sporadic and AIDS-associated forms have a less regular association with EBV (Haddow et al., 1970; de-Thé et al., 1978). Prognosis for lymphomas with histologic characterstics of Burkitt-like lymphoma without myc translocation is reported to be better than for those with a myc translocation. In the last years, specific mutations, related to myc in BL patients have been identified as crucial for the further estimation of survival chances and planning of treatment strategies (Dunleavy et al., 2016).

Hodgkin's disease

Hodgkin's disease is a heterogeneous group of lymphoproliferative diseases. Depending on the subtype, in 10 to 95% of the tumours associated with the disease, EBV can be detected mainly in so-called Reed-Sternberg cells. EBV could either indirectly support the pathogenesis of Hodgkin's disease, possibly by triggering certain pathological mechanisms or indicate the depression of immunoregulation that leads both to a malignant transformation and the reactivation of EBV. Data shows that in the western world, Hodgkin's disease is the most common lymphoma in adolescents and young adults (Glaser et al., 2003; Mueller et al., 1989).

Nasopharyngeal carcinoma (NPC)

In almost all cases of undifferentiated nasopharyngeal carcinoma, EBV can be detected in tumour cells. It has been shown that EBNA1, LMP1 and LMP2A are expressed within the tumour cells. Although the particular pathogenetic role of EBV in the carcinogenic process is not clearly defined, the establishment of a virus latency program in epithelial cells is a precursor of malignant transformation (Young et al., 2014). Furthermore, in nasopharyngeal carcinoma elevated EBV-antibody titers are associated with total tumour burden and affect long-term survival rates (Henle et al., 1977). NPC has a distinguishing racial and geographical allocation with the highest prevalence among the male population of Southern China and the Arctic region, indicating that numerous factors contribute to the development of NPC (Levine et al., 1995; Herold, Inn. Medizin, 1993).

Post-transplantation lymphoma

In immunosuppressed persons, after solid organ or hematopoietic stem cell transplantation, the suppression of T-cells can cause serious complications by EBV, as well as by other herpesviruses. These are summarised under the term PTLD (post-transplantation lymphoproliferative disease), either as a consequence of reactivation of the virus post-transplantation or a result of a primary EBV infection due to iatrogenic immunosuppression. They are associated with massive proliferation of B-cells and high mortality (Hsieh et al., 1995). The average probability of occurrence is about 2 to 10% for a solid organ transplant and higher for hematopoietic transplantations (Burney et al., 2006). The gold standard for diagnosing PTLD is tissue biopsy, but many authors have also investigated the role of EBV viral load. In B-cell NHLs rituximab has been established as an integral part of the PTLD treatment (Dierick et al., 2015).

Coincidence of EBV-associated diseases and HIV infection

HIV-related immunodeficiency benefits the incidence of EBV-associated diseases. These include Burkitt's and Hodgkin's lymphomas, diffuse large B-cell lymphomas with immunoblastic morphology, hairy cell leukoplakia and central lymphoma of the nervous system (McClain et al., 1995). The ability of this virus to infect oropharyngeal epithelial cells is demonstrated by EBV replication in AIDS-associated oral hairy leukoplakia (Zhao et al., 2011).

In addition to the described tumours, which are proven to be associated with EBV, other tumours have been associated with EBV in recent years. EBV genomes were identified within the gastric carcinoma and marginal dysplastic epithelial cells but not found in surrounding lymphocytes and healthy mucosa tissues. It has been reported that monoclonal EBV episomes can be found in EBV-associated gastric cancer cells, which suggests a contribution of the EBV infection to gastric carcinogenesis. While a causal involvement of EBV in gastric carcinomas (Levine et al., 1995) and leiomyosarcomas (McClain et al., 1995) can now be considered as certain, its association with carcinomas of the liver and breast cancer has been discussed controversially (Bonnet et al., 1999; Sugawara et al., 1999). It has been suggested that EBV-associated tumours might be prevented or even targeted by a prophylactic or therapeutic EBV vaccine (Cohen JI, 2015).

1.2 PLK1

1.2.1 The PLK protein

The polo-like kinase (PLK1) is a serine-threonine protein kinase. It consists of 603 amino acids and has an apparent molecular weight of approximately 66kDa. PLK1 has multiple regulatory roles in many processes of the cell cycle, including centrosome maturation, Golgi fragmentation, spindle assembly, kinetochore function, centromere assembly and cytokinesis, DNA replication, mitotic entry, removal of chromatid cohesion and chromosome condensation (Sumara et al., 2002; Lane et al., 1996; Spankuch-Schmitt et al., 2002; Neef et al., 2003)

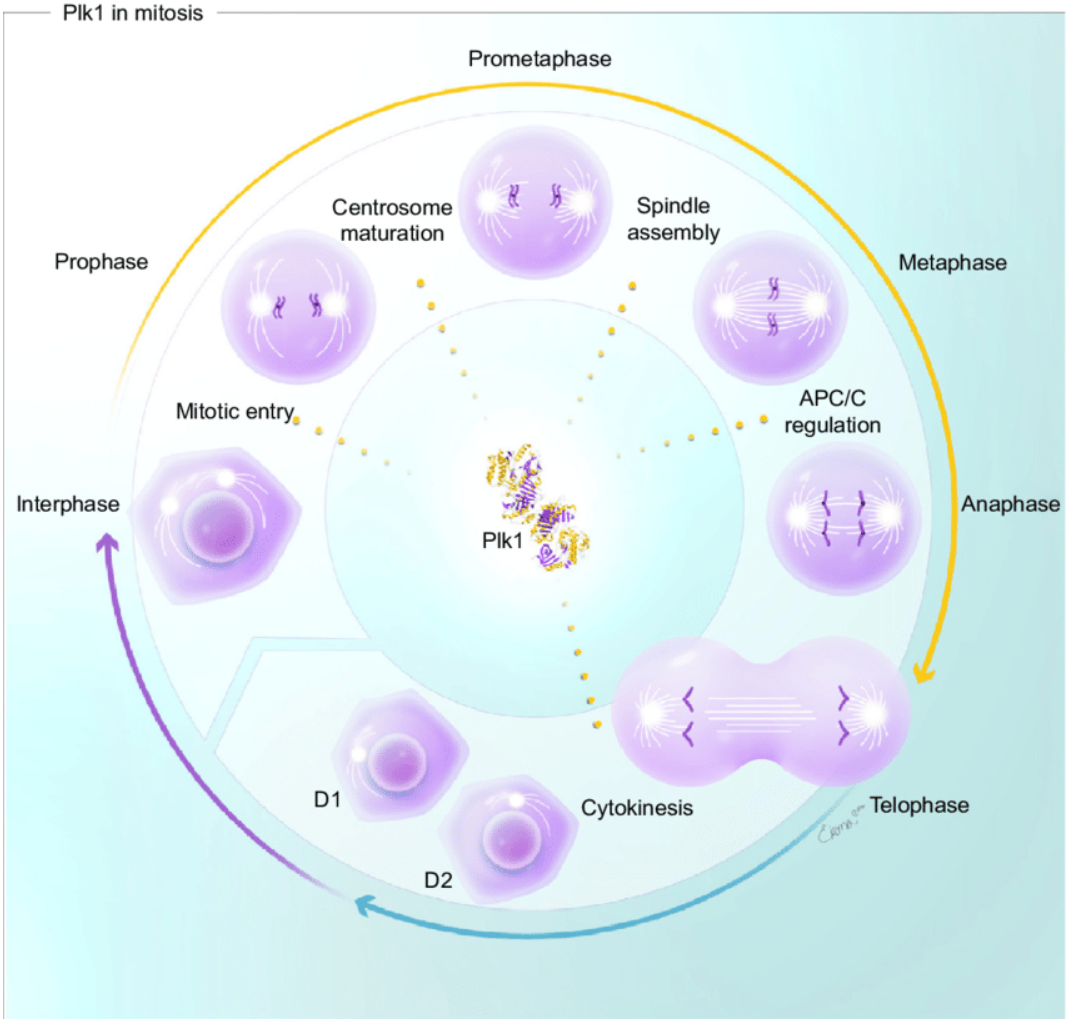

Fig. 2 PLK1's role in the cell cycle
Dashed lines show the sites of action. Yellow blue and violet lines show the progression of the cell cycle. Abbreviations: APC/C, anaphase-promoting complex/cyclosome; D, daughter cell (adapted from Hao and Kota, 2015).

During proliferation, the cells undergo synthesis of DNA (S-phase) and cell division (M-phase) with intervening gap phases to allow cell growth. Important

cell cycle checkpoints are mediated by cyclin-dependent kinases (Hunt et al., 2011).

To fulfil all its functions, PLK1 promotes mitotic entry by interaction with kinases Cdc25C Cdk1/Cyclin B complex, Aurora A and B (Seki et al., 2008). Nevertheless, non-mitotic roles for PLK1 have also been confirmed, including protection against physiological apoptosis and regulation tumour invasiveness (Gjertsen and Schoffski, 2015). Therefore, PLK1 has been the focus of a number of research studies. The specificity of PLK1-dependent biochemical reactions is regulated by PBD-dependent substrate binding and KD-dependent substrate phosphorylation. The PLK1 activation requires phosphorylation of a residue on the T-loop (Thr210) (Elia et al., 2003; Garcia-Alvarez et al., 2007).

PBD and KD are capable of mutual inhibition through intramolecular interaction with each other and allosteric regulation. PBD inhibits KD by restraining the flexibility of the hinge region between N-terminal and C-terminal lobes. KD stabilises a less active conformation of the PBD. The phosphorylation of the T-loop (T210 in PLK1 within the KD) increases the catalytic activity of KD. Phosphorylation of Ser137 or binding of PBD to a partner interrupts the intramolecular interaction between KD and PBD and releases the mutual inhibition. The flexibility of the hinge region and the interlobe cleft has been proposed as crucial for the catalysis of protein kinases, and the reduction of the interlobe flexibility of the KD by PBD binding might be one of the factors underlying the autoinhibition of PLK1 (Lee et al., 1998; Archambault et al., 2015).

PBD binds phosphorylated serine or threonine residues. PBD recognises a consensus phospho-Ser (p-Ser)/phospho-Thr (p-Thr) motif containing [Pro/Phe]-[Φ/Pro]-[Φ]-[Thr/Gln/His/Met]-Ser-[pThr/pSer]-[Pro/X] (Φ represents hydrophobic residues and X stands for any amino acid). PBD binds to its targets, either non-phosphorylated peptides or phosphor-peptides that were phosphorylated by PLK1 itself in a phospho-specific manner (Elia et al., 2003). PBD also appears to improve the spatial association of KD to its substrates. Therefore, PBD binds to a phosphorylated residue on the substrate or its target protein. The PBD-conducted interaction with a phosphorylated protein occurs after the creation of a phosphorylated binding motif and later binding of PLK1 to the already created phospho-target. PLK1 is able to recognise the phospho-epitope and bind to it in a concentration- and affinity-dependent manner (Barr et al., 2014).

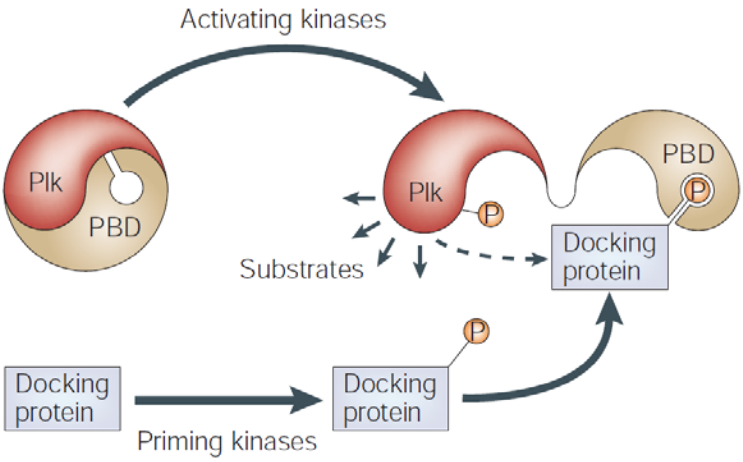

Fig. 3 Illustration of PBD-assisted substrate recognition and PLK1 activation
The initial phosphorylation by another kinase on threonine 210 (T-loop activation) enhances the kinase activity of PLK1. Protein substrates are pre-phosphorylated by priming kinases and directed to PLK1 when the intramolecular inhibition between the kinase domain and PBD is terminated (adapted from Barr et al., 2004).

The fact that PLK1 substrates can be activated by other kinases is of great importance, but PLK1 can also prime its targets (Lee et al., 2014). The phosphorylated residue, essential for PBD binding, is generated by either PLK1 itself (self-priming) or another upstream kinase (non-self-priming) as shown in Figures 4 A) and B) (Park et al., 2010; Lee et al., 2008).

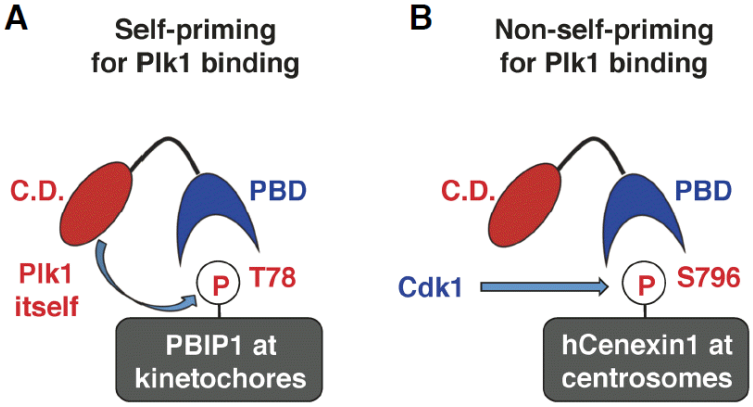

Fig. 4 Two pathways of PBD-dependent binding
(A) PLK1 phosphorylates and generates the p-T78 residue on a kinetochore protein before binding to it, in this case as exemplary, to PBIP1. This mechanism is known as self-priming and binding. (B) another kinase, Cdk1 phosphorylates a centrosomal protein, Cenexin1, and generates the p-S796 motif required for PLK1 PBD binding. The second mechanism is called nonself-priming and binding (adapted from Lee at al., 2014).

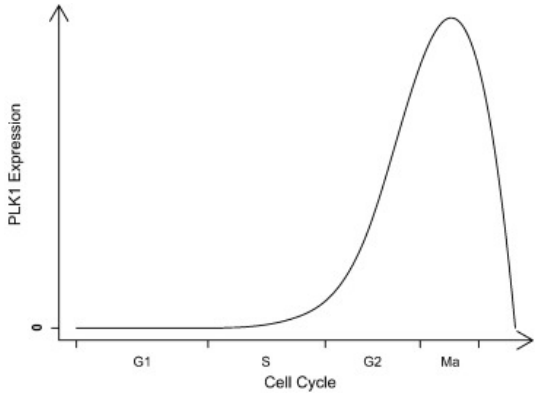

Fig. 5 PLK1 expression in different phases of mitosis
(adapted from Liu et al., 2016.)

PLK1 expression increases during S-phase, reaches its maximum during G2–M transition, and drops abruptly at the end of mitosis (Golsteyn et al., 1994). Following the more common mechanism of activation, PLK1 can be phosphorylated in its T-loop by Aurora A with Bora as co-factor during the G2-phase of the cell cycle. Temporally, at the G2-M transition, Bora facilitates the exposure of PLK1 activation loop for phosphorylation of the conserved threonine residue Thr210 in PLK1 by upstream kinases, and this prevents sequestration of the activation loop by the inter-domain linker and partially activates PLK1 (Macurek et al., 2008; Fischer et al., 2015).

In late mitosis, phosphorylation of the conserved serine motif at the end of the hinge region Ser137 in PLK1 by upstream kinases would partially activate PLK1 through disrupting the intramolecular interaction between the KD and PBD. Spatially, the binding of the PBD to the phosphorylated target at the proper subcellular location can disrupt the intramolecular interaction between the PBD and KD and relieve the inhibition of the PBD. These temporal and spatial controls can occur separately or additively, which allows multilevel regulation of PLK1 and satisfies its multiple functions in different stages of the cell cycle (Kang et al., 2006; Arnaud et al., 1998).

PLK1 associates dynamically to multiple subcellular structures throughout the interactions with various proteins. It localises at the centrosomes during interphase and prophase and can be traced to the kinetochores in pro-metaphase and metaphase. During anaphase it moves to spindles and shifts to the midbody during telophase. This temporal localisation of PLK1 corresponds with several particular tasks of PLK1 including its specific substrate recognition and kinase function throughout the mitotic cycle (Hanisch et al., 2006; Seong et al., 2002).

1.2.2 The PLK protein family

PLK1 is only one member of a whole family of serine-threonine kinases. All members appear to play specific roles that have little functional overlap with one another. PLK2 and PLK3 contribute to the DNA damage response. PLK2, which is expressed primarily in early G1-phase, mediates cellular stress-induced checkpoint arrest for survival, while PLK3 regulates G1/S-phase transition and other pathways, including spindle disruption (Bahassi et al., 2002; Conn CW et al., 2000; Drew M. L. et al., 2005). In addition, PLK2, PLK3, and PLK5 are required for proper neuronal function and differentiation, while PLK4 plays a key role in centriole duplication (de Cárcer et al., 2011; Zitouni et al., 2014; Bruns et al., 2003; Helmke et al., 2015). PLK4 contains a conserved central domain, also known as the ‘cryptic polo box’ (CPB), that connects the kinase domain and the carboxyl-terminal PB. This region was first described as a centriole targeting element, which is able to bind the kinase domain in s-trans conformation (Leung et al., 2002). Regarding this specific feature, the region is called the ‘cryptic polo box’ despite the sequence disparity to standard PBs (Swallow et al., 2005).

Although the primary sequence of PLK1 exhibits a high level of homology with closely related PLK2 and PLK3, the three PLKs have divergent substrate specificity and the PBDs of each PLK interact with specific phosphoepitopes on their binding targets.

PLK1 is characterised by a carboxyl-terminal polo-box domain (PBD) phosphopeptide binding domain, composed of two polo boxes PB1 and PB2. PBD1 and PBD2 are separated by Loop 2 switch linker region. KD and PBD are separated by inter-domain linker, containing a destruction box essential for PLK1 degradation and not conserved in PLK2, PLK3, PLK5 (Mundt et al., 1997; Archambault and Glover, 2009).

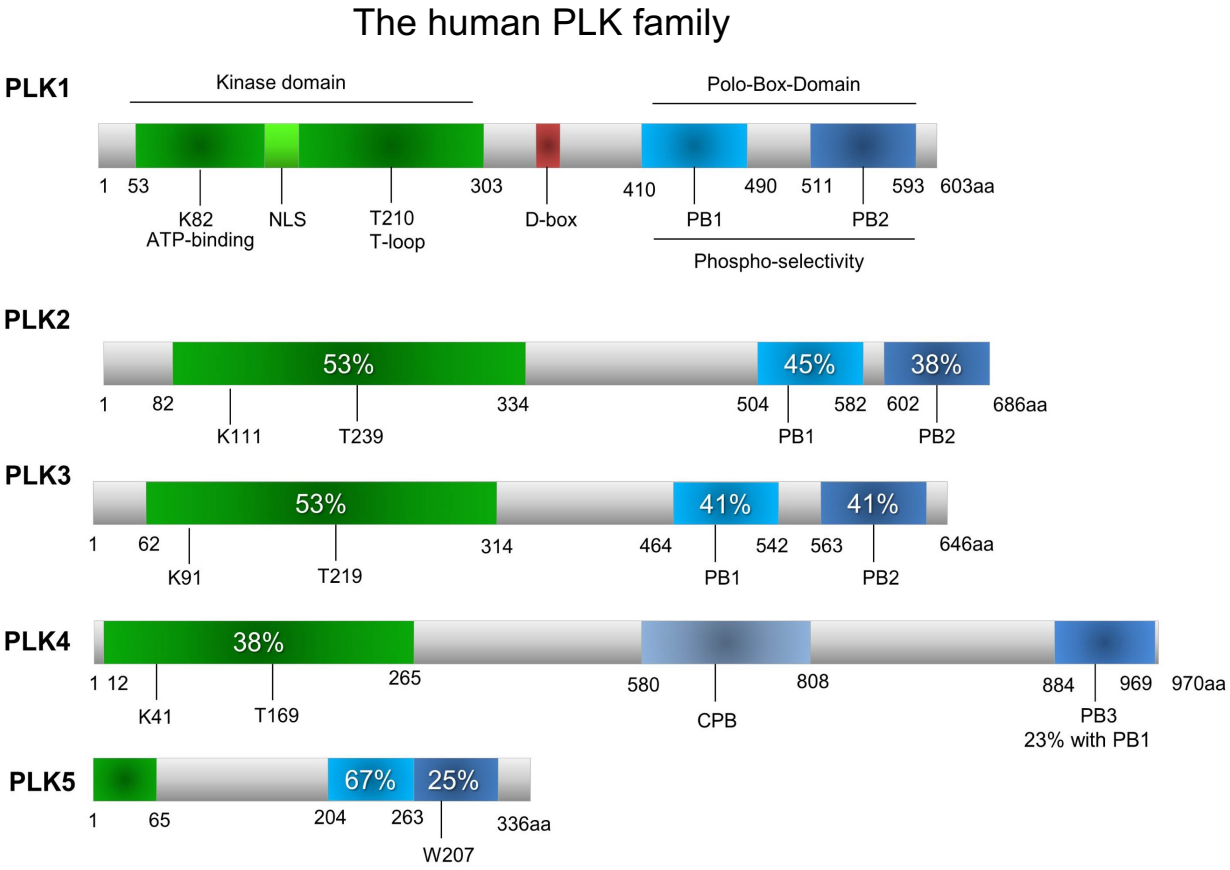

Fig. 6 PLK1 as a member of the family of serine-threonine kinases
The approximate level of sequence similarity to PLK1 is given as a percentage for all the other PLK members. The kinase domain is capable of ATP binding. T-loop activation of PLK1 occurs at Threonine 210 (T210) (Macurek et al., 2008; Seki et al., 2008). The destruction box (D-box) is a typical feature only of the PLK1. PB1 and PB2 are the polo-box domains with phopho-selectivity found in all the PLK-family members, apart from PLK4. PLK4 is the most divergent member of the PLK family and possesses a C-terminal PBD, called PB3 and a central domain known as the cryptic polo box (CPB) (Cizmecioglu et al., 2010).

1.2.3 PLK1 overexpression and associated tumours

PLK1 is expressed in all tissues (www.genecards.org) but overexpression of PLK1 has been observed in a variety of solid tumours, such as head and neck, esophageal, gastric, mamma, ovarian, endometrial, colorectal, pancreatic, papillary, thyroid, prostate carcinoma, melanomas, glioma, hepatoma, as well as in acute myeloid leukemia (AML). It has also been associated with advanced disease stage, low histologic grade, high metastatic potential and bad overall survival chances (Holtrich et al., 1994; Takai et al., 2005). AML is characterised by a differentiation arrest and dysfunctional proliferation of progenitor cells, caused by genetical aberrations or signal transduction malfunctions. Proteins linked to PLK1, such as Aurora A and B, but also PLK1 itself are overexpressed

in AML cell lines. Inhibition or knockdown of PLK1 preferentially disrupts further proliferation of leukemic rather than normal cells and sensitises AML cells to other chemotherapeutic agents (Renner et al., 2009).

Acute myeloid leukemia with a complex karyotype (CK AML) have an adverse outcome even treated with intensive therapies. PLK inhibition resulting in cell proliferation defects and autophagy has been suggested as the most selective approach for the primary CK AML (Moison et al., 2019).

Comparing the PLK1 expression in cancer and normal tissues shows significantly higher expression levels of PLK1 in malignant cells. Moreover, PLK1 protein expression has been reported to be increased in various human cancers compared with healthy tissue and is correlated to bad survival rates. Overexpression of PLK1 correlates to considerably worse overall survival in comparison to lower expression levels of PLK1 in a variety of cancer types (Liu et al., 2017). These observations have encouraged further investigation of the potential therapeutic application of PLK1 inhibitors for the pharmaceutical treatment of cancer (Strebhardt and Ullrich, 2006; Gjertsen and Schoffski, 2015).

Even though PLK1 overexpression and EBNA2 have never been linked to one another, their coincidental occurrence and association to certain tumours need to be narrowly inspected. Oro-/ nasopharyngeal carcinoma, gastric carcinoma, breast cancer and NHL are all potentially linked to PLK1 and EBNA2 conjunction (Table 2). In DG75 Burkitt lymphoma cells, PLK1 is overexpressed, and approximately five times stronger than the household gene GAPDH (Xiao et al., 2016). PLK1 signalling is known to promote the protein stability of the protooncogene myc and vice versa, myc can induce PLK1 transcription, establishing a feed-forward myc-PLK1 circuit in lymphomas (Xiao et al., 2016).

tumour	PLK1 overex-pression	prognostic value of PLK1 over-expression	reference	associa-tion with EBV	references
oro/nasopharyngeal carcinoma	+	+	Knecht et al., 1999	+	Henle et al.,1977;
gastric carcinoma	+	Ø	Tokumitsu et al., 1999	+	Levine et al., 1995
breast cancer	+	Ø	Weichert et al., 2005	+	Richardson et al., 2005
non-Hodgkin's lymphoma	+	+	Mito et al., 2005	+	Hummel, et al., 2006;

+ positive correlation: confirmed PLK1 overexpression / validated prognostic value / confirmed EBV association; Ø no prognostic value. The proposed prognostic potential of PLK1 overexpression in cancer patients is based on available completed studies. (Adapted from Strebhardt and Ullrich, 2006.)

Table 2 PLK1 and EBV coincidental overexpression in tumours

1.2.4 PLK1 functional inhibition

PLK1 inhibition can be achieved in a variety of ways. Historically the first down-regulation of PLK1 function was performed in 1996 by Lane and Nigg. They have reported that the treatment of HeLa cells with anti-PLK1-antibodies causes inhibition of cellular proliferation. Cells arrested in mitosis and are incapable of forming a bipolar spindle (Lane et al., 1996). These findings were later confirmed by using dominant-negative forms of PLK1 and single-stranded DNA antisense oligonucleotides, which bind to complementary mRNA and prevent translation of PLK1. Cells transfected with these antisense oligonucleotides were blocked in mitosis 48h post-transfection (Spankuch-Schmitt et al., 2002). A third mechanism of suppressing PLK1 expression is the use of small interfering RNA (siRNA). Only recently the possible clinical use of the siRNA as a class of therapeutics, which can selectively silence disease-causing genes, has been investigated. Several in vitro studies have already shown that PLK1 inhibition using siRNA significantly reduces the proliferation of multiple cancer cells (Weiß et al., 2012).

Inhibition of PLK1 triggers an aberrant mitotic activity that ultimately triggers cell death that occurs either during or after defective mitosis or

irreversible cell cycle arrest. Targeting mitosis for the treatment of human cancer is a validated approach and agents affecting the mitotic spindle are used as components of various therapeutic regimens. The so-called polo-arrest, caused by PLK1 inhibition is a perturbation of the spindle assembly and cell-cycle arrest at the prometaphase. Mitotic cells accumulate with monopolar spindles that are inappropriately attached to the kinetochores (Galluzi et al., 2012).

Volasertib

PLK1 specific inhibition can be achieved by targeting either the kinase domain (KD), which conducts the enzymatic phosphorylation function of PLK1, or the C-terminal polo-box domain (PBD), which implements the substrate recognition. One of the earliest PLK1 inhibitors, BI2536, was developed and described by scientists at the Boehringer Ingelheim Company. Although no longer used in monotherapy, due to suboptimal response rates (Mross et al., 2012), it has demonstrated efficacy when combined with other chemotherapeutic agents (Lian et al. 2018).

Volasertib (BI 6727), the most advanced PLK inhibitor in clinical development, is a dihydro-pepteridinone that targets the PLK family in an ATP-competitive manner and thereby induces mitotic arrest and apoptosis (Rudolph et al., 2009). Volasertib locates in the ATP binding pocket of PLK1 and causes competitive inhibition. Volasertib disrupts centrosome maturation and division and thus causes the composition of a monopolar spindle. Consequently, the cells are temporarily arrested in the prometaphase as they are unable to pass the spindle assembly checkpoint (Liu and Erikson, 2003; Sumara et al., 2004; Lenart et al., 2007; Steegmaier et al., 2007).

In vitro Volasertib potently curbs PLK1 enzymatic activity at a half-maximal inhibitory concentration (IC_{50}) of 0.87 nmol/L, but also two other members of the PLK family, the kinases, PLK2 (IC_{50}, 5nmol/L) and PLK3 (IC_{50}, 56nmol/L). However, the inhibitory activity against PLK4 (20mM) is comparatively low and Volasertib displays no inhibitory activity against many other unrelated kinases at concentrations up to 10mmol/L (Rudolph et al., 2009).

The US Food and Drug Administration (FDA) provided a novel therapy implementation for Volasertib in September 2013. All AML patients at the age of 65 or older who have not been treated previously were considered suitable for the purposes of this clinical study. Phase II clinical study on Volasertib showed

promising response to the drug and urged the start of the Phase III study, known as the POLO-AML-2 study. The Phase III study, POLO-AML-2, investigated Volasertib combined with low-dose cytarabine (LDAC chemotherapy), in patients aged 65 years and older who have not been treated for AML so far and were considered inadmissible for intensive remission induction therapy. The results presented at the 21st Annual Congress of the European Hematology Association (EHA) 2016 demonstrated that the percentage of patients with an objective response was higher with Volasertib plus LDAC, compared to placebo plus LDAC but the difference was statistically not significant. Further studies are required to identify a subset of AML patients with optimal response to Volasertib, and the molecules or pathways that associate with the response to Volasertib in AML cells. However, the study initiated a new trial program to explore the potential in the treatment of acute myeloid leukemia and myelodysplastic syndromes (Scharow et al., 2015).

Table 3 shows a list of selected PLK1 inhibitors as their number has been rapidly expanding. A new generation of PLK1 inhibitors is currently under development. Even though completed studies could not validate a breakthrough for the PLK1 inhibitors targeting the ATP-domain, the results were evaluated as encouraging enough to initiate the development of compounds that target the PBD of PLK1. These compounds are now the focus of preclinical research. This domain is characteristic for the PLK family and separates structurally individual members of the PLK family. Therefore, drugs targeting the PBD of PLK1 will be highly specific. One of the new small molecule PBD inhibitors, Poloxin has shown apoptotic potential in several cancer cell lines (Yuan et al., 2011; Reindl et al., 2008).

Inhibitor	Clinical trials	Status	Target	Reference
BI2536	Phase II	Completed 2008	ATP binding domain	Frost et al., 2012
GSK461364	Phase I	Completed 2009	ATP binding domain	Gilmartin et al., 2009
Volasertib (BI6727)	Phase III	active, not recruiting; estimated completion date December 2019	ATP binding domain	Rudolph, Steegmaier et al., 2009;
ON01910.NA (rigosertib)	Phase III	Completed 2015	PLK1 non-competitive and PI3K	Gumireddy et al., 2005
TAK960 hydrochloride	Phase I	Terminated 2013	ATP binding domain	Beria et al., 2010
Poloxin	None	-	Polo-box domain	Reindl, Yuan, 2008
Poloxin-2	None	-	Polo-box domain	Scharow, Raab, 2015

Table 3 List of PLK1 inhibitors

It is still to be determined whether ATP-competitive and PBD-specific inhibitors of PLK1 differ in their potential to suppress tumour growth. Common chemotherapeutical agents such as the vinca-alkaloids and taxanes, which have a proven response in the clinical treatment of cancer, have also been known for their side effects, including neurotoxicity and myelosuppression. Therefore, targeting PLK1 with the potential new compounds holds great promise for the development of anticancer therapies.

1.3 Aims of the project

In 2015, when this project was initiated, original findings in the laboratory of Prof. Dr. Kempkes led to the exciting discovery of a new protein complex between EBNA2 and PLK1. Epstein-Barr virus nuclear antigen 2 (EBNA2) is a well-known central viral transactivator protein. It is essential for the immortalisation of B-cells and has a supporting function in the regulation of viral and cellular genes. Unraveling EBNA2 interaction partners and intracellular signalling is crucial in order to understand the EBV-biology. PLK1, on the other hand, is an enzyme in the serine-threonine kinase family that plays a crucial role in mitosis. PLK1 overexpression has been associated with the development of various tumours and is verified as responsible for the aggressive proliferation of tumour cells in countless studies. However, although a considerable amount of information was known about these two proteins separately, there was no previous data regarding the interaction of EBNA2 and PLK1. Therefore, the further confirmation and investigation of this profound discovery is necessary. The main objective of this project was to characterise and better understand the molecular mechanism behind this interaction, its consequences for the cell cycle progression and its influence on the malignant transformation of EBV- infected B-cells.

Specifically, we asked ourselves if and how the protein complex EBNA2-PLK1 might be involved in the transformation of B-lymphocytes. This question prompted us to test the interaction of those proteins in EBNA2 transfected EBV-negative cells, as well as lymphoblastoid cell lines. As a relevant objective, co-immunoprecipitation analysis was performed to provide evidence that EBNA2 and PLK1 interact with each other. Furthermore, we aimed to investigate the molecular pathway of this interaction in the context of a dysregulation of the PLK1 activity. What consequences the interaction has between PLK1 and EBNA2, what happens if we disrupt it and how could we prevent the interaction in the first place are all questions we aimed to answer in this project. In this regard, we analysed the structure and the exact interaction surface within the protein complex. Additionally, the binding regions on EBNA2 and PLK1, which are essential for the formation of the complex, were inspected using PLK1 mutants. We wanted to know if EBNA2 is a substrate of PLK1 as a kinase enzyme and to what extent the EBNA2 phosphorylation is critical for the interaction of interest and the transformation of the lymphocytes. Therefore, we had to optimise protocols for

cell-cycle arrest of LCL and EBNA2 expressing cells. After achieving a cell-cycle synchronisation with nocodazole, we handed over the cell samples to the laboratory of Prof. K. Strebhardt an M. Raab in order to analyse the biological enzymatic activity of the PLK1 in the presence and absence of EBNA2.

Finally, to investigate whether the PLK1 activity can affect the interaction between the two proteins of interest, we sought to establish cell culture conditions and exact concentration levels for Volasertib treatment of LCLs and cells conditionally expressing EBNA2. By this means, we wanted to define the modulatory effects of PLK1 inhibition on EBNA2 positive and negative cells using MTT assay and evaluate the toxicity and efficacy levels of the PLK1 inhibitor treatment.

2. Materials

2.1 Plasmids

Table 4 Plasmids

Name	Description	Origin
pCKR74.2	Dox- (doxycycline) inducible HA-(haemagglutinin) tagged EBNA2 expression plasmid (pCKR74.2) based on pRTR.	et al. Bornkamm 2005
pSG5(pSG5-HA)	Empty vector used as a negative control	Stratagene
pAG155 (pAG155-EBNA2wtHA)	plasmid for expression of EBNA2 (B95.8) with C- terminal HA-Tag. Vector pSG5	Gordadze AV 2004
pEFC61 (pAG155-EBNA2-Δ377-387-HA)	plasmid for expression of EBNA2-ΔCR7 with C-terminal HA-Tag. Vector pSG5	Kempkes
Ga981-6 (12xluc)	contains the hexameric 50-bp EBNA-2 response element of the TP-1 promoter in front of the minimal β-globin promoter driving the luciferase gene	Minoguchi, S., 1997.
P3695 (Renilla)	pPGK:Renilla, Luciferaseplasmid	Promega
VA 32 (pSG5-EBNA2)	Full-length EBNA2 expression plasmid	Cohen and Kieff, 1991
VA 40 (pSG5-FLAG-EBNA2)	EBNA2 expression plasmid with N-terminal FLAG-tag	kind gift by Bill Schubach USA
VA 45 (pSG5-FLAG-EBNA2 Δ455 AAA)	EBNA2 expression plasmid with N-terminal FLAG-tag and conversion of three consecutive amino acids to Alanines	kind gift by Bill Schubach USA
VA 55 (pSG5-EBNA2 S457L)	EBNA2 expression plasmid with single-point mutant of pSG5 EBNA2. At position 457 serine is exchanged for leucine.	kind gift by Bill Schubach USA
VA 56 (pSG5-EBNA2 W458T)	EBNA2 expression plasmid with single-point mutant of pSG5 EBNA2. At position 458 Tryptophan is exchanged for threonine.	kind gift by Bill Schubach USA
VA57 (pSG5-EBNA2 S469L)	EBNA2 expression plasmid with single-point mutant of pSG5 EBNA2. At position 469 serine is exchanged for leucine.	kind gift by Bill Schubach USA
CKR355	empty expression plasmid with 3x N-terminal FLAG-vector and backbone pCDNA3.1 Hygro;	*Strebhardt, Raab*
CKR356	PLK1 expression plasmid with N-terminal FLAG-tag and backbone pCDNA3.1 Hygro;	*Strebhardt, Raab*
CKR357	PLK1 expression plasmid with N-terminal GFP vector and backbone pEGFP-C2	*Strebhardt, Raab*
CKR358	PLK1 expression plasmid with N-terminal FLAG-tag and backbone pCDNA3.1 Hygro; consists of the first 416 bp of PLK1	*Strebhardt, Raab*
CKR359	PLK1 expression plasmid with N-terminal FLAG-tag and backbone pCDNA3.1 Hygro; consists of the first 305 bp of PLK1	*Strebhardt, Raab*
CKR360	PLK1 expression plasmid with N-terminal FLAG-tag and backbone pCDNA3.1 Hygro; consists of both Polo-box domains; bp 372 to 603 from PLK1	*Strebhardt, Raab*

2.2 Cell lines

Table 5 Cell lines

Name	Description
DG75	EBV-negative Burkitt's lymphoma cell line (Ben-Bassat, Goldblum et al., 1977)
CKR 128-34	EBV-negative Burkitt's lymphoma cell line (DG75) transfected plasmid CKR74.2 that is based on the vector pRTR. pRTR (Bornkamm, Berens et al. 2005) is an expression vector for EBNA2 that carries a bidirectional doxycycline-inducible promoter that simultaneously drives the expression of a surrogate marker and a gene of interest.
LG 395 3.1	human lymphoblastoid cell line immortalised with recombinant wt EBV (p2089*BAC mid:* derived fromB95.8 virus) (Generated by L.G., Kempkes lab) (Delecluse, Hilsendege et al., 1998)
LG 396 3.1	human lymphoblastoid cell line immortalised with recombinant wt EBV (p2089*BAC mid:* derived fromB95.8 virus) (Generated by L.G., Kempkes lab) (Delecluse, Hilsendege et al., 1998)
CKR 178-10	DG75 transfected with a bidirectional doxycycline-inducible plasmid CKR74.2 in pRTR (Bornkamm, Berens et al., 2005)
P493.6	EREB cell line, a human B-lymphocytes cell line, coinfected with p3HR1 – Epstein-Barr virus and a mini EBV plasmid 554-4, in which the endogenous EBNA2 is replaced with an estrogen-inducible EBNA2-estrogen receptor (ER) fusion protein. Tetracycline-regulated expression of myc gene and estrogen-regulated expression of EBNA2: myc can be repressed with 1ug/ml tetracycline and further cell growth is prohibited, EBNA2 can be induced using 1ug/ml estrogen (Kempkes B, et al., 1995)
BL41.K3	EBV-negative Burkitt's lymphoma cell line transfected with p554-4; growth under supplementation of G418 (800µg/ml); estrogen induction of EBNA2 (1µM final concentration) leads to growth arrest and apoptosis (Kempkes B, et al., 1995)
BJAB. K3	EBV-negative lymphoblastoid cell line; P12978; transfected with ER/EBNA2; growth under supplementation of G418 (800µg/ml); estrogen induction of EBNA2 (1µM final concentration) leads to growth arrest and apoptosis (Klein et al., 1974, Kempkes et al., 1995)

2.3 Cell culture material

Table 6 Cell culture material

Name	used concentration	supplier
Ampicillin	100µg/ml	Sigma-Aldrich, USA
Dimethylsulfoxide (DMSO)	0,5 %	Merck (Calbiochem), Germany
Doxycyclin	1ug/ml	Sigma-Aldrich, USA
ß-estradiol (estrogen)	1ug/ml	Sigma-Aldrich, USA
FCS (Fetal calf serum)	10 %	GIBCO, UK

G418 (Geneticin)	800µg/ml	GIBCO, UK
L-Glutamine	2mM	GIBCO, UK
LB –Medium	1 % Bacto-Trypton; 0,5 % Yeast Extract; 1 % NaCl (pH 7,4)	GIBCO, UK
Opti-MEM Medium	-	GIBCO, UK
Penicillin/Streptomycin	100 U/ml	GIBCO, UK
Puromycin	1µg/ml	Merck, Germany
RPMI 1640 medium	-	GIBCO, UK
Volasertib (BI 6727)	1-100nM	Selleckchem

2.4 Antibodies

Table 7 Antibodies

Name	Description	Dilution	Supplier
Primary antibodies			
α-EBNA2 (R3) monoclonal	Rat, IgG2a kappa	WB 1:50, IP 1:3	E. Kremmer, HMGU
α-GAPDH (MAB374)	Mouse IgG1	WB: 1:5000	Merck Millipore, MAB374
α-GAPDH (5C4)	Rat, IgG2a	WB:1:2000	E. Kremmer, HMGU
α-HA (R1 3F10) monoclonal	Rat, IgG1	IP 1:3	E. Kremmer, HMGU
α-PLK1[35-206] monoclonal (ab17056)	Mouse, IgG2b	WB 1:1000, IP 1:100	abcam, UK Lot: GR137124--2
Phospho-Histone H3Ser10 (D2C8) XP monoclonal	Rabbit IgG	WB 1:2000	Cell signalling, Ref: 3377
α- PLK1 FLAG 6F7	Rat, IgG1	WB:1:20	HMGU
α- FLAG M2 F3165	Mouse, IgG1	WB:10µg/ml	Sigma-Aldrich, USA
Secondary antibodies			
α-rabbit GtXrb HRP	Goat anti-rabbit IgG Horseradish Peroxidase	WB 1:5000	Chemicon Lot LV1467501
α-rat-IgG-HRP (sc2006)	Goat anti-rat IgG Horseradish Peroxidase	WB 1:5000	Santa Cruz, USA
α-mouse-IgG-HRP (sc2005)	Goat anti-mouse IgG Horseradish Peroxidase	WB 1:5000	Santa Cruz, USA

2.5 Chemicals and reagents

Table 8 Chemicals and reagents

Name	Supplier
Acrylamide 30%	Carl Roth GmbH, Germany
Agarose	Byozym, Germany
Amersham ECL Western blotting detection reagents	GE Healthcare, UK
APS	MP Biomedicals, Germany
BSA (*Bovine serum albumin*)	Merck, Germany
Bromophenol blue	Merck, Germany
Complete EDTA free, Protease Inhibitor cocktail Tablets	Roche Diagnostics, Germany
Calyculin A (serine/threonine Phosphatase Inhibitor)	Cell Signaling Technology , USA
CIP Calf Intestinal Phosphatase	Sigma-Aldrich, USA
DNA Dye NonTox	ApplyChem,
Ethidium bromide	Carl Roth GmbH, Germany
Glycerin	Carl Roth GmbH, Germany
GeneRuler DNA 1 kb ladder	MBI Fermentas, Germany
IGEPAL	MP Biomedicals, Germany
Isopropanol	Serva, Germany
β-Mercaptoethanol	Sigma-Aldrich,USA
Milk powder	Carl Roth GmbH, Germany
MTT Thiazolyl Blue Tetrazolium Bromide	Sigma-Aldrich,USA
Nocodazole Methyl-(5-[2-Thienylarbonyl] -1H-benzimidazole-2-yl)carbamate	Sigma-Aldrich,USA
Na3VO4 (Sodium orthovandate)	Sigma S-6508
Propidium iodide	Sigma-Aldrich,USA
PageRuler Plus Prestained Protein Ladder	Thermo Scientific, USA
PhosStop	Roche Diagnostics, Germany
PMSF	ApplyChem Darmstadt UN 2923
Protein G-Sepharose	GE Healthcare, UK
RNase A	Invitrogen, Thermo Fisher Scientific, USA

TEMED	ApplyChem, Germany
Tris (hidroxymethyl) aminomethan	Merck, Germany
Trypan blue	Sigma-Aldrich,USA
Tween-20	ApplyChem, Darmstadt
Volasertib (BI 6727)	Selleckchem
Thymidine	Sigma-Aldrich,USA

2.6 Enzymes

Table 9 Enzymes

Name	supplier
BamHI	Fermentas (Thermo Fischer Scientific), USA
Xba I	Fermentas (Thermo Fischer Scientific), USA
HindIII	Fermentas (Thermo Fischer Scientific), USA
XhoI	Fermentas (Thermo Fischer Scientific), USA
SfiI	BioLabs New England
Eco47III	Fermentas (Thermo Fischer Scientific), USA
SphI	BioLabs New England

2.7 Kits

Table 10 Kits

Name	supplier
ECL	GE Healthcare Amerscham, UK
Dual Luciferase® reporter assay system	Promega, USA Ref: E1960
JETSTAR 2.0	Genomed, Germany
NucleoSpin® Plasmid	Macherey-Nagel GmbH Ref: 740588.50
Qubit® dsDNA BR Assay Kit	Life Technologies Ref: Q32850

2.8 Supplementary materials and devices

Table 11 Supplementary

Name	supplier
6K10 Centrifuge	SIGMA Centrifuges GmbH, Germany
BioPhotometer D30	Eppendorf, Germany
Cell-Incubator	Heraeus Instruments, Germany
Centrifuge 5415	Eppendorf, Germany
Centrifuge 5417 R	Eppendorf, Germany

CP1000 Developing device	AGFA, Cologne, Germany
Electrophoresis chamber	PeqLab, Germany
Electroporation Gene Pulser II	Biorad, Germany
FACS Calibur	BD Biosciences, USA
Film cassette	Amersham, Bioscience, Sweden
Fluoresce microscope Axiovert 200M	Zeiss, Germany
Fuji Medical X-Ray Film	FUJIFILM Corporation, Japan
Gene Pulser® cuvettes, 0,4cm electrode	Bio-Rad Laboratories, USA
GloMax Discovery System 11853TA	Promega, USA
Immobilion PVDF transfer membrane	Millipore, USA
Nitrocellulose blotting membrane premium 0,2µm	Amersham, GE Healthcare
Orion Microplate Luminometer	Berthold detection systems, USA
Odyssey IR scanner	Licor
Plasticware	GmbH, Eppendorf, Greiner GmbH
RC5C centrifuge	DuPont, USA
Rotanta 460 R centrifuge	Hettich, Germany
Shaker incubator	New Brunswick Scientific, USA
Thermomixer compact	Eppendorf, Germany
UV-Transiluminator	PeqLab, Germany
Whatman 3MM chromatography papers	GE Healthcare, UK

3. Methods

3.1 Cell culture methods

3.1.1 Cell counting

Cell number was determined using a Neubauer chamber. To detect the viability of the cells, an aliquot of cells was diluted 1:2 with 0.4% trypan blue. Dead cells showing blue colour and colourless living cells were counted.

The number of living cells was calculated with the following formula:

$$living\ cell\ no.per\ mL = \frac{counted\ no.of\ cells}{no.of\ counted\ big\ squares} \cdot 2 \cdot 10^4$$

3.1.2 Cell lines and cell culture conditions

All cell lines were cultivated at 37°C and 5% CO_2 in RPMI 1640 medium supplemented with 100U/ml Penicillin, 100µg/ml Streptomycin, 4mM L-Glutamine, and 10–20% FCS respectively. Cell density was determined by using a Neubauer counting chamber.

LG 395 3.1 and LG 396 3.1 are human lymphoblastoid cell lines immortalised with recombinant wt EBV (p2089BAC mid: derived fromB95.8 virus). The cells were maintained as suspension cultures in RPMI 1640 standard medium (Gibco Life Technologies) supplemented with 10% FCS (fetal calf serum, Bio&Sell), 4 mM L-Glutamine and 1 x penicillin/streptomycin (Gibco Life Technologies). Cells were grown at 37°C in a humidified atmosphere at 5% CO_2. The DG75doxHA-E2/CBF1 wt (CKR128-34) and the DG75doxHA-E2/CBF1 k.o. (CKR178-10) cell lines carry the doxycycline-inducible HA-EBNA2 expression plasmid (pCKR74.2). DG75doxHA-E2WW/CBF1 wt expresses a Dox inducible HA-EBNA2 WW325FF mutant. The cells were cultivated in standard 1µg/ml puromycin containing RPMI media at 37°C in a humidified atmosphere at 5% CO_2. EBNA2 expression was induced by doxycycline treatment (1µg/ml).

P493-6 cells were maintained in RPMI-1640 supplemented with 10% FCS (fetal calf serum, Bio&Sell) and 2 mM L-glutamine. Cells were grown at 37°C in a humidified atmosphere at 5% CO_2. For repression of the conditional pmyc-tet construct in P493-6 cells, 0.1µg/ml tetracycline was added to the culture medium and cells were incubated for 48hr. For myc re-induction, cells were washed three

times with growth medium and grown in tetracycline-free culture conditions. EBNA2 was induced using 1ug/ml estrogen.

BL41.K3 cells were cultivated in standard RPMI medium with 10% FCS (fetal calf serum, Bio&Sell) and 2 mM L-glutamine at 37°C in a humidified atmosphere at 5% CO_2. G418 (800µg/ml) was supplemented to induce growth. Estrogen induction of EBNA2 (1µM final concentration) led to growth arrest and apoptosis.

BJAB. K3 cells were cultivated in standard RPMI medium with 10% FCS (fetal calf serum, Bio&Sell) and 2 mM L-glutamine, at 37°C in a humidified atmosphere at 5% CO_2. Growth was induced under supplementation of G418 (800µg/ml). EBNA2 was induced using 1ug/ml estrogen.

3.1.3 Long-term cell depot

To preserve cells for a longer period of time, cells were frozen in liquid nitrogen. To this end, 10^7 cells were collected (suspension cells by centrifugation and adherent cells with preceding trypsin treatment), resuspended in 1.5 ml freezing medium and transferred to 1.8 ml Cryotubes (NUNC). Using a propanol freezing container cells were slowly cooled to -80°C and stored there for approximately one day. Finally, tubes were transferred to liquid nitrogen. To recultivate frozen cells, these were thawed in a 37°C water bath, washed with 30 ml medium to extract DMSO, and resuspended in fresh medium.

- Freezing medium 40% culture medium, 50% FCS, 10% DMSO.

3.1.4 Propidium iodide staining and FACS analysis

10^7 cells were centrifuged at 300 rcf for 10min at 20°C and washed once with FACS buffer (2% FCS in PBS). The supernatant was discarded and the cells were resuspended in 0.5ml PBS. Then cells were mixed with 100% Ethanol, dropwise while vortexing and incubated 15min on ice, kept at 4°C. Next, cells were centrifuged at 500rcf for 5min at 20°C, washed in 5 ml PBS/1%FCS, again centrifugated. The pellets resuspended in 1ml PI/RNase A solution (15ml PBS; 175µg/ml RNase A; 10µg/ml Propidium iodide in PBS) and incubated at 37°C for 30min and finally analysed by flow cytometry using a FACS Calibur system (Becton Dickinson) and CellQuest Pro software (BD Biosciences). Data was

analysed using FlowJo 7.6 software and its cell cycle analysis function (Tree Star Inc., Ashland, USA).

- PBS: 37M NaCl; 2.7M KCl; 7.3M Na2HPO4; 1.5M KH2PO4 pH 7.4.

3.1.5 MTT assay

Cells were cultivated at 37°C with 5% CO_2 in RPMI1640 standard culture medium. MTT (3-(4, 5-dimethylthiazolyl-2)-2,5-diphenyltetrazolium bromide) 5mg/ml solution (10 µl MTT per 100µl medium) was added to all wells of plates and plates were incubated at 37°C for 4h. The enzymatic reduction of yellow tetrazolium salt MTT to purple formazan crystals is a colourimetric reaction quantified by measuring absorbance at a certain wavelength with a multi-well spectrophotometer. After incubation, acid-isopropanol (100µl of 0.04 N HCl in isopropanol) was added to all wells and mixed thoroughly to dissolve the dark blue formazan crystals, and absorbance values were measured on a Sunrise microELISA plate reader, using a reference test wavelength of 550nm and a reference wavelength of 690 nm. The assays were performed in triplicate for each experimental condition.

The inhibitory concentration or (IC_{50}) (drug concentration that is required to reduce half of the cells from the total population) was ascertained using GraphPad Prism 7 software (San Diego, California). In order to analyse the data, the various concentrations of the inhibitor (Volasertib) were transformed into logs and plotted as X against the absorbance values as Y. Then, using the automatic analysis function of the program, nonlinear regression was calculated using the equation ‘Dose-response curves – Inhibition’ and applied the equation ‘log(inhibitor) vs. response’. Finally, to determine whether there is a significant difference between the IC_{50} scores, we performed an unpaired t-test and compared the p-values for each dataset.

3.1.6 Cell cycle arrest of cells at the onset of S-phase of the cell cycle by double thymidine block

Cells were grown in culture in standard media to approximately 40% confluence. 20ul of Thymidine solution for each 1ml of culture media was added to a final concentration of 2mM. Cells were incubated for 15h, then washed twice with

sterile PBS, transferred into new well plates, supplemented with 3ml fresh cell culture media per well and incubated for 9h. Again, 20mM of Thymidine blocking solution was added to the cells, followed by 15h incubation. Afterward, cells were washed twice with PBS, resuspended in fresh media and transferred into new plates. After the final addition of culture media, the cells were synchronised in G1 and were ready to be released into cycle over the next 15–20 hours.

3.1.7 Nocodazole arrest of cells in G2 M-phase of the cell cycle

Cells were cultured in DMEM standard medium. For the experiment, cells were either induced with doxycycline 1µg/ml to activate EBNA2 expression or left untreated with doxycycline. The asynchronously growing cells were treated with 100ng/ml nocodazole and incubated for 8/10/12/14/16h to induce G2-M-phase cell cycle arrest. The efficiency of synchronisation was tested by Propidium Iodide-based cell cycle analysis kit (Genscript) using flow cytometry.

3.2 Methods of protein analysis

3.2.1 Kinase assay

Table 12 Lysis buffer

final concentration	**stock**	**for 10 ml buffer**
20mM Tris pH 8.2	1M 1:50 dilution	200µl
150mM NaCl	5M 1:33 dilution	300µl
1% Triton X 100	10% 1:10 dilution	1ml
1mM PMSF	100mM 1:100	100µl
0,5mM Na3VO4 (Sodium orthovandate)	100mM 1:200	50µl
Complete Protease Inhibitor	1 tbl/2ml H20 1:25 dilution	400µl
PhosStop (Phosphatase Inhibitor)	1 tbl/1ml H20 1:10 dilution	1ml
H20		6.95ml

3.2.2 Co-immunoprecipitation

$1x10^7$ cells per sample were harvested and washed in 1ml PBS, then transferred into Eppendorf tubes and centrifugated with 500xg for 5min at 4°C, afterwards lysed with 500µl Lysis Buffer (NP-40)/IP and incubated for 30min rotating at 4°C on a falcon roller, then incubated on ice for another 30min. Next, cell debris were spun down at 16,000xg for 15min at 4°C and the supernatant transferred into new tubes. For the preparation of 50% slurry/equilibration beads (Protein G-Sepharose 4 Fast Flow); using 100µl 50% slurry per IP in total (50µl packed beads)) were centrifugated with 2000xg for 2min, washed 3x with 500µl Lysis buffer/spun down with 2,000xg for 2min and resuspended in equal quantity Lysis buffer. For pre-clearing the lysate 30µl equilibrated 50% slurry was added to the supernatant samples and incubated for 1h at 4°C under rotation.

Then, beads were spun down with 2,000xg for 2min to remove proteins binding unspecific to the beads. 100µl from the antibodies Anti-Ha R1 3F10 (Anti–rat igG1) were added to the supernatant samples and incubated at 4°C under rotation overnight. For the pre-blocking of the beads 1ml 0.5% BSA in Lysis Buffer was added to 50% slurry and incubated at 4°C under rotation overnight in order to avoid unspecific binding of the beads. On the next day, the beads were washed 3x with 500µl Lysis Buffer and spun down with 2,000xg for 2min. 50µl equilibrated 50% slurry was mixed with the antibody and supernatant samples and incubated for 2h at 4°C under rotation, then the beads were spun down with 2,000xg for 2min and the supernatant kept. Beads were washed 5x with 500µl Lysis Buffer and spun down with 2000xg for 2min, then resuspended in 60µl 2x Laemmli (IP-sample) and boiled for 5min at 92°C under occasional agitation to separate the beads from the target proteins.

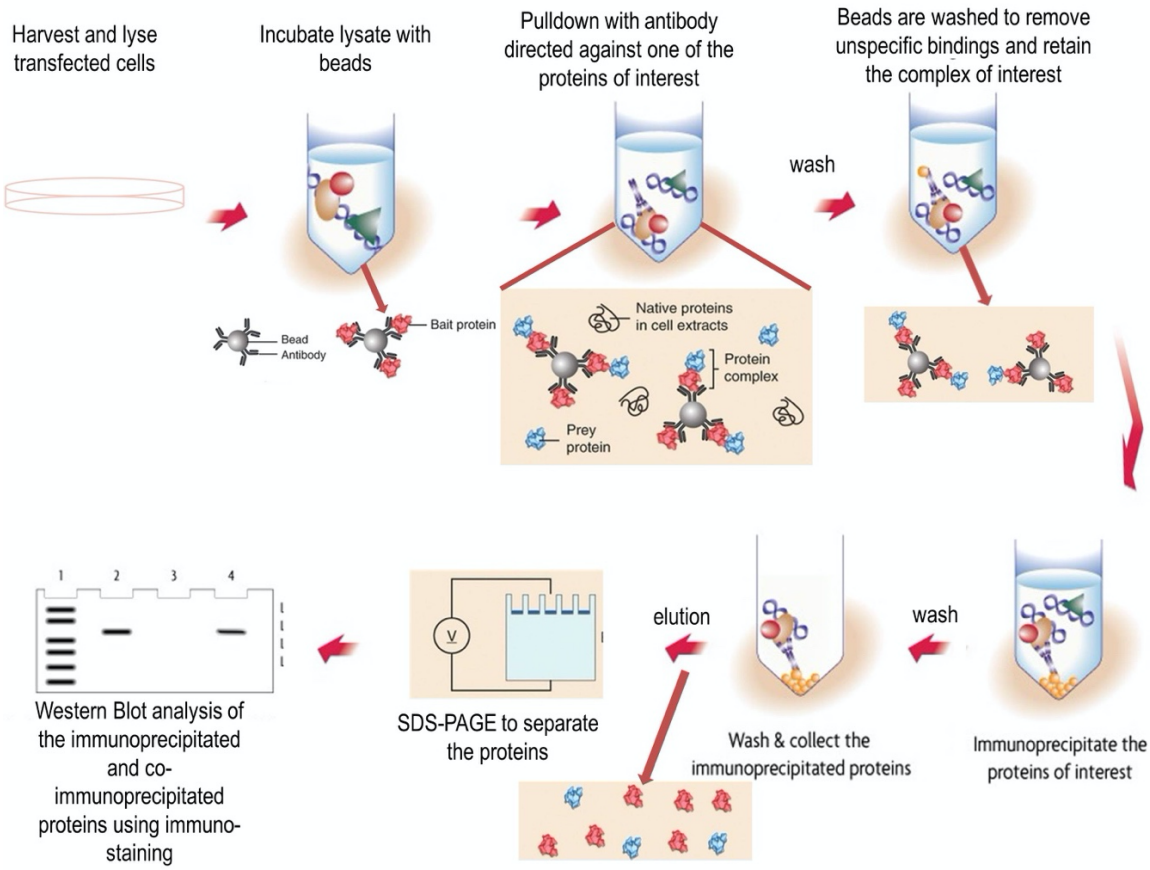

Fig. 7 Co-IP: Workflow for co-immunoprecipitation
In IP, an antibody is added first to a mixture containing an antigen and incubated to allow antigen-antibody complexes to form. Subsequently, the antigen-antibody complexes are incubated with an immobilised antibody against the primary antibody (secondary antibody) on protein-coated beads to allow them to absorb the complexes. The beads are then thoroughly washed, and the antigen is eluted from the beads by sodium dodecyl sulfate (SDS). Western blot is then performed using a secondary antibody directed against the second protein of interest (Adapted from Lee et al., 2013).

3.2.3 Sodium dodecyl sulfate-polyacrylamide gel electrophoresis

The glass plates are washed with 1% sodium dodecyl sulfate (SDS) and after that with 70% EtOH. The casting frames are set on stands and the gap between the glass plates filled with separating gel solution and isopropanol on top until overflow. After the gel has polymerised, the rest of the isopropanol is poured out, the free space filled up with the stacking gel and a comb placed to form wells.

The samples are mixed with Laemmli buffer and heated at 92˚C for 5min, then centrifuged for a couple of seconds and loaded into wells. The electrophoresis chamber runs at 25mA per gel; 100V in BioRad Mini-Protean Tetra Cell.

Table 13 Laemmli buffer

	SDS	Glycerol	Tris/HCl pH 6.8	Mercaptoethanol	Bromophenolblue	H2O
2x	4%	20%	120mM	5%		
	4ml from 10%	2ml	1.2ml from 1 M	500 ml	Tip of a spatula	2.8ml
5x	10%	50%	300mM	12.5%		
	1g	5ml	3ml from 1 M	1.25 ml	Tip of a spatula	0.75 ml

10xRunning Buffer (1l): 250mM Tris Base (30.4 g); 2M Glycine (150.2 g); 1% SDS 100 ml of 10% stock

Tris/Glycine SDS-polyacrylamide gel

Table 14 Separating gel 8%

8%	5 ml	10 ml	15 ml	20 ml	25 ml	30 ml	40 ml	50 ml
H_2O	2.3	4.6	7.0	9.3	11.6	13.9	18.6	23.2
30% Acrylamide	1.3	2.7	4.0	5.3	6.7	8.0	10.7	13.4
1.5 M Tris (pH 8.8)	1.3	2.5	3.8	5.0	6.3	7.5	10.0	12.5
10% SDS	50 ml	100 ml	150 µl	200 ml	250 ml	300 ml	400 ml	500 ml
10% APS	50 ml	100 ml	150 ml	200 ml	250 ml	300 ml	400 ml	500 ml
TEMED	3 ml	6 ml	9 µl	12 ml	15 ml	18 ml	24 ml	30 ml

Table 15 Separating gel 10%

10%	5 ml	10 ml	15 ml	20 ml	25 ml	30 ml	40 ml	50 ml
H_2O	2.0	4.0	5.9	7.9	9.9	11.9	15.8	20
30% Acrylamide	1.7	3.3	5.0	6.7	8.3	10.0	13.3	16.6
1.5 M Tris (pH 8.8)	1.3	2.5	3.8	5.0	6.3	7.5	10.0	12.5
10% SDS	50 µl	100 µl	150 µl	200 µl	250 µl	300 µl	400 µl	500 µl
10% APS	50 µl	100 µl	150 µl	200 µl	250 µl	300 µl	400 µl	500 µl
TEMED	2 µl	4 µl	6 µl	8 µl	10 µl	12 µl	16 µl	20 µl

Table 16 Separating gel 12%

12%	5 ml	10 ml	15 ml	20 ml	25 ml	30 ml	40 ml	50 ml
H_2O	1.7	3.3	5.0	6.6	8.3	9.9	13.2	16.4
30% Acrylamide	2.0	4.0	6.0	8.0	10.0	12.0	16.0	20.0
1.5 M Tris (pH 8.8)	1.3	2.5	3.8	5.0	6.3	7.5	10.0	12.5
10% SDS	50 µl	100 µl	150 µl	200 µl	250 µl	300 µl	400 µl	500 µl
10% APS	50 µl	100 µl	150 µl	200 µl	250 µl	300 µl	400 µl	500 µl
TEMED	2 µl	4 µl	6 µl	8 µl	10 µl	12 µl	16 µl	20 µl

Table 17 Stacking gel

15%	1 ml	2 ml	3 ml	4 ml	5 ml	6 ml	8 ml	10 ml
H_2O	680 µl	1.4	2.1	2.7	3.4	4.1	5.5	6.8
30% Acrylamide	170 µl	330 µl	500 µl	670 µl	830 µl	1.0	1.3	1.7
1.5 M Tris (pH 6.8)	130 µl	250 µl	380 µl	500 µl	630 µl	750 µl	1.0	1.25
10% SDS	10 µl	20 µl	30 µl	40 µl	50 µl	60 µl	80 µl	100 µl
10% APS	10 µl	20 µl	30 µl	40 µl	50 µl	60 µl	80 µl	100 µl
TEMED	1 µl	2 µl	3 µl	4 µl	5 µl	6 µl	8 µl	10 µl

3.2.4 Generation of cell lysates

For the generation of whole-cell lysates 10^7 cells were harvested by centrifugation, washed once with PBS, and resuspended and lysed in 100-200µl NP-40 Lysis Buffer. The reaction was incubated for 1h on ice and, subsequently, sonicated 3x for 10s. Cell debris was pelleted by centrifugation (20,000g, 15min, 4°C), the supernatant was transferred to a new 1.5 ml reaction tube and stored at -80 °C.

- NP-40 Lysis Buffer 50mM Tris-HCl, pH 7.5, 150mM NaCl, 1% NP-40, 1x Proteinase Inhibitor Cocktail (Roche).

3.2.5 Protein quantification via Bradford assay

The protein content of lysates was quantified by Bradford method using a defined serial dilution (1-10µg) of BSA as reference. To this end, 5x Bradford Solution was diluted 1:5 with H2O just before usage and 1-2µl of the lysates were added and mixed by inversion of the cuvette. The absorbance of the mixtures was measured at 595nm (A595) using a spectral photometer. Finally, 2µl of the cell lysates were measured at the same absorbance and the concentration was determined using the calibration curve.

Bradford-reagent: 0.01% Coomassie Brilliant Blue G-250; 4.7% Ethanol; 8.5% phosphoric acid

- 5x Bradford Solution 100mg Coomassie Brilliant Blue G-250, 47% Methanol, 42.5% phosphoric acid.

3.2.6 Western blot and immunodetection

The proteins separated by sodium dodecyl sulfate-polyacrylamide gel electrophoresis (SDS-PAGE) were blotted to a PVDF (Immobilon-P pore size 0.45µm, Millipore) membrane in a transfer unit. The membrane was initially incubated for 15s in 100% methanol for activation, washed for 2min in H2O and incubated for at least 5min in Transfer Buffer. The blotting stack was prepared as follows: one sponge, three pieces of 3MM Whatmann filter paper, the gel from SDS PAGE, activated PVDF membrane, three more pieces of 3MM filter paper and one sponge on top. 10µg of protein from cell lysate 10-20µg of purified protein from the immunoprecipitation was loaded. The transfer was carried out at 400mA for 1h.

Subsequently, the membranes were blocked with blocking buffer for 30min at room temperature, then incubated overnight at 4°C with the primary antibodies. Next, membranes were washed 3X for 10min with washing buffer and incubated with the corresponding HRP-conjugated secondary antibodies for 1h at room temperature and, afterwards, washed with PBST 4x for 15min. The signals were detected by Amersham™ ECL western blotting detection reagent following the manufacturer's instruction and exposed to Fujifilm 100 NUF X/raz film.

- Blocking buffer 50mM Tris-HCl, pH 7.5, 150mM NaCl, 5% non-fat milkpowder
- PBS (1l): NaCl – 8g; KCl0 – 2g; Na2HPO4 – 1.44g; KH2PO4 – 0.24g; pH 7.4

- Washing Buffer (PBS/Tween): PBS with 0.05% Tween
- Transfer buffer 25mM Tris Base, 192mM Glycine, 0.1% SDS, 20% Methanol.

3.3 Methods of DNA analysis

3.3.1 Small-scale purification of plasmids

For small-scale purification, 2ml of saturated bacteria culture were centrifuged at 5000rcf for 5min at 4°C. Plasmid DNA was purified using the NucleoSpin® Plasmid kit (Macherey-Nagel). To test the plasmid DNA, 2µl of DNA was digested with restriction enzymes and separated in an electrophoresis gel.

3.3.2 DNA isolation from agarose gels

DNA fragments were isolated using NucleoSpin® Gel and PCR Clean-up kit (Macherey-Nagel) according to the manufacturer's protocol.

3.3.3 Cloning of recombinant plasmids

Digestion using restriction enzymes

For the digestion, 2µl of the corresponding restriction enzyme was mixed with 6µl of the corresponding buffer and 10µg of DNA and filled with autoclaved water to the volume of 60µl. The mixture was incubated for 2h at 37°C.

3.3.4 Ligation of DNA fragments

Vector fragment and insert fragment were mixed at 1:3 ratio. Ligase buffer was also added at 1:10 and the T4 DNA ligase at 1:20 dilution to the final volume of 20µl. The mixture was incubated overnight at 16°C. The ligation reaction was used for bacterial transformation.

3.3.5 Electrophoresis in agarose gel

Agarose gel was prepared to dissolve 2g of agarose in 200ml of TAE solution (40mM Tris-Acetate; 1mM EDTA (pH 8.0)) and 10µl of ethidium bromide. The digested DNA samples were mixed 1:5 with the loading dye. The agarose gel was run at 100V and the DNA fragments were controlled using UV light at 254nm using a UV transilluminator.

3.3.6 Transformation or re-transformation: (incubation of bacteria with DNA on ice and heating shock)

Approximately 150µl competent bacteria were thawed out slowly on ice (DH5 bacteria). The plasmid DNA (approximately 50ng) were transferred in tubes. Then the plasmid was incubated with the bacteria for 30min on ice, followed by heat shock at 42 °C for exactly 2min and incubated on ice for at least 2min. The samples with bacteria and plasmids were added to 1ml LB-medium and incubated at 37 °C shacking for 1h. 200µl of the bacteria culture was spread on an agar plate with antibiotics and incubated at 37°C overnight.

3.3.7 Transfection (electroporation)

One day before the transfection, cells were split 1:2 and on the day of the transfection, the cells were counted in the Neubauer chamber and the amount of $1x10^7$ cells needed for the transfection were harvested in 10ml cell volume per sample. The falcons with cell volume were centrifuged at 300rcf, 10min, 20°C and the supernatant discarded. Then the pellet was washed with 20ml of Opti-MEM and again centrifugated at 300rcf, 10min, 20°C, the supernatant was discarded and the pellet dissolved in 250µl of Opti-MEM per sample. Cells with Opti-MEM were transferred in tubes together with 5µg of DNA per sample.

The cells with the DNA were transferred into 0.4cm electro ‘Gene pulser’ cuvettes (Biorad) and electroporated at 250V and 950µF. After the transfection, the cell suspensions were incubated with the DNA on a small flash with 10ml of 20% FCS medium at 37°C for 24h. Each transfection sample was prepared in triplicates.

3.3.8 Luciferase assay

$5x10^6$ cells were used per sample. Cells were transfected with 5µg of promoter Ga981-6, 0.5µg of Renilla plasmid and 3µg of the plasmid of interest. Cells were harvested 24h after transfection by centrifugation at 300 rcf at 20°C for 10min. The pellet was washed with PBS. Dual Luciferase assay was performed following the Promega kit E1960 protocol. Cells were lysed with 100µl of passive lysis buffer 1x, and incubated on ice for 15min before being frozen at -80°C. Next day, the cell lysates were thawed and centrifuged at 15.300rpm for 15min at 4°C. The supernatant was transferred into new tubes and stored at -

20°C. To measure luciferase activity, 10µl of supernatant were transferred into a 96 well-plate.

The measurement of the luciferase activity was carried out using the Orion Microplate Luminometer and the following stored program per well: addition of 50µl 1x Luciferase assay reagent II (LARII), followed by the first measurement, then the addition of 50µl 1x Stop&Glo reagent and second measurement.

(The results of the luciferase activity were given in relative light units RLU.)

4. RESULTS

4.1 MTT assays of Volasertib- (BI 6727-) treated cells

4.1.1 MTT assay with immortalised B-lymphocytes in the context of PLK1 inhibition on a molecular level

MTT assays have been proven suitable for the initial stage of in vitro drug screening as it measures proliferation rate or conversely the reduction in cell viability after drug exposure. In order to investigate the effect of the PLK1 inhibitor Volasertib on EBNA2 positive cells, two equivalent cell lines of immortalised B-lymphocytes: LG395 and LG396 were treated with the inhibitor in serial dilutions ranging from 100nM to 0.09nM and compared to additional controls without Volasertib. To quantify the effect of the PLK1 inhibitor on the cell proliferation we calculated the concentration of the drug that resulted in the half-maximal response, value called IC_{50} score. IC_{50} scores (Fig. 7 A) were similar, however not identical for the two cell lines with IC_{50} of 38.65nM for LG395 and 24.96nM for LG396. The significant difference between the IC50 scores (as shown in Fig. 7 B) is probably due to an overall higher proliferation state of the LG395 cell line and not necessarily a consequence of the Volasertib treatment.

As expected, we were able to show that EBV infected cells were sensitive to a PLK1 inhibition via Volasertib. The calculated IC_{50} scores were comparable to the established EC_{50} scores of other cell lines, derived from cancer tissues such as colon (HCT 116 cell line) and hematopoietic malignancies (Raji cell line) with IC_{50} scores within the range vales of 11 to 37nM (Rudolph et al., 2009).

A)

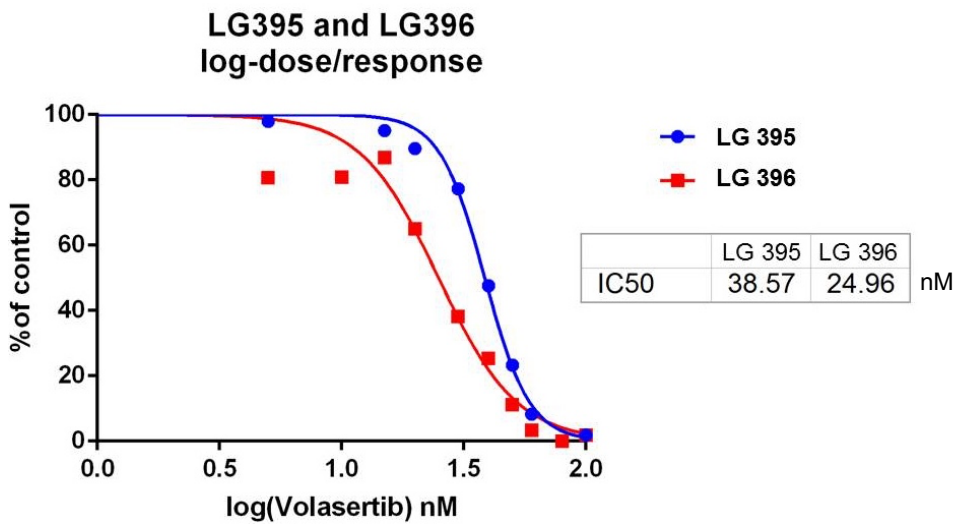

B)

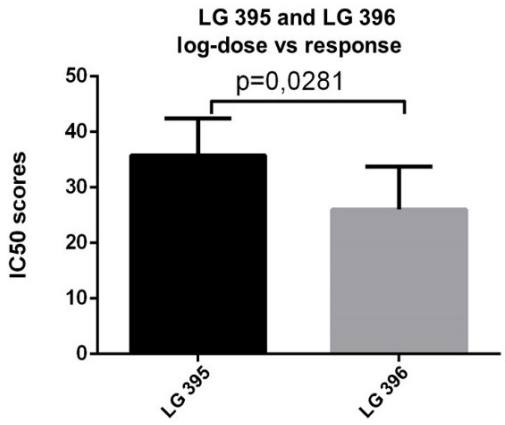

Fig. 8 EBV infected B-cells are sensitive to Volasertib
$4x10^4$ B-cells, infected with EBV (LG 395 and LG396) were seeded as 100µl cultures in 96 well plates and cultured in the presence of increasing amounts of Volasertib for 48h or were left untreated. The viability of treated and untreated cells was analysed by MTT assays. Results of three biological replicates performed in technical triplicates were combined and analysed by GraphPad Prism 7. A) Combined dose-response curves; B) The mean IC_{50} scores were then analysed using unpaired t-test in the GraphPad Prism 7 and visualised as bars. Error bars represent the corresponding standard deviation. p-value with $\alpha = 0.05$ as significance level. (All assays were performed in triplicates and the results were obtained in three independent experiments.)

4.1.2 MTT assay with EBNA2 transfected EBV-negative B-lymphocytes in the context of PLK1 inhibition

When two equivalent EBV-negative cell lines BJAB.K3 (Figs. 9 A and B) and BL41.K3 (Figs. 9 C and D), both EBV-negative lymphoma cell lines, transfected with EBNA2 (as described in section 2.2. Cell lines) were treated with increasing concentrations of Volasertib for 48h, they displayed equal IC_{50} scores, without EBNA2 expression. The IC_{50} scores for the EBNA2 positive cells were lower in all experiments than those of the EBNA2 negative cells: 20.44nM compared to 25.37nM for BL41.K3 (Fig. 9 A) and 15.65nM compared to 25.38nM for BJAB.K3 (Fig. 9 C). However, the difference was not significant ($p>0.05$). Thus, we identified a clear trend of EBNA2 expressing cells being slightly more sensitive to the PLK1 inhibition.

A)

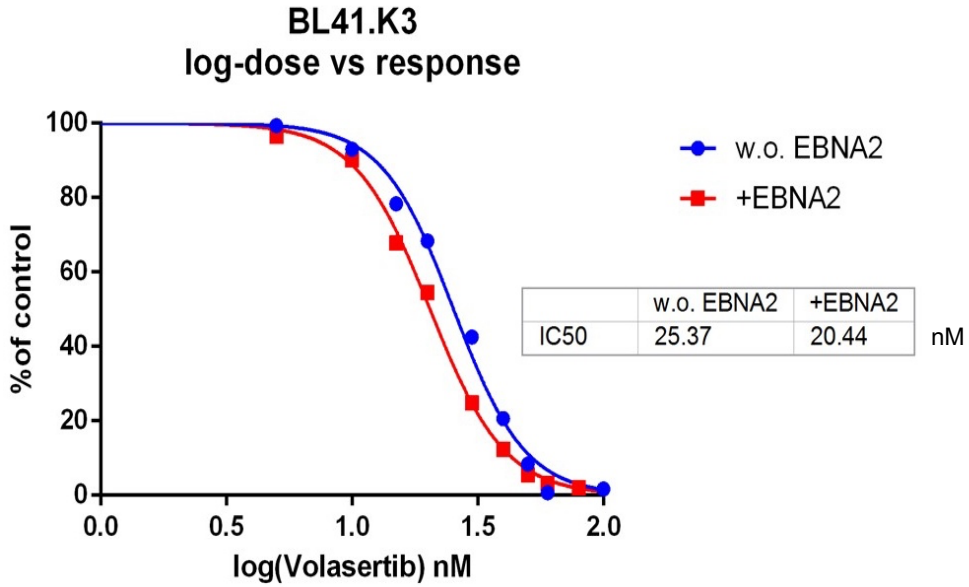

	w.o. EBNA2	+EBNA2	
IC50	25.37	20.44	nM

B)

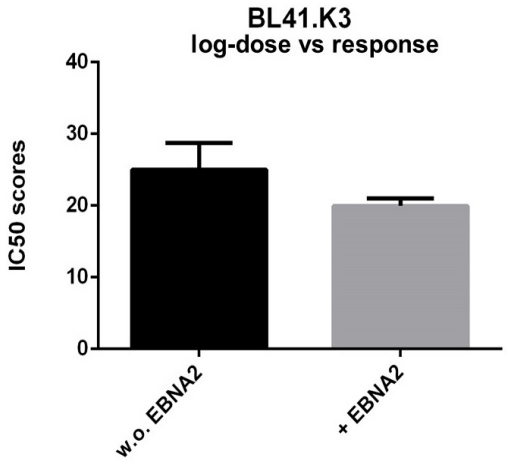

C)

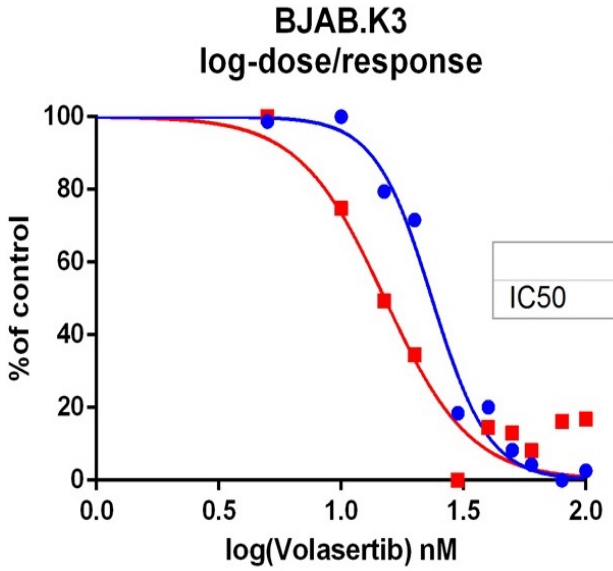

	w.o. EBNA2	+ EBNA2	
IC50	25.38	15.65	nM

D)

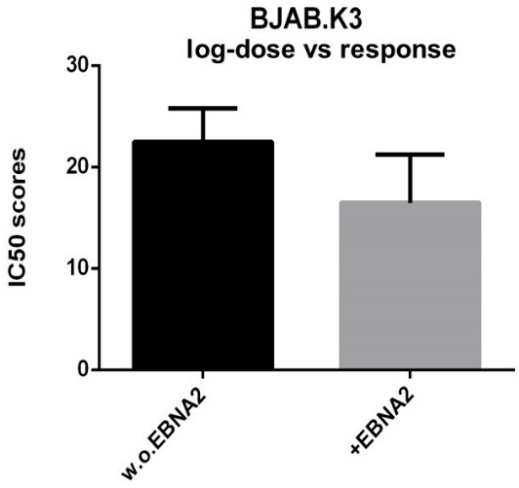

Fig. 9 EBNA2-expressing B-cells are more sensitive to Volasertib
Two EBV-negative cell lines: BL41.K3 and BJAB.K3, transfected with EBNA2, were cultivated 24h in medium with estrogen (0.1µg/ml) for the induction of EBNA2 (+EBNA2) or were left untreated (w.o. EBNA2). $4x10^4$ cells were then seeded as 100µl cultures in 96 well plates and cultured in the presence of increasing amounts of Volasertib for 48h or were left untreated. The viability of treated and untreated cells was analysed by MTT assays. The results of three biological replicates performed in technical triplicates were combined and analysed by GraphPad Prism 7. A) Combined dose-response curves. B) The IC_{50} scores were calculated using unpaired t-test in the GraphPad Prism 7 and visualised as bars. Error bars represent the corresponding standard deviation. p-value with $\alpha = 0.05$ as significance level. (All assays were performed in triplicate and the results were obtained in three independent experiments.)

4.1.3 MTT assay with EREB B-lymphocytes in the context of PLK1 inhibition

To further investigate if EBNA2 is the one component that makes the cells more susceptible to the Volasertib treatment we used an EREB B-Lymphocytes cell line with conditional expression of the protooncogene myc and EBNA2 (see section 2.2 Cell lines). Figure 9 displays our findings that there is a significant difference between EBNA2 positive and negative cells only if the expression of our protein of interest is switched on three days before the start of the Volasertib incubation. Moreover, the simultaneous expression of EBNA2 and myc, but even more with EBNA2 alone, resonances in lower IC_{50} scores with 15.70nM and 10.31nM accordingly. The lowest IC_{50} score of the cell subpopulation with suppressed myc gene (Fig. 10 C, w.o. myc) can be explained by the fact that further cell growth is prohibited by the switch-off of myc in the presence of

tetracycline and the cells arrest in the G0/G1-phase of the cell cycle (Kempkes et al., 1995). These findings suggest that EBNA2 positive cells respond stronger to PLK1 inhibition.

A)

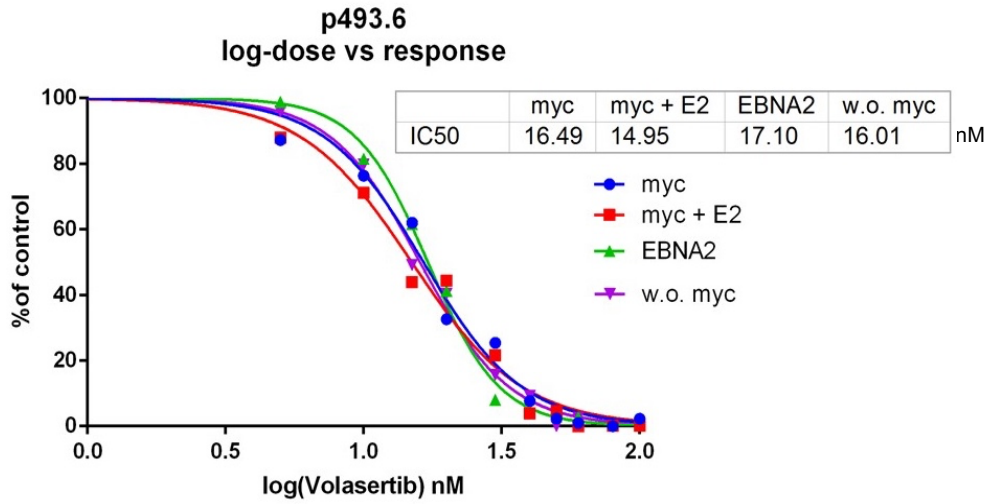

B)

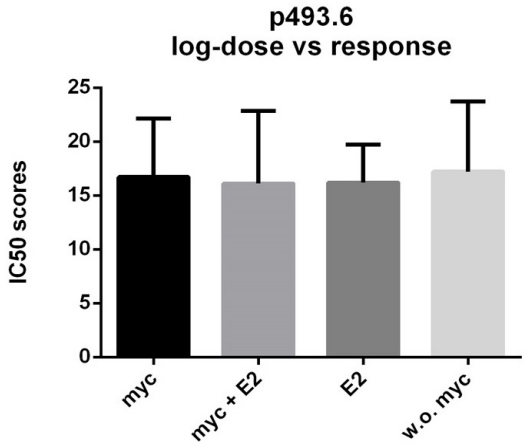

C)

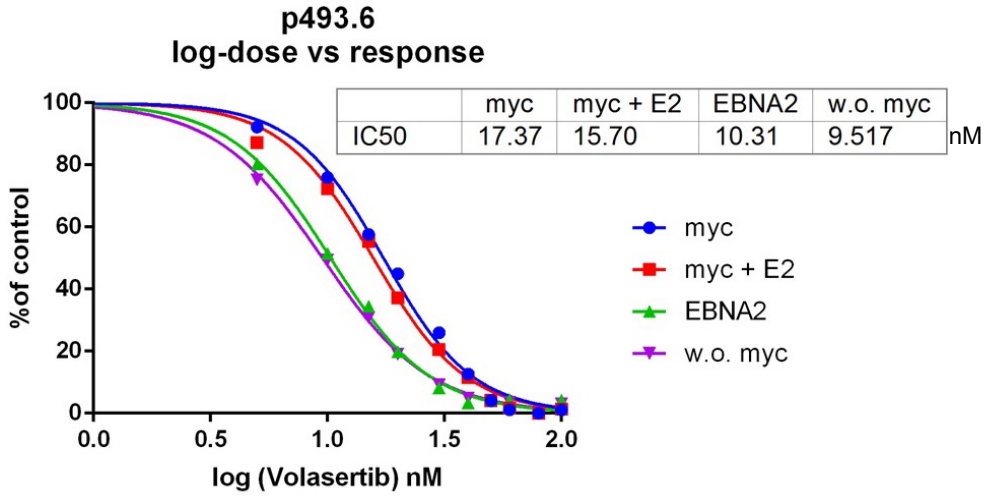

D)

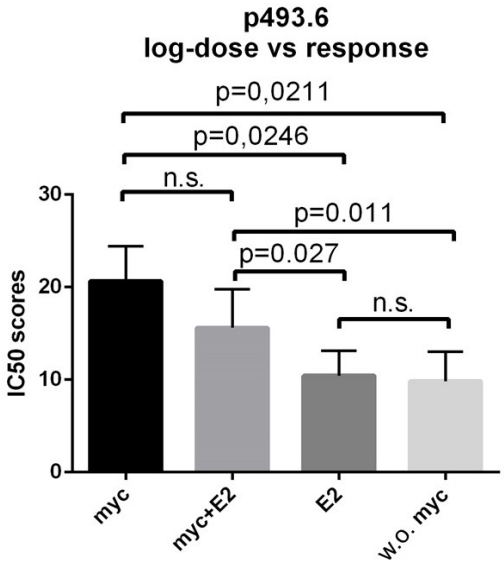

Fig. 10 EBNA2 expressing cells display different sensitivity to Volasertib only if EBNA2 is switched on three days prior to analysis
The p493.6 cells, an EREB B-cell line with tetracycline-regulated myc plasmid, were left untreated (myc), treated with 0.1µg/ml estrogen for the induction of EBNA2 (myc + E2), treated with estrogen and tetracycline for induction of EBNA 2 and repression of myc (EBNA2) or treated only with tetracycline for the repression of myc (w.o. myc). All cells were treated either simultaneously with Volasertib or tetracycline/ estrogen in panel A) or treated with tetracycline/estrogen. The Volasertib treatment was started after 72h in panel C). The cells were then seeded in 96-well plates with constant cell density at $4x10^5$ cells/ml and incubated with the inhibitor in serial dilutions ranging from 100nM to 0nM Volasertib. Incubation times varied between 0 and 48h as described. The inhibition of cell growth was detected by MTT assay as described in Materials and Methods. Representative data sets from three independent experiments were then analysed using GraphPad Prism 7. Dose-response curves were plotted to determine the mean IC_{50} value for each condition of the cell line. B) and D). The IC_{50} scores were then calculated using unpaired t-test in the GraphPad Prism 7 and visualised as bars. Error bars represent the corresponding standard deviation. p-value with $\alpha = 0.05$ as significance level. (All assays were performed in triplicate and the results were obtained in three independent experiments.)

4.2 FACS analysis of the cell cycle distribution of Volasertib-treated cells

4.2.1 FACS analysis of immortalised B-lymphocytes in the context of PLK1 inhibition

Next, we aimed to prove the efficacy of the PLK1 inhibition by Volasertib, expecting an increase in the G2/M population as well as an increase in apoptosis (Fig. 11 and 12). Cells were harvested 48h after the administration of Volasertib. The success of the PLK1 inhibition was determined using the DNA content

increase measured in FACS analysis as a typical phenomenon in the G2/M-phase of the cell cycle. The respective fluorescence intensity provided information about the DNA content of a cell, as well as the percentage of apoptosis and cell cycle phases. Apoptotic cells were characterised by DNA fragmentation, indicated by a sub-G1 peak. For each phase of the cell cycle, we identified a standard DNA content. The respective fluorescence intensities of each cell population resulted in the histogram plots as shown below.

Using different concentrations of the PLK1 inhibitor in the range of the calculated IC_{50} scores for the immortalised B-lymphocytes LG395 and LG396 (Fig. 11 A), we expected modification of the normal cell cycle distribution. DNA content doubled from G0/G1 to G2/M. The first peak in the histogram at 0.2K fluorescence intensity was representative of G0/G1, whereas, the second peak at 0.4K is representative of G2/M. As predicted, the increase of the mitotic and apoptotic cells in the populations occurred after treatment with concentrations >25nM Volasertib and their number increased further at 50nM. We measured up to a twofold increase of the mitotic cells (Fig. 11 B) from 12% up to 18% G2 increase for LG395 and from 85 up to 16% G2 increase for LG396). However, at the same time the sub-G1 population representing apoptotic cells expanded from 6% up to 13% for LG395 and from 5% up to 18% for LG396 at the highest Volasertib levels (Fig. 11 B).

We also observed a strong increase of the S-phase population for both cell lines. At this point of our studies we do not know whether these cells are still actively replicating DNA, or whether they have been arrested in the S-phase of the cell cycle.

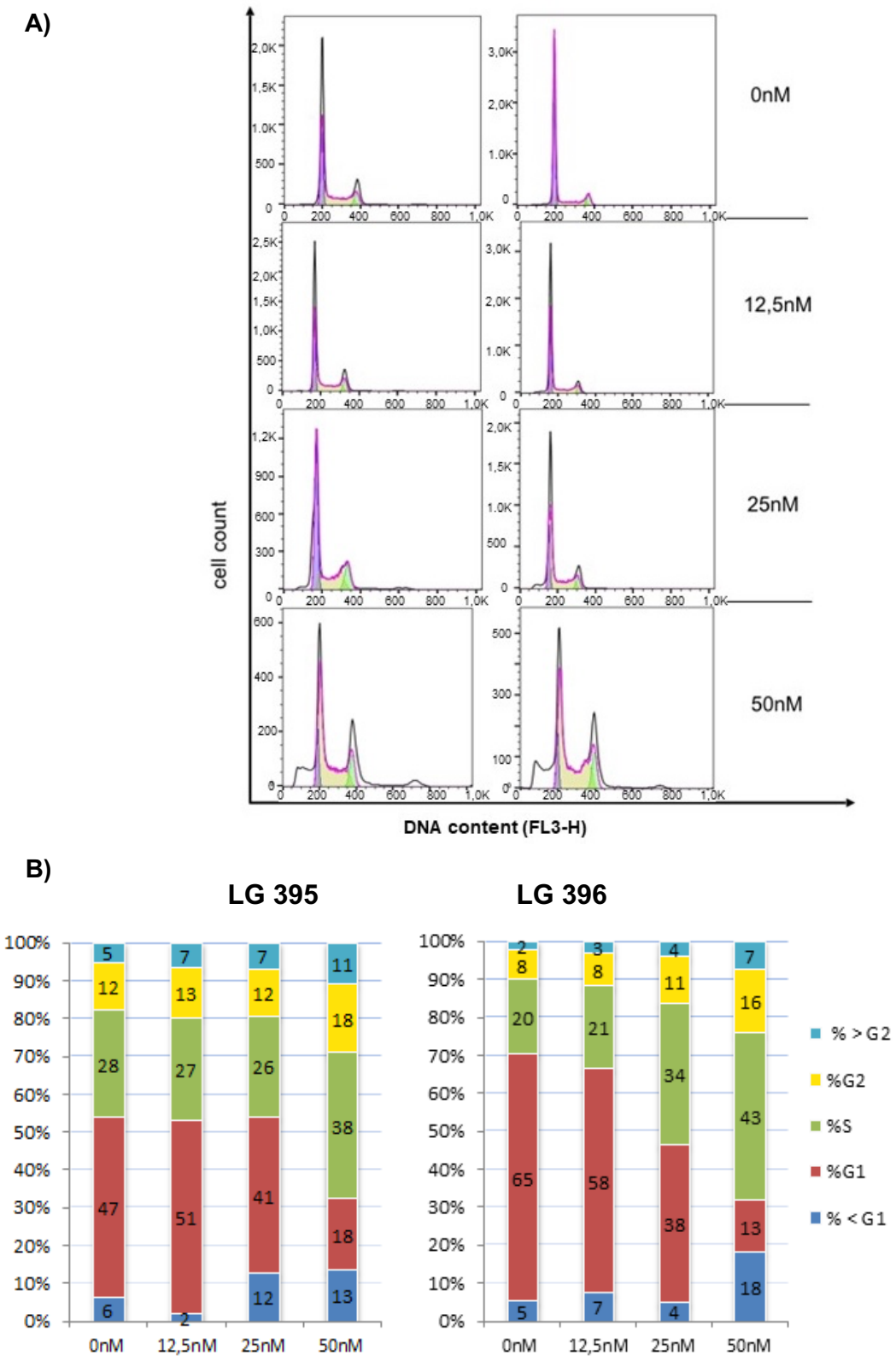

Fig. 11 Volasertib treatment causes a reduction of the G1 population and increase of the G2 population of immortalised B-lymphocytes

For cell cycle analysis from each cell line of immortalised B-lymphocytes: LG 395.3.1 and LG396.3.1. cells were treated with different Volasertib concentrations ranging from 0 to 50nM, harvested after 48h, the nuclei were fixed by ethanol treatment, washed in PBS and processed for DNA staining and analysed by Propidium Iodide-based cell cycle analysis kit (Genscript) using flow cytometry. Flow cytometry data was then analysed by using FlowJo V10 software and the cell cycle analysis was performed after excluding doublets.

A) Histograms showing the cell cycle distribution of cells treated with Volasertib. G1-phase cells are marked in purple, S-phase cells are marked in yellow and G2/M-phase cells are marked in green. B) Quantitative analysis of cell cycle phase distribution of the LG 395 and 396 cells treated with different Volasertib concentrations (as indicated). The total of G1-, S- and G2/M-phase cells was set to 100%. The colour bars represent the different subpopulations: dark blue for sub-G1-phase (apoptotic cells), red for G1-phase, green for S-phase, yellow for G2/M-phase (mitotic cells) and light blue for >G2-phase (polyploid cells).

4.2.2 FACS analysis of B-lymphocytes with conditional expression of EBNA2 in the context of PLK1 inhibition

Of great interest was the toxicity effect of PLK1 inhibition on EBNA2 positive cells in contrast to EBNA2 negative cells. Therefore, we treated the p493.6 cell line with conditional EBNA2- and suppressible myc – expression with Volasertib concentrations also ranging between 0 and 50nM (Figs. 12 A and B). We observed an alternation of the normal distribution of the cell cycle stages even after treatment with 12.5nM Volasertib, which became more prominent proportionally to the Volasertib concentration. As the percentage of apoptotic cells (displayed as a white peak in the <0.2K fluorescence intensity in Fig. 11 A)) reached the highest rates at 50nM concentration, the automatic evaluation of the cell cycle analysis via FlowJo had to be manually modified in order to visualise the cell cycle distribution in histograms. The exact quantification in bars showed 1.5x up to threefold increase of the G2/M cells in all populations. While Volasertib only led to mild apoptosis at the concentration of 12.5nM (~ 6 to 23% early apoptosis versus ~ 6% up to 11% in untreated control cells Fig. 12, the absence of myc seems to increase the proportion of apoptotic cells (~20 and ~30%, respectively), presumably contributing to the reversal of resistance. Of note, the response of the cells to Volasertib at high concentrations (25nM and 50nM), shows an appreciable difference in the presence of EBNA2. While the sub-G1 population in myc depleted cells (- myc) and cells expressing only (+ myc) reached a maximum of 36% at the highest concentration of the drug treatment, cells expressing only EBNA2 displayed with 41%, the highest distribution of apoptotic cells.

At this point, we also have to consider that the initial proliferation status of the EBNA2 expressing cells without Volasertib incubation have together with the cells expressing only myc the lowest rates of sub-G1 contribution, accordingly

8% for +E2 and 7% for +myc. All cells expressing EBNA2, either EBNA2 and myc or only EBNA2 exhibit the highest decrease of the G1-population if treated with 25nM and 50nM Volasertib. All in all, we see a slight increase in the toxic effect of Volasertib on the cells as soon as EBNA2 expression is switched on for at least two days prior to Volasertib administration.

A)

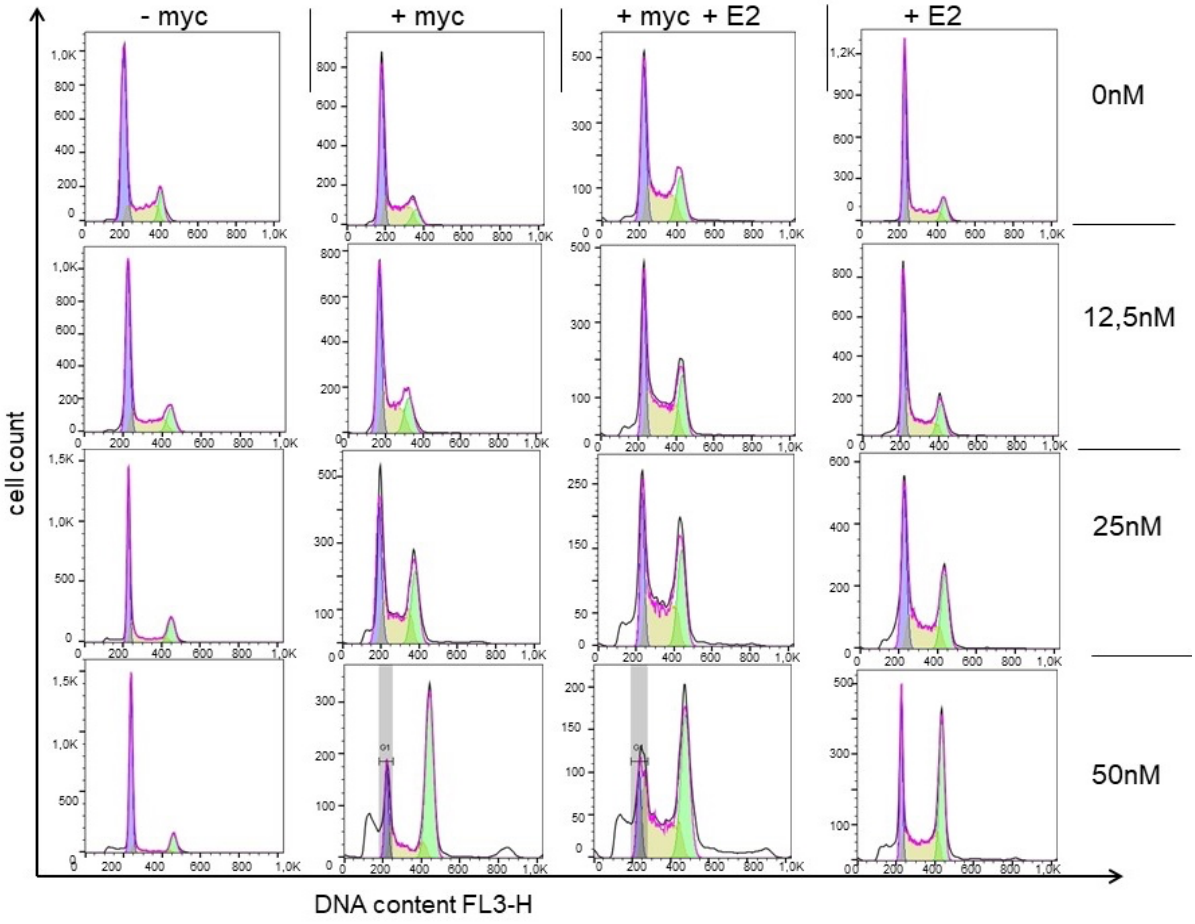

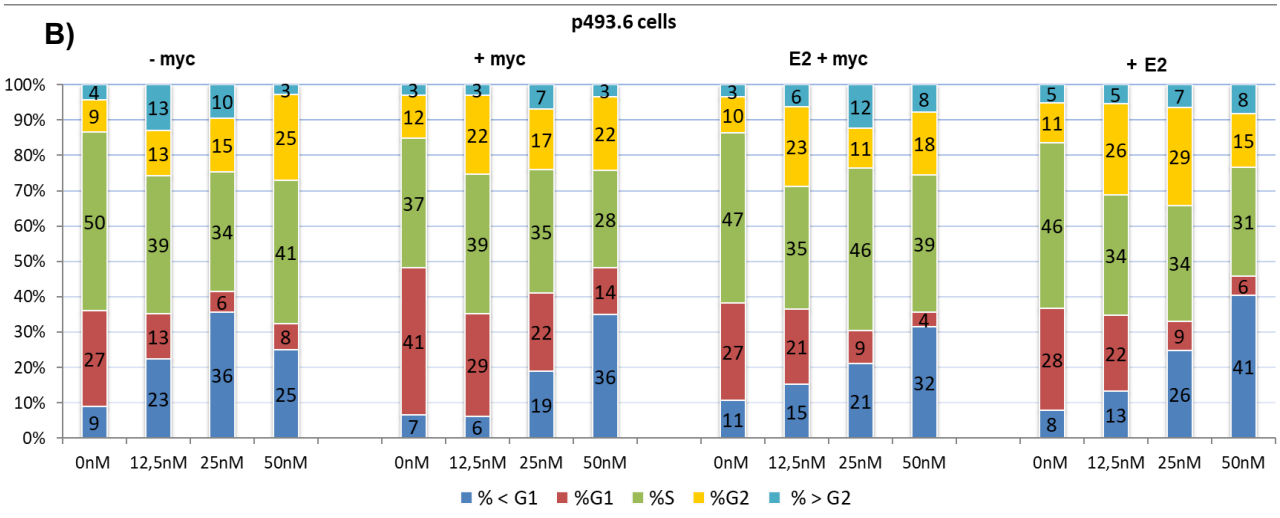

Fig. 12 Volasertib treatment is more toxic for EBNA2-positive p493-6 cells
For cell cycle analysis p493.6 cells were treated either with tetracycline 1µg/ml in order to suppress the expression of myc (- myc), with estrogen (1µg/ml), in order to induce EBNA2 expression (+myc +E2), with tetracycline and estrogen (+ E2), or left untreated in a condition, in which myc is primarily expressed (+myc) for three days prior to the start of the experiment. The cells were then treated with the inhibitor in serial dilutions ranging from 100nM to 0nM Volasertib for 48h, harvested, the nuclei were fixed by ethanol treatment, washed in PBS and processed for DNA staining and analysed by Propidium Iodide-based cell cycle analysis kit (Genscript) using flow cytometry. Flow cytometry data was then analysed by using FlowJo V10 software and the cell cycle analysis was performed after excluding doublets.
A) Histograms showing cell cycle distribution of cells. G1-phase cells are marked in purple, S-phase cells are marked in yellow and G2/M-phase cells are marked in green.
B) Quantitative analysis of cell cycle phase distribution of p493.6 cells treated with different Volasertib concentrations as indicated. The total of G1-, S- and G2/M-phase cells was set to 100%. The colour bars represent the different subpopulations: dark blue for sub-G1 phase (apoptotic cells), red for G1-phase, green for S-phase, yellow for G2/M-phase (mitotic cells) and light blue for >G2-phase (polyploid cells).

4.3 G2/M cell cycle arrest of DG75 B-lymphocytes

4.3.1 Double thymidine block and nocodazole treatment vs. sole nocodazole treatment for G2/M arrest

Cell synchronisation was used for the examination of cell cycle regulated events, including the progression of the cell cycle. When cells in G2-phase are exposed to DNA damage, several key mitotic regulators such as Cdk1/Cyclin B, Aurora A and PLK1 are down regulated in order to restrain mitotiv activity (Bahassi et al., 2011). PLK1 is known to be most active during the G2/M-phase of the cell cycle.

Its activation starts in G2, about 5 to 6h before mitotic entry, when PLK1 is phosphorylated on T210 in its T-loop by Aurora A, resulting in activation of the kinase domain (Macurek et al., 2008). To test the role of EBNA2 in the regulation of PLK1-arrest, we first performed experiments to achieve G2/M cell cycle arrest in EBNA2 expressing DG75 cells (see Fig. 13).

Thymidine is a DNA synthesis inhibitor that can arrest cells at G1/S boundary, prior to DNA replication, whereas treatment of nocodazole, which is an inhibitor of microtubule formation, can arrest cells at G2/M-phase (Ho et al., 2001). We aimed to establish a cell cycle synchronisation and G1/S arrest and release and in a second step, a G2/M block. First, we treated the cells with thymidine for 15h. Then, cells were released from a thymidine block for 9h. Within these 9h, we expected most of the cells to exhibit an increase of the PLK1 activity, as T210 phosphorylation is reported to be first detected approximately at this point. A second application of thymidine for 15h with a consequent drop of PLK1 activity was followed by a release from G1/S arrest and treatment with nocodazole to enrich the cells for the G2/M-phase (see Fig. 13, upper panel). Strategy I shows high levels of apoptosis and insufficient enrichment of the G2/M-phase of the cell cycle. Next, we compared this method to a single nocodazole application in an attempt to simplify the cell cycle arrest (Fig. 13, bottom panel).

A double thymidine block is reported to promote the synchronisation of the cells. However, our findings suggest that a double thymidine block prior to a nocodazole application does not improve the arrest of the cells in the G2/M-phase compared to nocodazole treatment only. On the contrary, the histograms from the cell cycle analysis show that cells treated with thymidine and nocodazole have a smaller population of mitotic cells than those treated only with nocodazole. (Fig. 14 A G2/M cells in green colour. For a precise quantification of the difference see Fig. 14 B). As indicated, strategy I led to as much as 36% (EBNA 2 negative) and 21% (EBNA 2 positive cells) G2/M population expansion and displayed a high percentage of G1 distribution. By contrast, sole nocodazole incubation for 15h led to an increase of the G2/M population up to 42% (EBNA2 negative cells) and 40% (EBNA2 positive cells).

Strategy I:

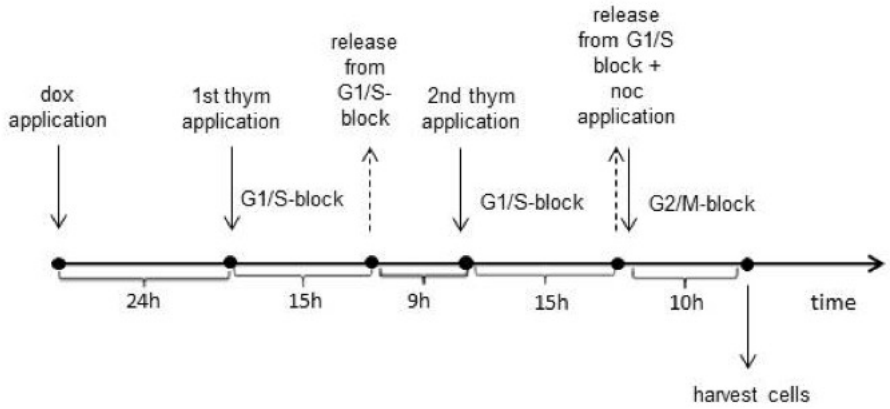

Strategy II:

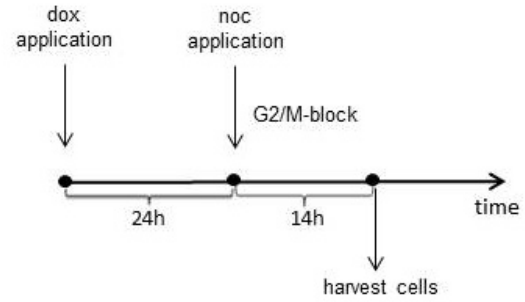

Fig. 13 Pilot study to establish assay conditions
Comparative analysis of two strategies to achieve G2/M cell cycle arrest in DG75 B cells (CKR128-34): CKR 128-34 cells have been generated from an EBV-negative Burkitt's lymphoma cell line (DG75) by transfection of a bidirectional doxycycline-inducible plasmid CKR74.2. In response to doxycycline, EBNA2 and GFP are expressed.
Strategy I) Double thymidine (thym) block followed by nocodazole (noc) treatment or II) nocodazole treatment only. For both strategies, CKR128-34 cells were either cultivated in medium containing doxycycline (1µg/ml) for 24h to express EBNA2 or left untreated. For strategy I asynchronously growing cells were treated with thymidine (2mM) for 15h, thymidine was removed by washing of the cells and the cells were cultivated for 9h in the absence of thymidine to release the block. Thymidine (2mM) was added again and cells were cultivated for an additional 15h to induce the second G1/S arrest. This second G1/S block was again released by washing of the cells. Nocodazole (100ng/ml) was added to induce a G2/M block. For strategy II asynchronously growing cells were treated with nocodazole (100ng/ml) for 14h. Arrows indicate the time points at which cells were harvested for cell cycle analysis. The success of the cell cycle arrest was assessed using PI-staining and FACS analysis.

In order to confirm these results, we repeated the experiment using Strategy II in order to achieve the possibly most efficient G2/ M cell cycle arrest and further analyse the PLK1- activity under these circumstances in the presence and absence of EBNA2.

As Figure 15 shows, single nocodazole application for 14h resulted in an almost threefold increase of the G2/M population from 25% to 75% for EBNA2

negative cells and from 22% to 74% for EBNA2 positive cells (green bars in Fig. 14 D) and no significant apoptosis in the cell population, represented by sub-G1 population, which is not visible in the histograms (Figs. 14 C and D). However, we observed a loss of cells also in the other cell populations, which were not treated with thymidine. One may claim that polyploid cells, typically occurring after the nocodazole treatment, might not have been sorted out as single cells and automatically left out by the automatic cell sorting, which excludes doublets.

Overall, we could demonstrate that cell cycle synchronisation using a double thymidine block does not improve the success of nocodazole induced G2/M cell cycle arrest. To test the effect of the cell cycle block on the kinetics of PLK1 during G2 and the cell cycle checkpoint, we performed a nocodazole incubation for 15h. Afterward PLK1 and EBNA2 expression were analysed by western blotting (Fig. 15).

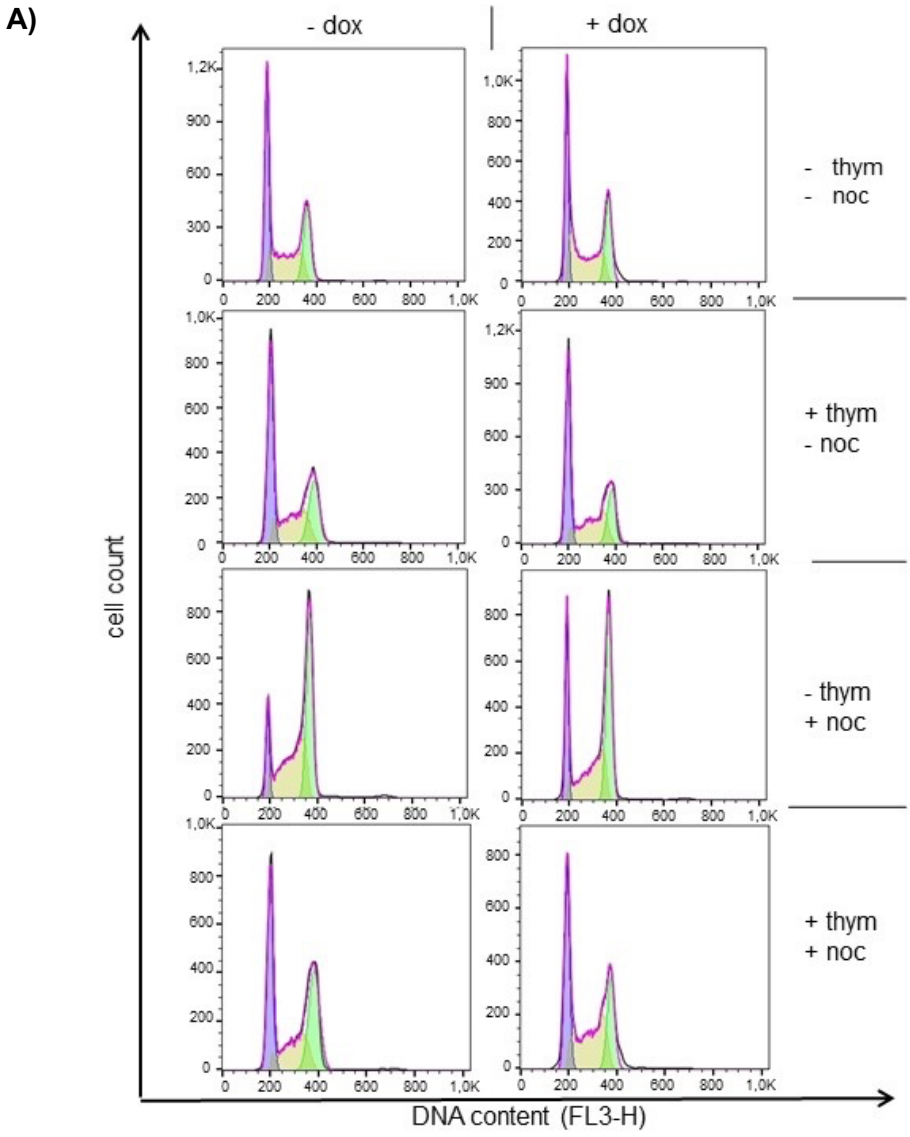

B)

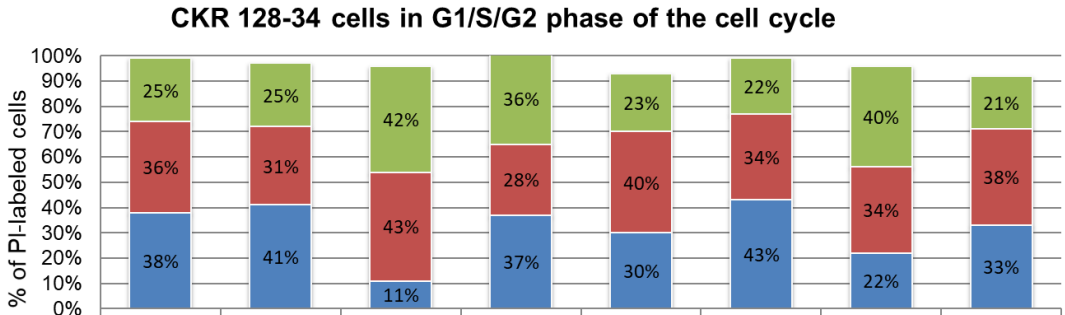

dox	-	-	-	-	+	+	+	+
thym	-	+	-	+	-	+	-	+
noc	-	-	+	+	-	-	+	+
cells in G2/M	25%	25%	42%	36%	23%	22%	40%	21%
cells in S	36%	31%	43%	28%	40%	34%	34%	38%
cells in G1	38%	41%	11%	37%	30%	43%	22%	33%

C)

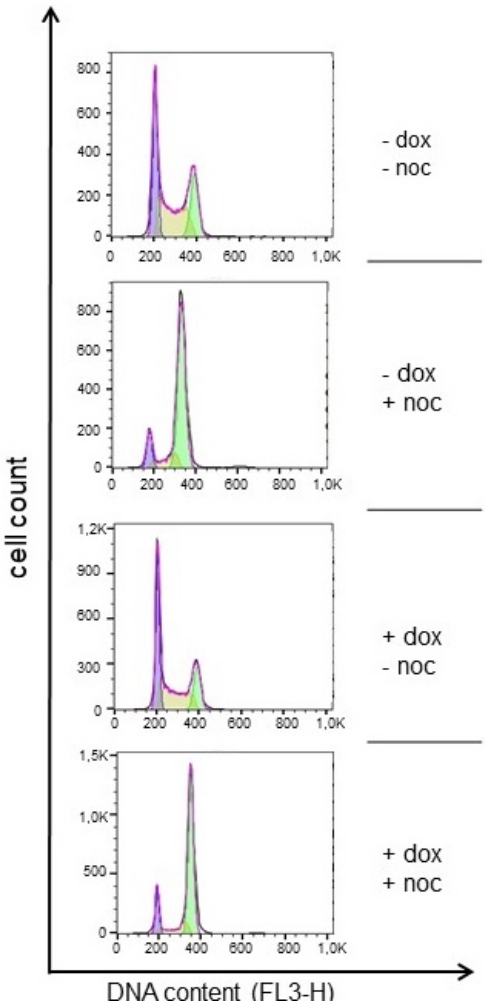

D)

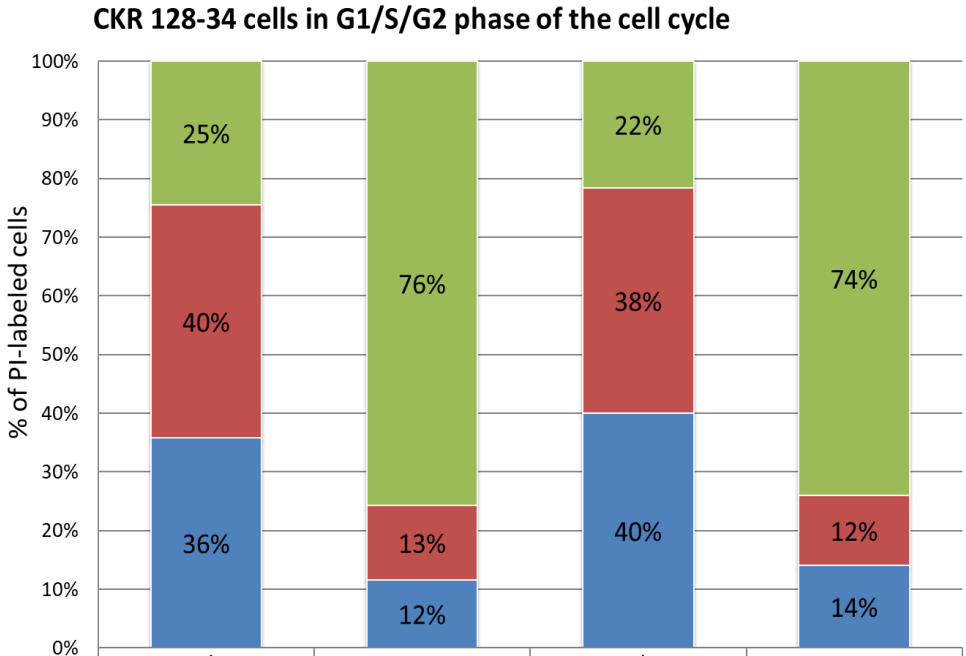

noc	Ø	0,1	Ø	0,1
dox	Ø	Ø	1	1
cells in G2/M-phase	25%	76%	22%	74%
cells in S-phase	40%	13%	38%	12%
cells in G1-phase	36%	12%	40%	14%

Fig. 14 Nocodazole treatment increases the population of cells in the G2/M-phase of the cell cycle

For cell cycle analysis CKR 128-34 cells were cultivated under specific conditions as explained in Fig. 12. $2x10^6$ cells were harvested, the nuclei were fixed by ethanol treatment, washed in PBS and processed for DNA staining and analysed by flow cytometry. A) and C): histograms showing cell cycle distribution of cells: A) presents strategy I and C) strategy II. G1-phase cells are marked in purple, S-phase cells are marked in yellow and G2/M-phase cells are marked in green. Cells with < 2n or > 4n DNA content were excluded from the analyses. B) and D): Quantitative analysis of cell cycle phase distribution. Figure B) represents the results from strategy I and D) from strategy II. Concentration as indicated dox 1 = doxycycline (1µg/ml) and noc 0,1 = nocodazole (0.1µg/ml) or Ø for none.

As the western blot in Fig. 15 A) shows, EBNA2 expression is stable if cells are treated with doxycycline independently from the cell cycle stage and the nocodazole arrest via Strategy II. GAPDH as a housekeeping gene, expressed in a steady state was used as a marker for the normalisation of the target gene expression (Fig. 15 B)).
Surprisingly, the PLK1 expression seemed to be also unaffected by the cell cycle progression (Fig. 15 C). However, in the following experiments performed by M. Raab and Prof. K. Strebhardt, with the same cell extracts, a clear difference between the PLK1-protein levels at different cell cycle stages can be observed.

The phosphorylation of Histone 3 as a hallmark of mitosis, correlates with the successful G2/M arrest as its bands were detected only in the nocodazole-treated cell populations (Fig. 15 D). Phosphorylation of Histone 3 occurs first in the late G2-phase and is completed at the prophase. At the end of mitosis Histone 3 is dephosphorylated (Hendzel et al., 1997), which also explains the absence of protein bands in the first and third lines in Fig. 15. D), where cells were not exposed to nocodazole treatment and, therefore, exhibit low rates of mitosis.

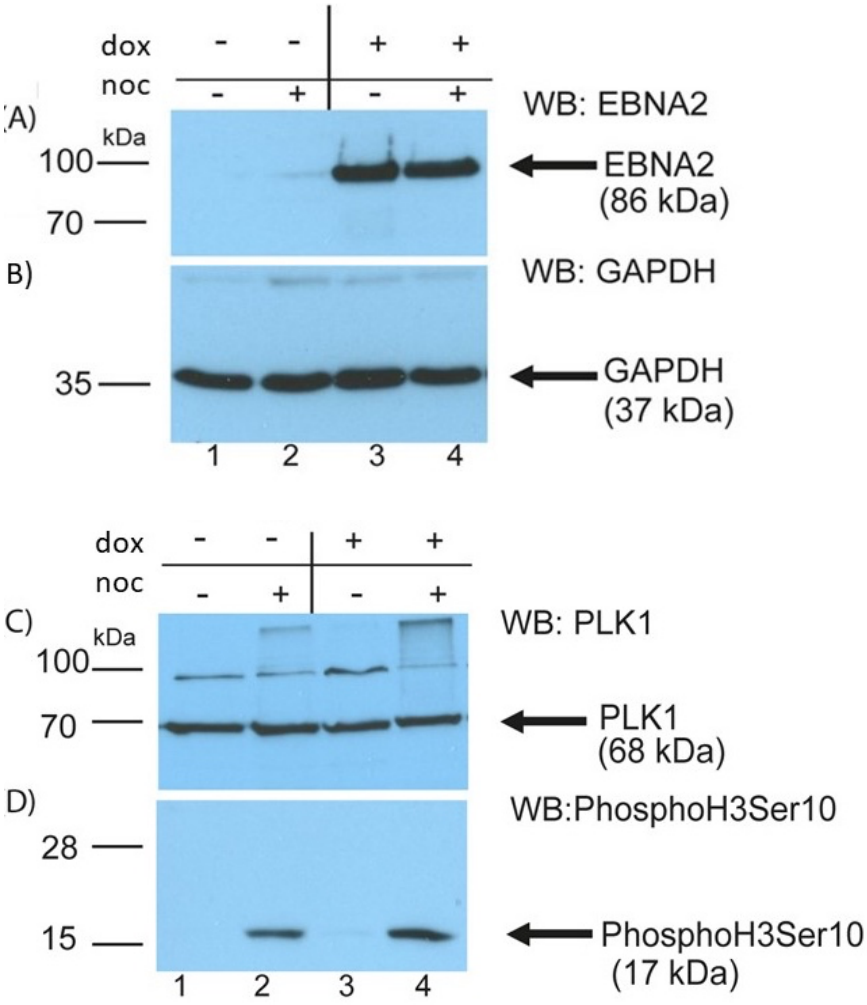

Fig. 15 Nocodazole treatment enriches DG75 cells in the G2/M-phase of the cell cycle

A) CKR128-34 cells were either induced with doxycycline 1µg/ml (+ dox) in order to activate EBNA2 expression or left untreated (- dox). The asynchronously growing cells were treated with 100ng/ml nocodazole (+/-noc) and incubated for 14h to induce G2-M-phase cell cycle arrest. Total cell lysates were submitted to SDS-PAGE (10% for EBNA2 and 12% polyacrylamide for PLK1 detection) 20µg of protein from each sample was loaded per lane and transmitted to

immunoblotting. (A): anti-EBNA2(R3) antibody and HRP-anti-rat secondary antibody, (B) anti- GAPDH mab 374 and (C): anti-PLK1 (ab17056) antibody and HRP-anti-mouse secondary antibodies, (D) Phospho- H3Ser10 (D2C8) antibody and goat-anti-rabbit HRP secondary antibody, respectively. Signals were visualised using chemiluminescent detection reagents (Amersham ECL).

4.3.2 PLK1 kinase assay

The previous experiments were only done as preparation for the PLK1 kinase assays. We asked ourselves whether EBNA2 has an impact on the PLK1 activity as a kinase protein, mainly active during the mitosis. To investigate this, we used the cell extracts from the B-lymphocytes CKR 128-34 with conditional EBNA2 expression, treated with nocodazole, following strategy II (Fig. 13, bottom panel) and because we did not have the capacity and technical equipment to perform a kinase assay in our laboratory, we used lysis buffer to prepare the cell extracts (as described in 3. Methods, section 3.2.1 Kinase assay) and sent these to M. Raab and K. Strebhardt, who kindly offered their cooperation.

First, they performed a western blot with the cell extracts (Fig. 16 A)) and were able to confirm our previous findings that the cells were arrested at early M-phase of the cell cycle. Hence, they used as proof the positive staining for histone H3phosphoserine10 and the increase of the signal from Cyclin B1 as a mitotic marker in the cell extracts treated with nocodazole (third and fourth row, Fig. 16 A)). Additionally, active PLK1, phosphorylated at threonine 210 (T210) was identified also in the nocodazole treated cell extracts (see second lane, Fig. 16). PLK1 can be activated by a phosphorylation of the conserved threonine residue (T210), which is located at the T-loop of the kinase domain. Phosphorylation of this residue starts in G2-phase of the cell cycle and similarly to the kinase activity continuously raises reaching its peak in the beginning of the mitosis. These findings correspond also with the increased total protein levels during the G2/M-phase of the cell cycle (as shown in the first row, Fig. 16). EBNA2 expression is dependent only on doxycycline induction and seems to be constant throughout the cell cycle arrest with nocodazole.

Next, a co-IP confirmed our findings that EBNA2 is a binding partner of PLK1 and the higher the PLK1 levels, accordingly in the G2/M-phase, represented by the nocodazole-arrested cells in Fig. 16 B). The signal from EBNA2 is stronger, because a greater amount of the protein could be pulled down using the PLK1 primary antibody. The kinase assay (Fig. 16 C) showed equal

PLK1 activity for the nocodazole-treated cells in EBNA2 presence and absence. The signal from the cytoplasmic retention sequence (CRS) of Cyclin B serves as a substrate for the PLK1 enzyme activity. Phosphorylation of the GST-marked Cyclin B resulted in the incorporation of the radiolabelled phosphate from the gamma-32P-ATP. The quantification of radioactivity incorporated into the substrate as a function of time and enzyme concentration provides an evaluation of the enzyme activity. PLK1 is equally active in doxycycline-treated cells, which express EBNA2 and doxycycline-untreated cells. The difference from the signal strength for CRS resulted only from the nocodazole cell cycle arrest. The higher the percentage of mitotic cells, the higher the PLK1 activity, the more prominent the Cyclin B phosphorylation. Interestingly, other phosphorylating substrates of PLK1 with the molecular weight of approximately 80 to 100kDa became visible, especially in the doxycycline induced cell population. Phosphorylated EBNA2 with a molecular weight in this exact range is one possible candidate that might be phosphorylated when PLK1 is most active, but this hypothesis needs further investigation.

4.4 EBNA2 as a potential substrate of PLK1

In the context of PLK1 functional significance as a kinase enzyme, we aimed to define possible phosphorylation sites for PLK1 within EBNA2. An in vitro kinase assay (Fig. 17 A) and B)) suggested that GST-EBNA2 mutants with a deletion of the amino-acid-sequence distal to residue 422 cannot be phosphorylated. Therefore, GST-marked EBNA2 was compared to GST-marked mutants containing either only 214 amino acids (aa 246-422) or the last 362 amino acids of the protein (aa 246-487). The first and second lane from the kinase assay in Fig. 17 A serve as controls, GST alone is the negative control, which shows no signal, and GST-CRS is a positive control as CRS is an acclaimed PLK1 phosphorylation target. Interestingly, the EBNA2 protein with deletion of the last 64 amino acids could not be phosphorylated by the kinase, whereas, the EBNA2 mutant containing the last 65 amino acids (aa 246-487) in the last lane (Fig 17. A)) exhibits a stable signal for ATP incorporation.

Since PLK1 phosphorylates serine and threonine residues as potential phosphorylation substrates (Elia et al., 2003), these are also found within EBNA2, precisely at residues 455-459 and 463-467 at the C-Terminus of the protein (Fig. 17. B). The PBD of PLK1, however, could bind to residues 266-268 of EBNA2,

precisely serine threonine proline (STP) as shown in Fig. 17 B) (Elia et al., 2003). Taking these findings into consideration, it is possible that the interaction site for PLK1 within EBNA, containing both a phosphorylation domain and a binding sequence, is located within the 250 amino acids on the carboxyl-terminus of EBNA2 and correspondingly includes the conserved regions CR5 to CR9.

We are grateful to M. Raab and Prof. K. Strebhardt for performing both kinase assays.

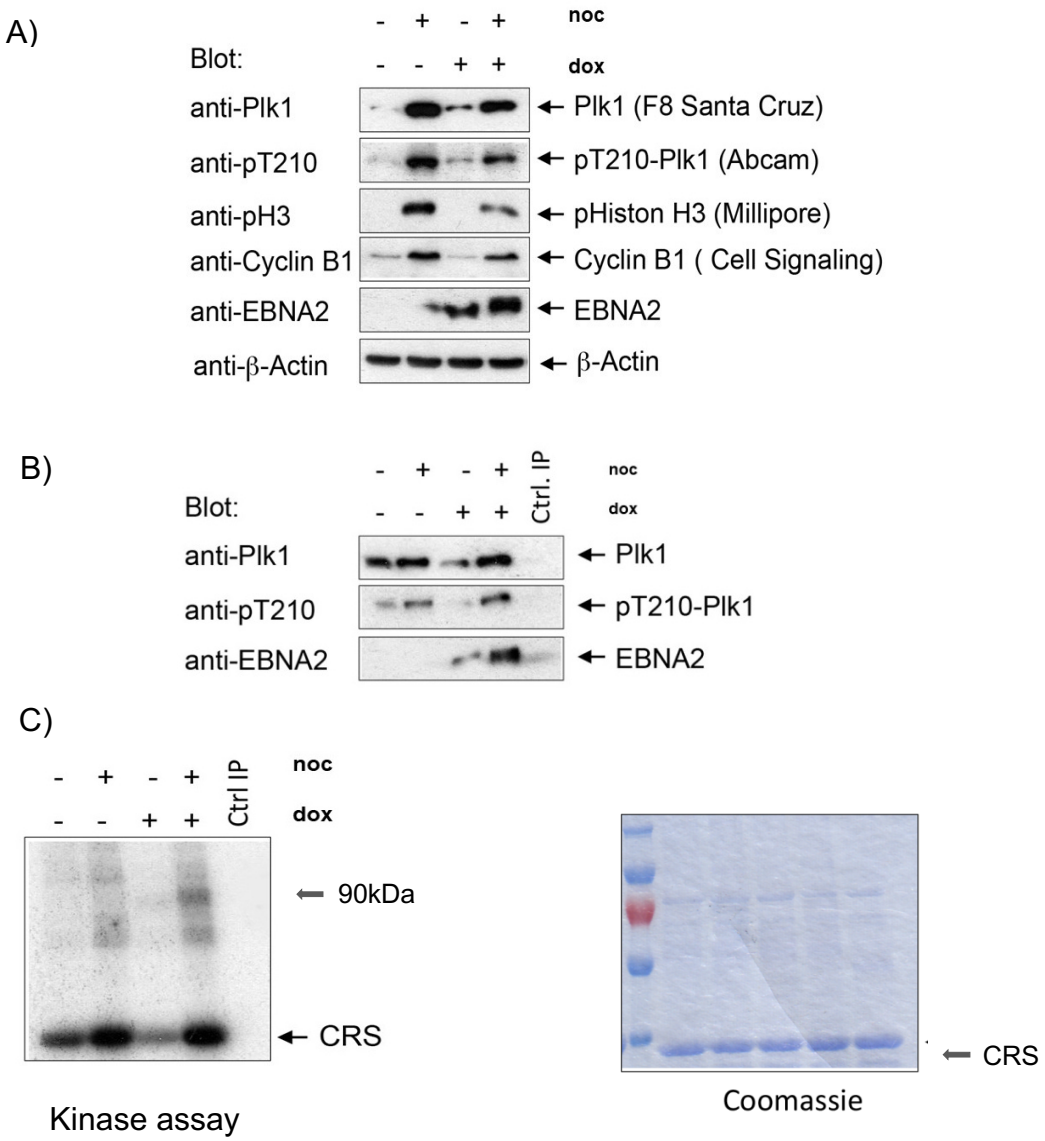

Fig. 16 PLK1 kinase assay in DG75 cells: no major impact of EBNA2 on PLK1 activity in G2/M arrested cells

CKR128-34 cells were cultured in standard RPMI medium. For the purpose of the experiment, cells were either induced with doxycycline 1µg/ml (+ dox) in order to activate EBNA2 expression or left untreated (- dox). The asynchronously growing cells were treated with 100ng/ml nocodazole (+/-noc) and incubated for 14h to induce G2-M-phase cell cycle arrest. pT210-PLK1 was used as marker for the PLK1 phosphorylation/activation. p-Histone3/ pH3Ser10 served as G2/M marker. Cyclin B also a G2/M marker was used as a control. A) western blot with total cell lysates from the nocodazole treated cells B) western blot with the

samples from the co-immunoprecipitation using anti-PLK1 antibody C) PLK1 – IP- Kinase assay with γ-P32 ATP; Cytoplasmic retention sequence (CRS) is a region of Cyclin B1 and contains four conserved serine phosphorylation sites, glutathione S-transferase (GST)-marked Cyclin B is phosphorylated by PLK1. Phosphorylation is detected by gamma P32 ATP Adenosine triphosphate, well-established substrate routinely used by M. Raab. Coomassie blue was used to stain proteins in polyacrylamide gel. It serves as a control of the amount of protein that was loaded on the gel.

The experiments were performed by M. Raab and Prof. K. Strebhardt (University of Frankfurt Medical School).

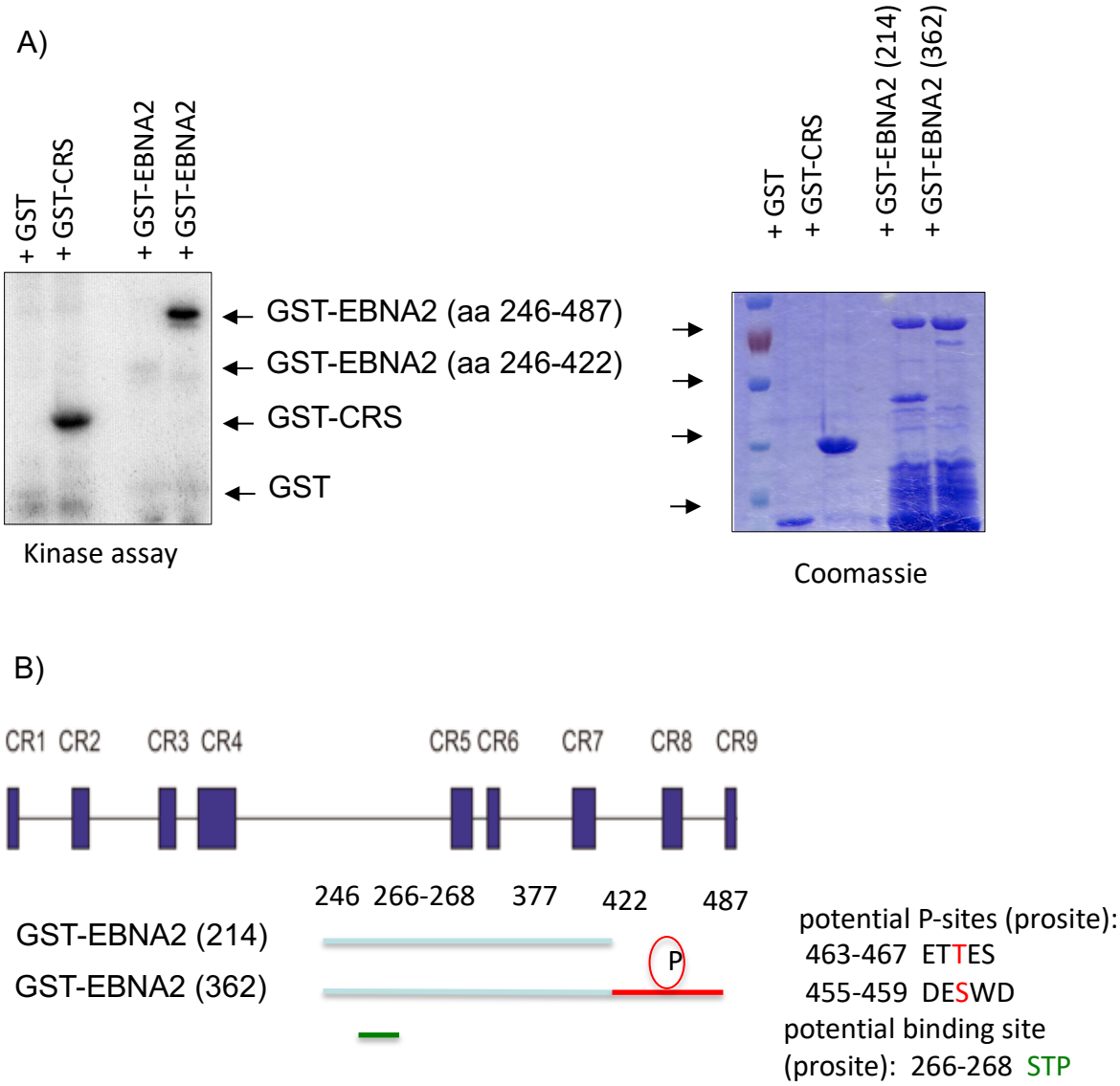

Fig. 17 EBNA2 as a potential substrate of PLK1

A) in vitro GST- kinase assay: DG75 cells transfected with HA-tag were incubated with purified GST (lane 1) or with the GST-EBNA fusion proteins: lane 2 GST-CRS, lane 3 GST-EBNA2 amino acids (aa) 246-422 and lane 4 GST EBNA2 aa 246–487. Bound protein was detected by immunoblotting using anti-HA-tag antibody. Coomassie blue was used to stain proteins in polyacrylamide gel. It serves as a control of the amount of protein that was loaded on gel. B) schematic representation of EBNA2 containing conserved regions CR1-7 and the GST-EBNA2 proteins, showing suggested phosphorylation sites within EBNA2: serine and threonine amino acids are localised in this region. The predicted phosphorylation sites (P-sites) within EBNA2 are serine (S) and threonine (T)

amino acids shown in red are localised at residues 455–459 and 463–467. The potential binding site for PLK1, which contains the typical consensus motif contains residues 266–268 of EBNA2, precisely serine threonine proline (STP) shown in green. The experiments were performed by M. Raab and Prof. K. Strebhardt (University of Frankfurt Medical School).

4.5 Transactivation activity and expression stability of the EBNA2 mutants

These final findings prompted further investigation of the EBNA2 sequence and the significance of sequence alternations to the protein expression and transactivation activity. Figure 18 is a schematic representation of the EBNA2 mutants used. These were not created specifically for the purposes of the experiment but rather coincidentally discovered in the laboratory stock (see section Materials 2.1 Plasmids). As the figure shows, the wild type EBNA2 full-length protein was modified by point mutations: in EBNA2 S457L serine at the residue 457 is exchanged for leucine and for the establishment of EBNA2 S469L the serine at position 469 is exchanged for leucine. Both point mutations are close to the C-terminus of EBNA2 and the CR8 and CR9, which are associated with the functional activation domain of the protein. In order to test the transactivation activity of these proteins, we compared it in a luciferase assay, as shown in Fig. 18 B). DG75 cells were co-transfected with the promoter Ga981-6 and reporter plasmid p3695-Renilla and EBNA2 expression plasmids (as described in Materials 3.3.8 Luciferase assay). 24h after transfection cells were harvested and luciferase activity was measured in RLU (relative light units), normalised to the Renilla activity and visualised as bars in Fig. 18 B), the comparison of the pSG5 marked full-length EBNA2 (pSG5-E2) to the mutants S457L and S469L, the point mutants display an up to fourfold increase of the transactivation activity. Interestingly, the mutations do not disturb the expression of the protein, on the contrary, the EBNA2 expression is analogically stable for both mutants as the western blot in Fig. 18 C) shows.

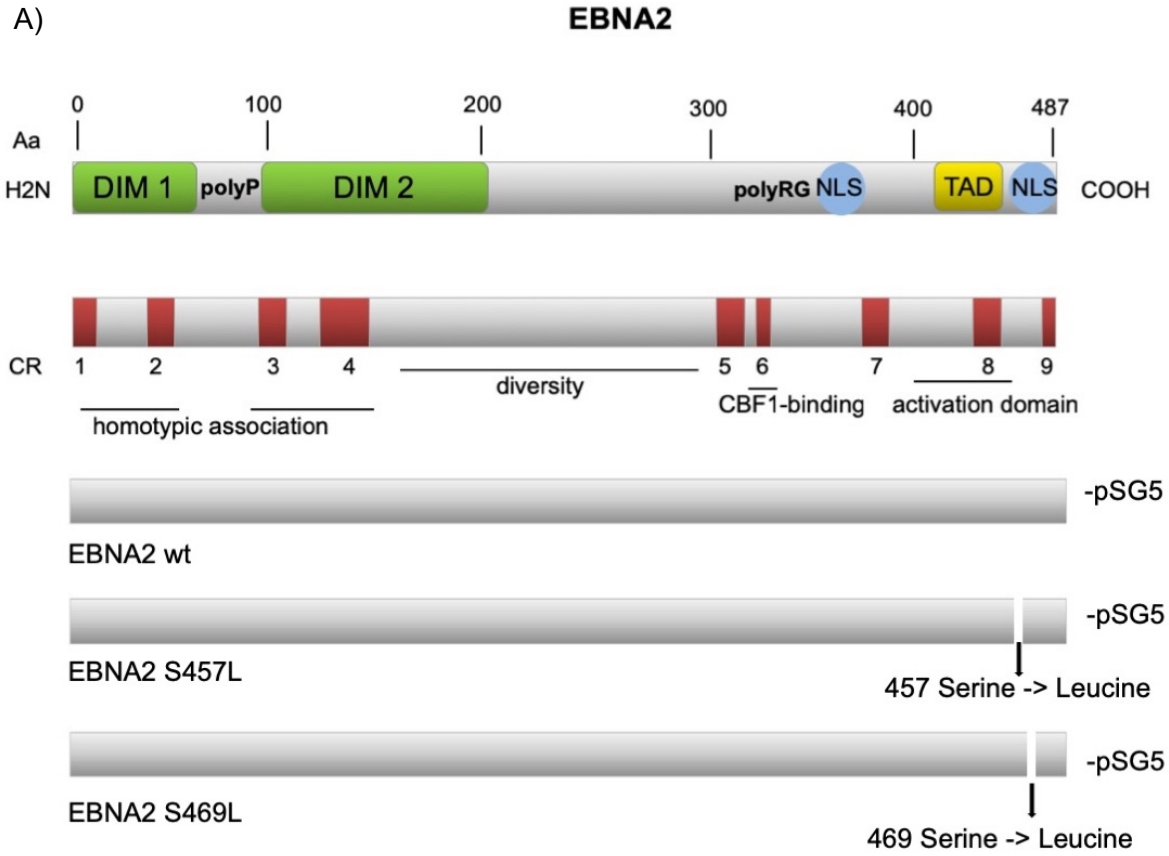
A)
EBNA2
Aa
0
100
200
300
400
487
H2N
DIM 1
polyP
DIM 2
polyRG
NLS
TAD
NLS
COOH
CR
1
2
3
4
diversity
5
6
7
8
9
homotypic association
CBF1-binding
activation domain
-pSG5
EBNA2 wt
-pSG5
EBNA2 S457L
457 Serine -> Leucine
-pSG5
EBNA2 S469L
469 Serine -> Leucine

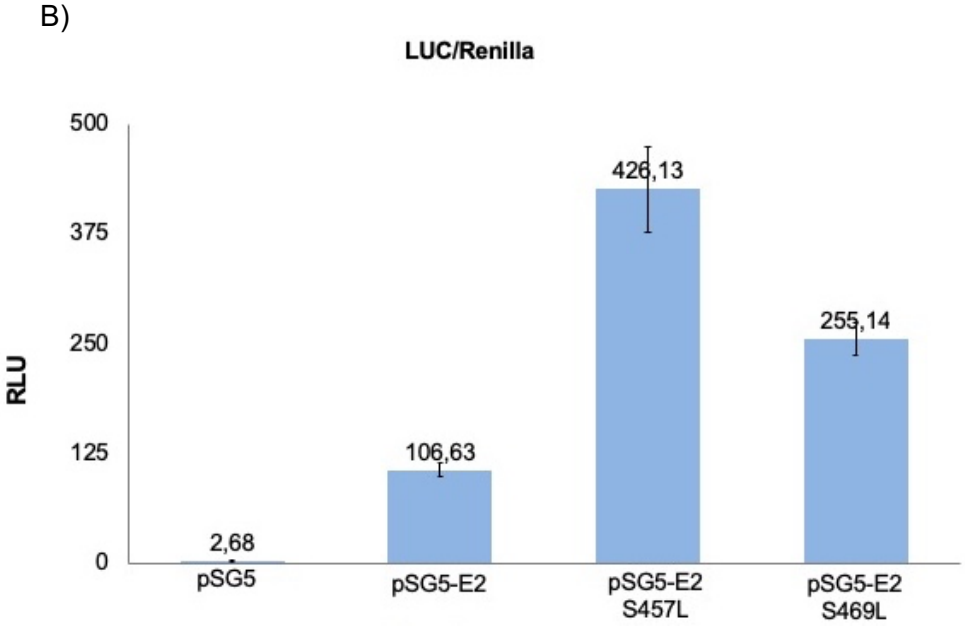
B)
LUC/Renilla
RLU
500
375
250
125
0
2,68
106,63
426,13
255,14
pSG5
pSG5-E2
pSG5-E2
S457L
pSG5-E2
S469L

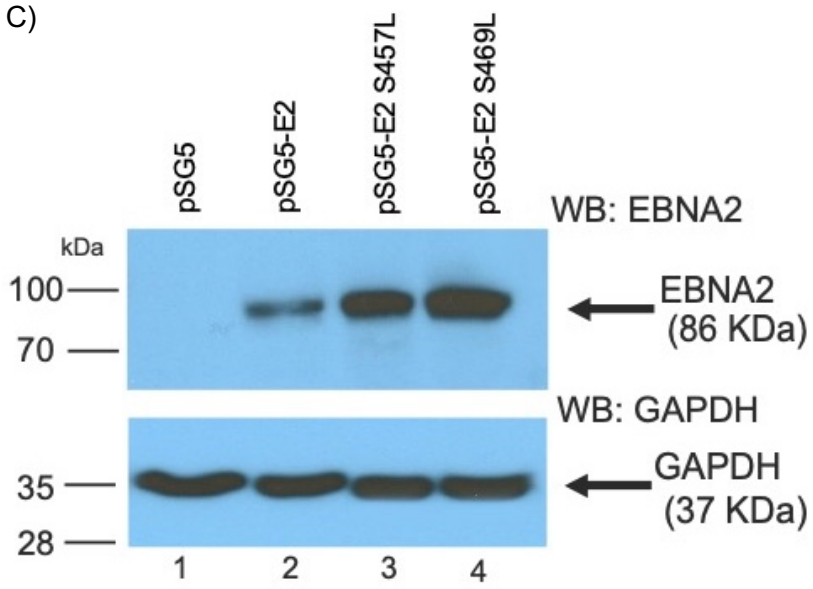

Fig. 18 EBNA2 protein fragments with inactivated potential phosphorylation sites, show an increase of transactivation activity and stable EBNA2 expression in the immunoblotting

(The data shown above are representative of four independent experiments and four western blots)

A) schematic representation of the EBNA2 mutants

- pSG5-EBNA2 wt is a full-length EBNA2 expression plasmid;
- pSG5-EBNA2 S457L is an EBNA2 expression plasmid with a point mutation at position 457, serine is exchanged for leucine;
- pSG5-EBNA2 S469L is an EBNA2 expression plasmid with a point mutation at position 469, serine is exchanged for leucine.

B) Increase of the transactivation activity of the EBNA2 mutants in the luciferase assay: DG75 cells were co-transfected with 5µg of promoter Ga981-6 and reporter plasmid p3695-Renilla and EBNA2 expression plasmids, pSG5 as an empty vector or EBNA2 mutants: pSG5-E2, pSG5-E2 S457L or pSG5-E2 S469L. Renilla luciferase reporter vector (p3695-Renilla) was used as an internal control for transfection efficiency. 24h after transfection cells were harvested and luciferase activity was measured using the dual luciferase assay system (Promega) and Orion Microplate Luminometer. The activity of the Ga981-6 promoter as luciferase activity was normalised to Renilla activity in relative light units (RLU). The error bars are graphical representations of the standard deviation calculated from the mean values of the four experiments.

C) western blot with the DG 75 cells transfected with EBNA mutants 24h after transfection cells were harvested and visualised in western blot using a primary ab: anti-EBNA2-rat and anti-rat HRP as the secondary antibody. The EBNA2 protein expression was normalised to GAPDH expression. GAPDH was detected using GAPDH MAB 374 as primary and anti-mouse HRP IgG as secondary antibody. Protein complexes coupled to agarose beads were washed and subjected to immunoblotting. Finally, signals were developed with a chemiluminescent film reagent after 20s exposure.

4.6 EBNA2 phosphorylation

As discussed, EBNA2 needs to be phosphorylated as any other protein in order to interact with PLK1. The question this statement raises is whether PLK1 itself phosphorylates EBNA2 or other kinases are needed for the phosphorylation prior to the protein interaction. Considering this, we aimed to perform an analysis of the EBNA2 phosphorylation and dephosphorylation, while PLK1 activity was normal or artificially increased by nocodazole treatment. Thus, we used DG75 cells with conditional expression of EBNA2 and treated them with nocodazole to achieve a G2/M arrest. Before western blot analysis, we additionally incubated the cells with Calyculin A prior to lysis in order to suppress the intrinsic phosphatases activity and enable a better examination of the phosphorylation state of all proteins. As Fig. 19 shows, we detected EBNA2 only after doxycycline induction of its expression and the signal from lanes 5-8 was comparably strong. If cells were treated with nocodazole and enriched for the G2/M-phase of the cell cycle when PLK1 was most active, EBNA2 in lanes 7 and 8 displayed a weak second band with a slightly higher molecular weight than the normal EBNA2, known to be 86kDa. This finding suggests that EBNA2 is phosphorylated and the peak of PLK1 kinase activity might be related in time of occurrence. By adding Calyculin A, we were able to show that EBNA2 is phosphorylated in lanes 6 and 8 and even though a quantification of the phosphorylation is not possible in the western blot analysis, it seems that the PLK1 activity does not necessarily affect the EBNA2 phosphorylation status, suggesting that kinases other than PLK1 also play a role in the EBNA2 phosphorylation. The PLK1 expression is once again stable and seems to be only insignificantly affected by the nocodazole treatment, which, as already discussed in section 4.3.1, is probably due to a sensitivity problem of the antibodies we used for the pull down. The PLK1 signal should rather be stronger in mitotic cells as the expression of the protein increases. GAPDH constant expression is the positive proof for normalisation of the results.

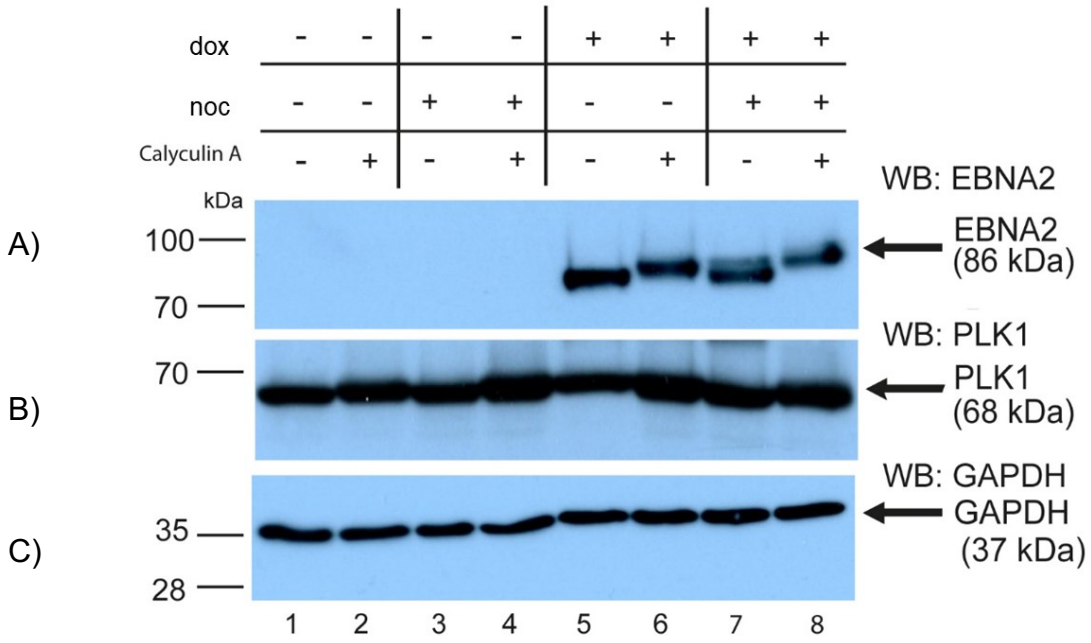

Fig. 19 Calyculin treatment of the PLK1 and EBNA2

Cell cycle arrest with nocodazole 100ng/ml 14h incubation and 45min incubation with Calyculin A 100nM were performed immediately before the cells were harvested. CKR128-34 cells were either induced with doxycycline 1µg/ml (+ dox) in order to activate EBNA2 expression or left untreated (-dox). The asynchronously growing cells were treated with 100ng/ml nocodazole (+/-noc) and incubated for 14h to induce G2-M-phase cell cycle arrest. Cells were treated with 100nM Calyculin A for 30min prior to lysis in order to suppress intrinsic phosphatases. Total cell lysates were submitted to SDS-PAGE (10% for EBNA2 and 12% polyacrylamide gel for PLK1) and transmitted to immunoblotting. (A): anti-EBNA2 (R3) antibody, (B): anti-PLK1 (ab17056) antibody and C): anti-GAPDH mAb 374. Finally, signals were developed with a chemiluminescent film reagent after (A) 20, (B) 15 and (C) 10s exposure accordingly.

4.7 Interactions sites for PLK1 within EBNA2

Next, we sought to define the PLK1-EBNA2 interaction interface. As a transient interaction, the proteins form a dynamic association in order to mediate biological functions, which are yet to be explored. To understand how PLK1-EBNA2 complex functions, we needed to examine how mutations can affect the strength of the interactions that result in protein binding. In this experiment, we sought to map more precisely the binding interface between PLK1 and EBNA2 by modifying key residues that might impact on the binding. The conserved region CR7 in EBNA2 close to the activation domain of EBNA2 and the binding site of EBNA2 to CBF1 were analysed as possible sites of binding for PLK1.

We transfected DG75 cells with four EBNA2 plasmids: pSG5 as an empty vector used as a negative control, pAG155, a full-length EBNA2 labelled with HA-Tag, pEFC61, a transformation of the pAG155 with deletion of the amino acids 377 to 387 forming the CR7 domain and finally pGFP only for an examination of the transfection rate success. 24h after transfection we performed an immunoprecipitation targeting the HA-Tag of EBNA2 and detected the proteins of interest by immunoblotting using anti-EBNA2 and anti-PLK1 antibodies. As Fig. 20 B) shows, we were able to pull down PLK1 only in the immunoprecipitation samples from the cells transfected with pAG155, the full-length EBNA2. The missing signal from PLK1 in lane 6 suggested that the EBNA2 construct with deletion of CR7 (pEFC61) was impaired to form a stable complex with PLK1. Isolated deletion of the CR7 prohibited the interaction of PLK1 and EBNA2.

In view of the PLK1 function as a kinase and its substrate recognition of phosphorylated partners, we repeated the experiment under other conditions. Additionally, we investigated the influence of a targeted dephosphorylation of the cell lysates. Therefore, we incubated the samples with phosphatase enzyme CIP after cell lysis and immediately before immunoblotting and compared the phosphorylation state of PLK1 and EBNA2. Fig. 20 D) displays the results. We were able to confirm again that the constructs of EBNA2 with deleted CR7 cannot efficiently bind to PLK1 as lanes 7 and 8 detected no signal for PLK1. Interestingly PLK1 and EBNA2 both displayed higher molecular weight if the samples were not treated with the phosphatase, than those incubated with the CIP (signal from the EBNA2 in lanes 5 and 8 compared to lanes 4 and 7 accordingly, and signal from PLK1 in lane 5 compared to lane 4).

A) DG75 cells 10x objective

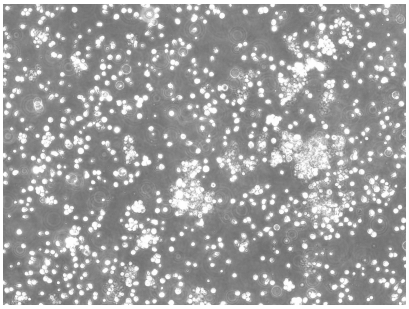

DG75 cells 10x objective; GFP filter

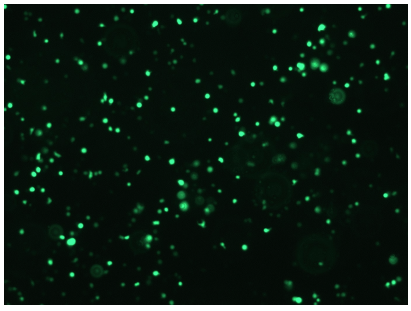

B)

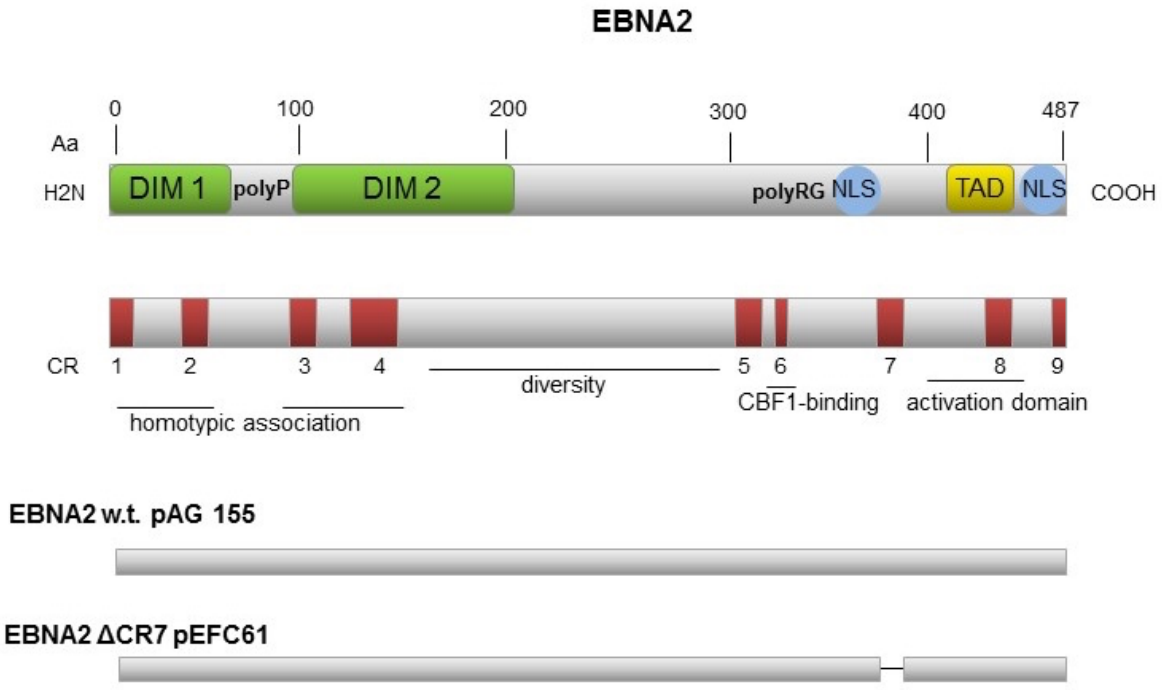
EBNA2
0
100
200
300
400
487
Aa
H2N
DIM 1
polyP
DIM 2
polyRG
NLS
TAD
NLS
COOH
CR
1
2
3
4
5
6
7
8
9
diversity
CBF1-binding
activation domain
homotypic association
EBNA2 w.t. pAG 155
EBNA2 ΔCR7 pEFC61

C)

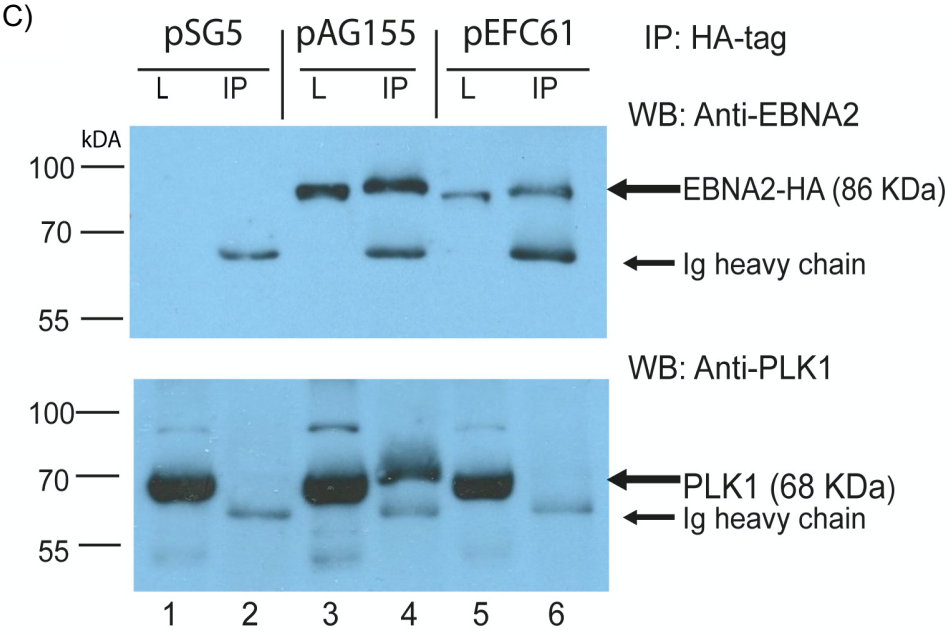
pSG5
pAG155
pEFC61
L
IP
L
IP
L
IP
IP: HA-tag
WB: Anti-EBNA2
kDA
100
70
55
EBNA2-HA (86 KDa)
Ig heavy chain
WB: Anti-PLK1
100
70
55
PLK1 (68 KDa)
Ig heavy chain
1
2
3
4
5
6

D)

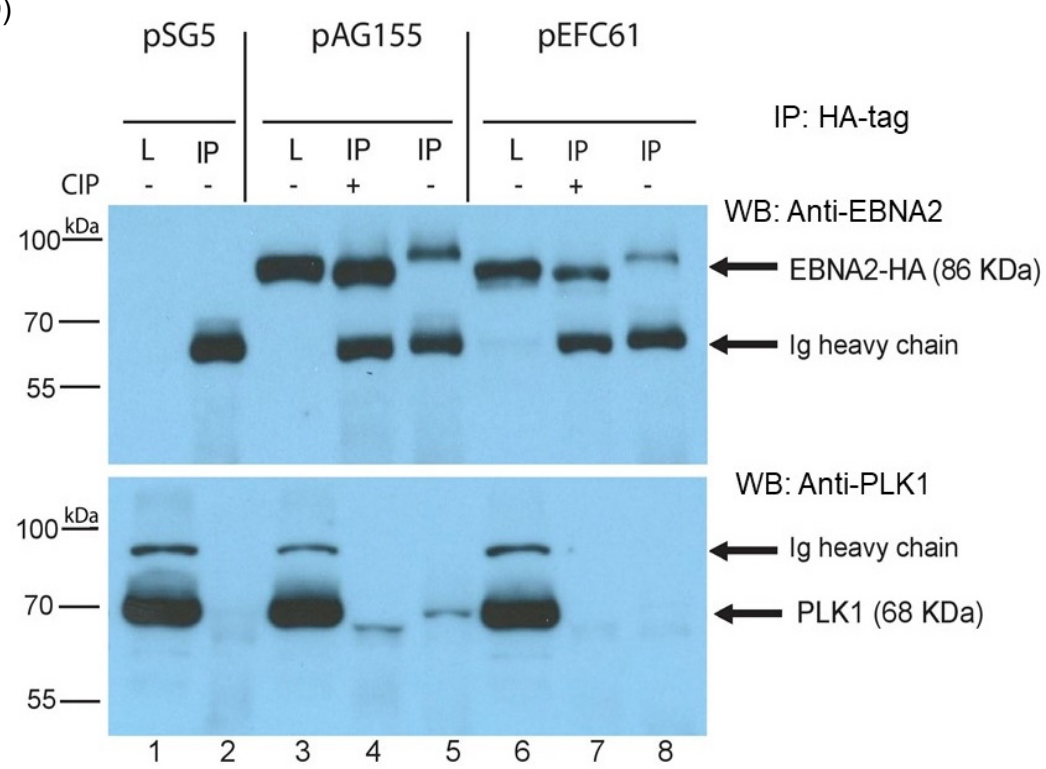

Fig. 20 The CR7 domain of EBNA2 is essential for the EBNA2-PLK1 interaction

DG75 cells were transfected with three different plasmids: pSG5, pAG155 and pEFC61.

A) Immunofluorescence of DG75 cells transfected with the pGFP plasmid. pGFP expression was monitored by fluorescence microscopy 24h after transfection. Using equivalent conditions for all the plasmids, pGFP as control allows approximate evaluation of the transfection rate for the other EBNA2 constructs.

B) Schematic representation of the EBNA2 and the EBNA2 constructs used for the transfection of DG75 cells:

- pSG5 as an empty vector used as a negative control
- pAG155 is an EBNA2-HA expression plasmid
- pEFC61 is a transformation of the pAG155, where the EBNA2 gene has a deletion from amino acid 377 to 387 and lacks the CR7 domain
- pGFP was used only for examining the transfection rate success and was not submitted to co-immunoprecipitation.

C) western blot with the IP samples and total cell lysates

24h after transfection the total cell lysates were co-immunoprecipitated (co-IP) with HA-Tag antibody, the resulting protein complexes were submitted to SDS-PAGE, loaded on 10% gel and detected by immunoblotting using (A): anti-EBNA2(R3) antibody and HRP-anti-rat secondary antibody and (B): anti-PLK1 (ab17056) antibody and HRP-anti-mouse secondary antibody. Total cell lysates (L) and immunoprecipitation samples (IP) were detected by immunoblotting. Finally, the signal was developed with a chemiluminescent detection reagent after 15s exposure.

D) western blot with the IP samples and total cell lysates after CIP incubation

24h after transfection the total cell lysates were immunoprecipitated (IP) with HA-Tag antibody, the resulting protein complexes submitted to SDS-PAGE, loaded on 10% gel and detected by immunoblotting using anti-EBNA2(R3) antibody and HRP-anti-rat secondary antibody and anti-PLK1 (ab17056) antibody and HRP-

anti-mouse secondary antibody. Total cell lysates (L) and immunoprecipitation samples (IP) were detected by immunoblotting. Certain IP samples were treated with phosphatase enzyme CIP (P) before immunoblotting. Finally, the signal was developed with a chemiluminescent detection reagent after 30s exposure.

4.8 The influence of PLK1 inhibition on the interaction between PLK1 and EBNA2

All previous experiments suggested that the EBNA2-PLK1 complex can be detected in unsynchronised cell populations. To further analyse this hypothesis, we used the clinically approved PLK1 inhibitor Volasertib and applied it in concentrations ranging from 1nM to 20nM prior to performing a co-immunoprecipiation via HA-Tag for the EBNA2-PLK1 complex. Once again, EBNA2 was labelled with an HA-Tag and only conditionally expressed in the doxycycline-treated cells. Additional CIP incubation after lysis aimed to target the phosphorylation of the two proteins of interest. Fig. 21 shows the results from the immunoblotting using EBNA2 and PLK1 antibodies.

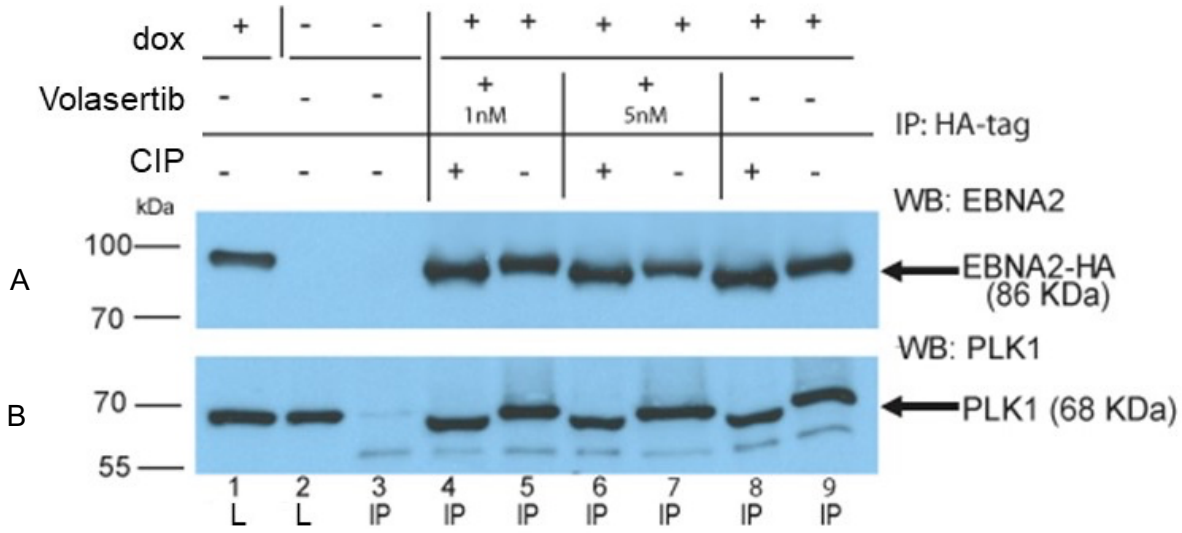

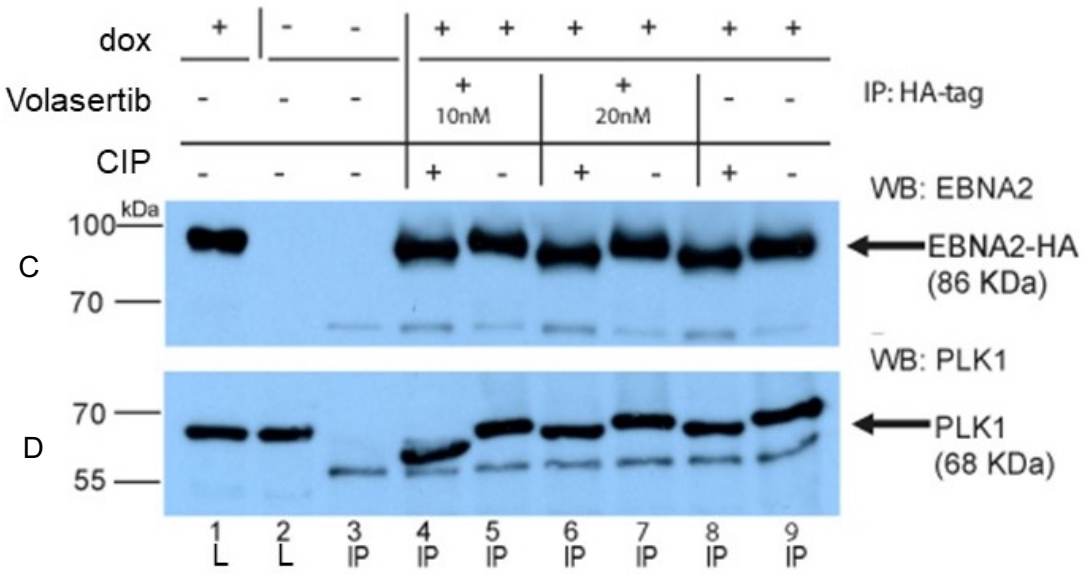

Fig. 21 Volasertib does not affect the interaction between EBNA2 and PLK1
10^7 DG75 cells with characterised by a doxycycline-inducible EBNA2-HA expression plasmid were treated with doxycycline and with different concentrations of Volasertib (BI6727 PLK1-Inhibitor: 1nM, 5nM, 10nM and 20nM) for 24h or left untreated. The cell lysates were submitted to co-immunoprecipitation using an HA-Tag specific antibody. Protein complexes coupled to agarose beads were washed and subjected to SDS-PAGE (10% polyacrylamide). Total cell lysates (L) and immunoprecipitation samples (IP) were detected by immunoblotting.
A and C: anti-EBNA2(R3) antibody and HRP-anti-rat secondary antibody and
B and D: anti-PLK1 (ab17056) antibody and HRP-anti-mouse secondary antibodies. Some of the samples were treated with phosphatase enzyme CIP (calf intestinal alkaline phosphatase) before immunoblotting in order to analyse the phosphorylation status of the proteins of interest. Finally, signals were developed with a chemiluminescent detection reagent after 20s exposure.

EBNA2 was detected in the doxycycline induced samples only. PLK1 was successfully co-immunoprecipitated in all samples with positive EBNA2 expression. The incubation with 1nM, 5nM, 10nM and 20nM Volasertib was compared to the results from cells without Volasertib treatment as a reference. All in all, we obtained strong signals from all immunoprecipitation samples (lanes 4–9 in Fig. 21 A, B, C and D) for EBNA2 and PLK1, independently on the PLK1 inhibition. Additionally, CIP incubation causes a minimal shift of the molecular weight of PLK1 and EBNA2 as both proteins were dephosphorylated by the enzyme in a manner unaffected by the PLK1 inhibition. PLK1 inhibition does not prevent the phosphorylation of EBNA2 and has no significant impact on the interaction between EBNA2 and PLK1. In conclusion, the phosphorylation status of both proteins does not exclusively depend on PLK1. Native and inactive PLK1 can bind to EBNA2.

4.9 Interaction sites for EBNA2 within PLK1

Modulating the binding affinity of transient protein–protein complexes offers new opportunities to control their interaction. Beyond this, structural modifications on the protein surface of PLK1 can reveal crucial sites for the interaction with EBNA2. Here, we attempted to map the precise interaction sites for EBNA2 within the amino-acid-sequence of PLK1 using PLK1 mutants. Therefore, we tested whether the selective deletion of functional units of PLK1 can influence the interaction with EBNA2. For the purposes of the experiments, we used three PLK1 fragments and compared them to the full-length PLK1. All constructs were labelled with a FLAG-tag and a triple FLAG-tag was used as negative control. Fig 22 A) is a schematic representation of the wild type PLK1 and the constructs we used in the experiment. The mutant KD416, composed of the first 416aa from the amino terminus of the protein, contains the entire kinase domain of PLK1, including the ATP binding site and the destruction box as a specific feature of PLK1. KD 305 consists of the first 305aa of PLK1, accordingly only the kinase domain. The PBD construct contains the last 231aa on the C-terminus of PLK1, forming the polo-box domain. The immunoprecipitation was performed with a FLAG-tag antibody and the immunoblotting using anti-FLAG-tag and anti-EBNA2 secondary antibodies. Figs. 22 B) and C) display the visualisation of the immunoblotting. The PLK1 constructs were distinguished by the molecular weight: FLAG-PLK1 wt with approximately 66kDa, KD 416 with 50kDa, KD305 with 35kDa and PBD with 30kDa. The signal from full-length PLK1 wild type (wt) and EBNA2 in lane 5 clearly implies that wild type PLK1 can efficiently interact with EBNA2. The equivalent staining from the IP samples in lanes 10, 14 and 18, which represent the three PLK1 mutants, show a considerably weaker signal. However, EBNA2 was pulled down using all three PLK1 mutants, suggesting that the interaction of the two proteins of interest is possible despite the targeted deletion of KD or PBD. The weakest signal for EBNA2 was detected in the IP with KD416. This could indicate that the deletion of PBD disturbs the PLK1-EBNA2 interaction, however, the mutant KD305, only a shorter sequence of KD, which also lacks the PBD, displays comparatively stronger signal for EBNA2 and therefore suggests stronger protein interaction. The only difference between the mutants KD305 and KD416 being approximately 100 amino acids of the PLK1 sequence contains the D-box. We can speculate that KD416 might not be able

to fold properly. KD305 and PBD show similar affinity for EBNA2. Hence, we observed positive staining for EBNA2 in all cases.

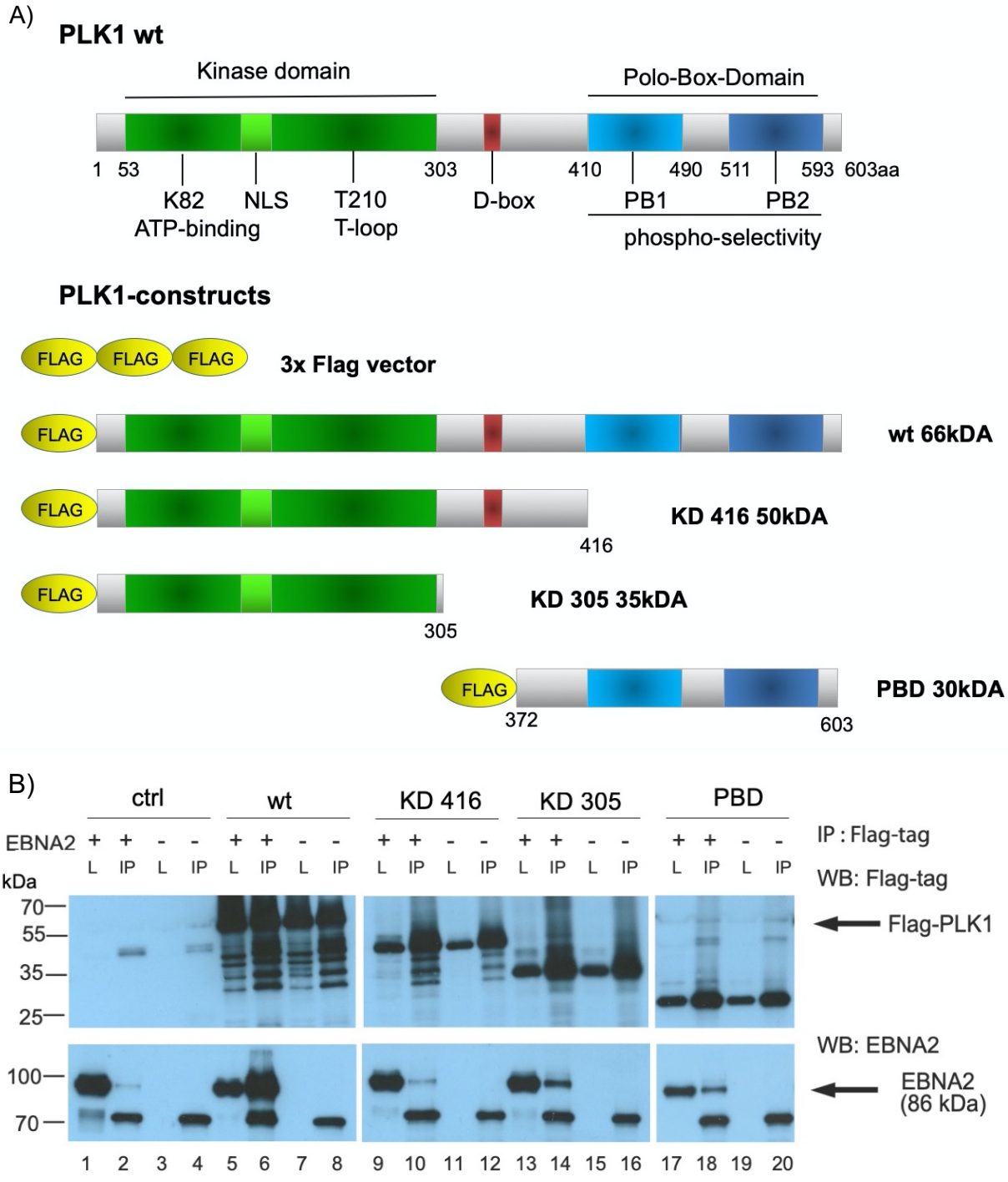

Fig. 22 Interaction of PLK1 fragments with EBNA2
A) Schematic representation of the polo-like kinase (PLK1) in human cells
The amino-acid (aa) sequence lengths are displayed for every protein. The kinase domains (green) and polo-boxes 1 and 2 (blue) are depicted. The PLK1 sequences responsible for its nuclear localisation (NLS, which is indicated in light green) and its destruction at the end of mitosis (D-box, which is indicated in red) are also displayed. Specific residues that secure phosphorylation and enzymatic

activation (T-loop) of the kinase domain and enable the phospho-selectivity of the polo-boxes are indicated.
The PLK1-constructs are composed as follows:

- 3x FLAG-tag vector with pCDNA + Hygromycine as a backbone
- PLK1 wt: molecular weight 66kDa
- KD 416: 416 residues without PBD, molecular weight 50kDa
- KD 305: 305 residues, molecular weight 35kDa
- PBD: residue 372 to 603, molecular weight 30kDa

B) PBD- and KD- PLK1 mutants can all interact to a certain extent with EBNA2
DG75 FLAG-PLK1-cells were transfected with four different PLK1 mutants and 24h later subjected to co-immunoprecipitation using FLAG-tag beads. Immunoblotting was conducted using FLAG-tag and EBNA2 antibodies accordingly. Finally, signals were developed with a chemiluminescent detection reagent after 20s exposure. Total cell lysates (L) were loaded on the gel and the corresponding immunoprecipitation samples (IP). The experiment was performed in doublets using identical conditions for all the samples transfected with EBNA2 wt (EBNA2+) or with pSG5 as an empty vector (EBNA2-).

5. Discussion

The exact mechanism of how viruses interact with their host cell on a molecular level is of great interest for the elucidation of the functional response that triggers lifetime changes in a single cell and an organism as a victim of subsequent pathological transformations.

The discovery of the Epstein-Barr virus as the first identified human tumour virus (Epstein et al., 1964) triggered extensive research that has gone on for decades on the pathological mechanisms employed by EBV. Despite a frequency of up to 95% of the worldwide population, there are no EBV-specific drugs to treat the primary infection. The standard therapy is largely supportive and mostly harmless for healthy individuals. Today it is known that Epstein-Barr virus is etiologically associated with a number of malignancies, including Burkitt's lymphoma, Hodgkin's lymphoma, nasopharyngeal carcinoma, certain T-cell lymphomas, and immunoblastic lymphoma (Rickinson and Kieff, 1996). The immortalisation of primary human B-lymphocytes serves as a model in vitro for the investigation of EBV-associated tumourigenesis. The understanding of the molecular mechanisms involved in the immortalisation of B-lymphocytes by EBV is of great importance with regard to oncological diseases. In addition to the EBV-encoded proteins, which play a crucial role in the uncontrolled growth of B-lymphocytes and EBV-associated tumourigenesis (Kempkes et al., 1995; Elgui de Oliveira et al., 2016), a number of genes are regulated by EBV in their expression. The detection of interaction partners for the viral antigens assembled after EBV infection has still not been completed. To date no antiviral drug has been approved for treatment of primary EBV infection, although the therapy of EBV-related malignancies of lymphoid and epithelial cell origin undoubtedly represents a major unmet medical need.

This project aims to give an insight into the newly found interaction between EBNA2 and PLK1, the networking of cellular processes in human B-lymphocytes after EBV infection and characterises the significance of the interaction between the viral antigen EBNA2 and the ubiquitously expressed protein PLK1, essential for the cell cycle progression. PLK1 is a major kinase during mitosis and cytokinesis (Liu et al., 2017). The depletion of PLK1 protein in cancer cells dramatically inhibits cell proliferation and induces apoptosis. Hence,

PLK1 inhibitors have already found implementation in clinical studies for tumour treatment.

Approaching EBV from a new perspective, we investigated the interaction of EBNA2 with PLK1 under various conditions on a cellular and subcellular level and sought to examine details of the protein-protein interactions, to analyse the complicated biological processes in which they participate.

The interaction of PLK1 and EBNA2 was already identified in LCLs by the Kempkes group and confirmed in this project. Thus, we validated the protein-protein interaction in different cell cultures in view of protein sequence alternations by using EBNA2 mutants and PLK1 fragments. Our aim was to provide information about the specific protein and amino-acid residues participation in the given protein-protein interaction in order to analyse the exact molecular mechanism of how the two proteins interact and facilitate the understanding of biological and clinical observation, which is potentially relevant in anticancer treatment. For the exact definition of the protein-protein interaction interfaces of PLK1 and EBNA2 we tested the impact of mutations on the protein binding affinity. Furthermore, we studied the expression and phosphorylation of EBNA2 with respect to the cell cycle stage and PLK1 activity, as well as the influence of PLK1 inhibition on the proliferation of EBNA2-positive and -negative cells.

We succeeded in verifying a robust interaction of PLK1 and EBNA2 under various conditions, different cell cycle stages and despite phosphorylation alternations. However, we could not establish a clear correlation between the kinase activity of PLK1 and the proliferation of immortalised B-lymphocytes or EBNA2-transfected cells. Thus, we claim that EBNA2 and PLK1 have more than one exact interaction site as targeted mutations of both proteins did not fully impair the proteins in binding to one another. The questions remaining are whether and how the PLK1-EBNA2 association contributes to immortalisation of B-cells by EBV.

5.1 Inhibition of the proliferation of immortalised and EBNA2 transfected B-lymphocytes by targeting PLK1

Drugs targeting PLK1 have been the focus of extensive clinical studies but have never been analysed in the context of EBV infection or tested the effect on

EBNA2 expression. In this work, using proliferation assays, we were able to show that EBV- infected cells are sensitive to PLK1 inhibition. The IC_{50} scores shown in Fig. 8, section 4.1 reveal that immortalised B-lymphocytes have IC_{50} scores in the same range as other cell lines derived from cancer tissues (Rudolph et al., 2009). Volasertib disrupts centrosome maturation and division and thus causes the composition of a monopolar spindle, which terminates cell cycle progression temporarily at the spindle assembly checkpoint during prometaphase. The longer the cells are arrested, the more become apoptotic (Lenart et al., 2007; Steegmaier et al., 2007). In vitro experiments suggest that Volasertib could be employed in the adverse cytogenic AML treatment, which appears to be more sensitive to PLK1 inhibition than normal karyotype AML specimens and normal hematopoietic cells (Moison et al., 2019). A phase II clinical trial with Volasertib was conducted in patients over 65 years with previously untreated acute myeloid leukemia, who were ineligible for intensive remission induction therapy, to evaluate their response to subcutaneous low-dose cytarabine with or without Volasertib (Mertens et al., 2012). The phase III trial did not meet the initial expectations and failed to verify the encouraging conclusions from the phase II study. However, competing risk modeling of survival rates confirmed the antileukemic effect of Volasertib in combination with low-dose cytarabine and supports an investigation of modified Volasertib doses as well as further examination of the possibilities for an increase of the treatment tolerance (Döhner et al., 2016).

Volasertib has proven drug potency in various solid tumour xenograft models of human cancer at acceptable doses (Rudolph et al., 2009), and a desirable effect has been reported in early clinical trials in patients with solid tumours (Janning and Fiedler, 2014). The FACS analysis we performed (Fig. 11, section 4.1) confirmed that Volasertib treatment causes a reduction of the G1 population and an increase of the G2 population of immortalised B-lymphocytes. Of note is the fact that we also saw a clear expansion of the S-phase in the cell populations treated with the highest amount of Volasertib. However, questions remain as to whether we can differentiate clearly cells in the S-Phase and G2-blocked cells.

The assessment of the experiments was problematic since the increasing levels of apoptosis shown in Fig. 11 could also be associated with the p53 status of the lymphocytes. It has been reported, that p53 gene expression is induced in

LCL to the level of mitotic cells and, therefore, immortalised B-cells are more sensitive to the p53 mediated effect by various drugs (Allday et al., 1995). The immortalised B-cells could, in our case, be targeted with a PLK1 inhibitor successfully, but whether the presence of the virus in cells could actually alter the reaction to the drug inhibition remains unclear.

For this reason, we sought to differentiate the influence of the virus and EBNA2 expression on the drug efficacy and toxicity. Thus, we used EBV-negative lymphoma cell lines, transfected with EBNA2 and were able to prove that the IC_{50} scores for the EBNA2 positive cells were slightly lower. Although, per definition, we saw an insignificant difference between EBNA2 expressing and EBNA2 negative cells, we can speculate that within the repetition of the experiment we witnessed an obvious reproducible tendency that the EBNA2 positive cells were more prone to the Volasertib suppression of PLK1. Next, we tested the influence of the PLK1 inhibition via Volasertib in EREB B-lymphocytes with conditional expression of myc and EBNA2 and found that the response of cells to the drug treatment was stronger the longer EBNA2 was switched on (Fig.12, section 4.2). For the assessment of this experiment with FACS we had to manually define the cell cycle stages for the cells treated with the highest concentration of Volasertib according to the DNA content because the cells showed distribution, which was not automatically perceptible for the FlowJo Software.

Overall, we can confirm that myc correlates with increased proliferation activity as already reported (Kempkes et al., 1995). Therefore, proliferation rates of the myc expressing cells were also the highest. The corresponding FACS analysis of the cells we tested using proliferation assays suggests that Volasertib treatment is more toxic for EBNA2-positive p493-6 cells. At a drug concentration as high as 50nM the cells were not able to proliferate (Fig. 12, section 4.1). In the quantification histograms of Fig. 12 A) we see a clear expansion of the apoptotic population, especially at the highest drug levels and a decrease of the G1 contribution. However, as previously discussed, the significant difference appears only if the expression of EBNA2 is switched on for three days prior to the drug application. Whether the presence of EBNA2 can intensify the efficacy of drugs targeting PLK1 and if these findings have a clinical value for anticancer therapies in vivo should be an object of future research.

Although PLK1 functional suppression with Volasertib, a small molecule, adenosine triphosphate-competitive kinase inhibitor, did not show a major

difference in the proliferation rates between EBNA2 positive and negative cells, the impact of the Volasertib treatment might be alternated by the interference with other intrinsic kinases. Volasertib is a selective inhibitor for the PLK family but it also inhibits PLK1 and PLK2 with IC_{50} values of 0.87 and 5nM, respectively, and shows somewhat lower potency on PLK3 (56nM) (Rudolph et al., 2009). The PBD differs more between the PLKs than the KD does, and PBD binding motifs differ between PLKs (Lee et al., 2012). Future experiments with specific drugs targeting the PBD of PLK1, such as Poloxin, might give a new perspective on the specific PLK1 inhibition in view of the PLK1-EBNA2 interaction. The most recent development of Poloxin 2 is reported to have significantly improved potency and selectivity for PBD of PLK1 (Scharow et al., 2015).

5.2 EBNA2 as a substrate of PLK1

PLK1 is required for entry into mitosis during normal cell cycles and its functional activation reaches the highest level at the late G2 stage and decreases again after the transition to mitosis (Sumara et al., 2014). To determine how PLK1 maximum activity as a kinase can influence EBNA2 on a molecular level, we established a cell cycle arrest at the G2/M-phase of the cell cycle using nocodazole treatment. B-lymphocytes with conditional expression of EBNA2 were successfully trapped into mitosis. Fig. 16 confirms that PLK1 and EBNA2 can interact in all stages of the cell cycle and even if the cells were not enriched for the G2/M population, PLK1 binds efficiently to EBNA2. At this point, we considered the interaction of PLK1 and EBNA2 to be independent of the kinase activity of PLK1. However, the phospho-dependent ligand recognition by PBD is crucial for the association of PLK1 to a specific substrate, also known as processive phosphorylation. It has been appreciated that the release from the intramolecular inhibitory state between the two functional domains of PLK1 emerges from conformational alternation induced in PBD when phosphopeptide binding leads to the affiliation of KD to the specific substrate (Park et al., 2010; Jang et al., 2002; Seki et al., 2008). All previous studies taken together suggest a sequence D/E-X-S/T-Φ-X-D/E (X, any amino acid; Φ, a hydrophobic amino acid) as an optimal phosphorylation sequence by PLK1 (Nakajima et al., 2003). The KD of PLK1 recognises serine and threonine residues as potential phosphorylation substrates (Elia et al., 2003). These are also found within

EBNA2, precisely at residues 455–459 and 463–467 at the C-terminus of the protein (Fig. 17. B, section 4.4).

In latently infected cells, EBNA2 is hyperphosphorylated by cyclin-dependent-kinase 1 also known as CDK1 or cell division cycle protein 2, the key regulator of mitosis (Yue et al., 2005). Of great interest in the context of the kinase function of PLK1 is a possible regulation of EBNA2 function through phosphorylation during the EBV lytic cycle. In this study, we examined whether PLK1 is able to phosphorylate EBNA2 and how this phosphorylation affects EBNA2 function. Interestingly, the kinase assay, as shown in Fig.16, revealed that an increase of the PLK1 enzymatic activity results in phosphorylation of a protein with a molecular weight of approximately 90kDa, which could be the hyperphosphorylated EBNA2. The results from the kinase assay performed by M. Raab and Prof. Strebhardt as collaborative work on our project (Fig. 16, section 4.4) demonstrated that EBNA2 might be a substrate of PLK1 in the G2/M-phase. There is still a question as to which protein with an approximate molecular weight of 90kDa was identified as the kinase substrate of PLK1. One possible explanation is that this is phosphorylated or even hyperphosphorylated EBNA2, but more evidence is needed to support this suggestion.

Determination of crystal structure of KD bound to PBD in future studies could help to narrow the range of possible phosphor-priming dependent and independent interactions of PLK1.

EBNA2 is a phosphoprotein, but whether constitutive phosphorylation of EBNA2 influences its transactivation function is unknown. It has been shown that phosphorylation of EBNA2 in latent infection is regulated during the cell cycle and that the protein is hyperphosphorylated and, thus, inhibited during mitosis (Yue et al., 2005). Precisely, the transcriptional activity of the hyperphosphorylated protein is suppressed. As already discussed in section 4.4, the predicted phosphorylation sites (P-sites) within EBNA2 are serine (S) and threonine (T), localised at residues 455–459 and 463–467 (PhosphoSitePlus®). Interpretation of Fig. 18 allows the argument that inactivation of these phosphorylation sites causes an increase of the transactivation activity. Hence, our results confirm the hypothesis that a hyperphosphorylation decreases the transactivation activity, because mutants with impaired phospho-sites could not be restricted in their functional activity. Moreover, the expression of these EBNA2 mutants is stable on the protein level. At this point, the next step would be to compare the affinity

of PLK1 mutants containing only KD or only isolated PBD to these EBNA2 mutants with impaired phosphorylation sites.

The inhibition of the function of PLK1 as mitotic kinase on a molecular level did not significantly affect the protein-protein interaction. Fig. 19 (section 4.6) shows that the cells arrest in the G2/M-phase of the cell cycle after nocodazole treatment, when PLK1 reaches the peak of its kinase activity (Petronczki et al., 2008), and EBNA2 phosphorylation is enhanced. However, other kinases are also increasingly active during the G2/M transition and do not allow a final conclusion to be drawn as to whether PLK1 itself is responsible for the EBNA2 phosphorylation.

Next, the probable phosphorylation of EBNA2 in the course of interaction with PLK1 led us to the question of whether we can better examine the phosphorylation state of our binding partners. Therefore, in Section 4.7 we used a phosphatase after performing a co-immunoprecipitation. As Fig. 20 implies, dephosphorylation with an extrinsic phosphatase showed a clear change of the phosphorylation state of the two proteins of interest. After treatment with the phosphatase, both proteins displayed slightly lower molecular weight when depleted from the phosphoryl groups. Of question is whether we were able to efficiently target the phosphorylation sites of EBNA2 with the phosphatase enzyme of choice. Another critical point we acknowledge is that it is not clear whether once the protein complex is formed the phosphorylation sites remain available for the CIP reaction. CIP might not be able to approach the target residues if they are out of its reach in the protein complex.

5.3 Functional inhibition of the kinase activity of PLK1

PLK1 expression and activity increase at the G2/M transition and peak during mitosis (Petronczki et al., 2008). Phosphorylation of Thr210, located in the T-loop inside the KD is characteristic for mitosis and appreciated as the most important post-translational modification on PLK1 during mitotic division. Phosphorylation of Thr210 by upstream kinases is considered the first step in triggering PLK1 activation during mitosis (Macurek et al., 2008). Not only does the PBD of PLK1 require phosphorylation for substrate recognition (Elia et al., 2003), but the kinase function of the KD of PLK1 itself is dependent on ATP incorporation for its activation (Sumara et al. 2014).

Taking the results from Fig. 21 into consideration, we argue that functional inhibition of PLK1 with Volasertib does not affect the association of the PLK1-EBNA2 protein complex. We claim, that the kinase enzymatic activity of PLK1 is not essential for the interaction with EBNA2 as both active and inactive PLK1 can bind to EBNA2.

The priming phosphorylation of EBNA2 needed for the substrate recognition by PLK1 is conducted by other kinases and seems to be independent of the main function of PLK1. This initial phosphorylation of EBNA2 by other kinases allows the PLK1 recruitment in a process called non-self-priming (Lee et al., 2014). Although we cannot exclude the possibility that PLK1 can also create its own docking site on EBNA2 under certain circumstances, our experiments do not rule out the so-called non-self-priming mechanism of PLK1 being an alternative preliminary condition for the EBNA2 recognition as suitable substrate.

5.4 Mapping of the interaction sites within PLK1 and EBNA2

PLK1 mutants lacking PBD or KD were not impaired in their protein-protein interaction with EBNA2 (Fig. 22, section 4.8). PBD alone, as well as isolated KD of PLK1, could both be used for a pull down of EBNA2. Considering that PBD plays an essential role in targeting PLK1 to various subcellular elements and, thus, determines the mitotic allocation of PLK1 (Lee et al., 2008), we expected a clear loss of affinity for EBNA2 as interaction partner, if PBD was deleted. However, our results did not confirm these assumptions. One of the PLK1 mutants with deletion of the entire PBD showed a similar affinity to EBNA2 as the isolated PBD itself. These findings were rather unexpected as we thought that KD alone would not be able to bind to EBNA2.

We can speculate that the KD fragments show different affinity to EBNA2 due to the presence or absence of the destruction box in the protein sequence. Interestingly, the inter-domain linker region of PLK1 between KD and PBD contains the canonical destruction box motif RKPLTVLNK (aa 337 to 345). These residues are essential for the recognition by APC/C, which is reported to be one of the main regulators of the transition from metaphase to anaphase and mitotic exit in human cells. Targeted mutation of residues forming the destruction box renders PLK1 non-degradable and leads to a delay in mitotic exit (Schmucker and Sumara, 2014). Whether the destruction box as a functional unit of PLK1

actually modifies the stability of the protein itself or modulates the structure of the protein in a way that prohibits efficient interaction with EBNA2, still remains to be elucidated. Another probable explanation for the impaired interaction of the KD416 protein with EBNA2 (Fig. 22, section 4.8) is the protein folding problem, which disturbs the tertiary structure of the protein.

Of notice is also the fact that between the PBD and the kinase domain in full-length PLK1 mutual inhibitory interaction occurs (Jang et al., 2002). Isolated PBD is reported to bind strongly and specifically to pSer/pThr-containing peptides (Elia et al., 2003). However, in our experiment visualised in Fig. 22, we also do not see an increase of the PLK1 affinity for EBNA2, when PBD is isolated. Even though the deletion of PBD prevents possible inhibition by the kinase domain near the N-terminus, the isolated PBD and isolated KD showed a comparable affinity for EBNA2. In this case, we consider at least two binding sites for EBNA2 within PLK1, one of them located approximately within the first 300–400aa and another one within the last 400–603aa. Certainly, further analysis of these binding sites needs to be performed.

Vice versa, modification of the EBNA2 structure brought more insight to the exact interaction sites within the EBNA2 protein. CR7 deletion mutants (aa 376 to 425 deleted) of EBNA2 were impaired for efficient interaction with PLK1 (Fig. 20). Next, plasmids from truncated CR7, composed only of the residues aa 376–425, could be transfected in B-lymphocytes in order to investigate whether CR7 alone is sufficient for the interaction with PLK1. However, even if CR7 of EBNA2 is one of the key residues for the PLK1 interaction, we still cannot exclude the existence of a second and third interaction site within EBNA2. As shown in Fig.17 (section 4.4) another potential binding site for PLK1, suggested by sequence alignment, is located at the residues 266–268 of EBNA2 and contains the typical consensus motif of serine-threonine proline (STP). In order to verify this hypothesis, further experiments with deletion mutants for these residues, assayed for interaction with PLK1, should be performed.

5.5 Outlook

EBNA2 is an EBV multifunctional viral oncoprotein, crucial for the immortalisation of B-lymphocytes. The interaction with PLK1 might involve a key mechanism in

the malignant transformation of cells caused by the virus. Our data imply that EBNA2 can bind to PLK1 in a reversible but stable manner. Whether this particular interaction triggers a pathway that can influence the viral ability to establish and maintain immortalised B-cells and, thus, benefit tumourigenesis, is still unclear. Investigation of the PLK1-EBNA2 interaction and downstream signalling pathways emerging from this interaction could help to improve our knowledge concerning EBV-associated malignancies. So far, we were able to show that EBNA2 can, to a certain extent, sensitise cells for PLK1-targeted inhibitory treatment. However, the clinical relevance of this discovery remains questionable. Implementation of selective PLK1 inhibitors on EBV-infected or EBNA2 transfected B-lymphocytes might bring valuable insights into the consequences of this interaction and enable identification of direct drug targets in cancer treatment. The exact principles that guide the proliferation activity of EBV-immortalised cells and their potential in immunotherapeutic application remain to be fully explored in the future.

6. References

Abbot SD, Rowe M, Cadwallader K, Ricksten A, Gordon J, Wang F, Rymo L and Rickinson AB (1990). "Epstein-Barr virus nuclear antigen 2 induces expression of the virus-encoded latent membrane protein." J Virol 64(5): 2126-2134.

Alfieri C, Birkenbach M and Kieff E (1991). "Early events in Epstein-Barr virus infection of human B lymphocytes." Virology 181(2): 595-608.

Allday MJ, Crawford DH and Griffin BE (1989). "Epstein-Barr virus latent gene expression during the initiation of B cell immortalization." J Gen Virol 70 (Pt 7): 1755-1764.

Allday MJ, Sinclair A, Parker G, Crawford DH, Farrell PJ (1995) Epstein-Barr virus efficiently immortalizes human B cells without neutralizing the function of p53. EMBO J.;14(7):1382–1391.

Amoroso R, Fitzsimmons L, Thomas WA, Kelly GL, Rowe M and Bell AI (2011). "Quantitative studies of Epstein-Barr virus-encoded microRNAs provide novel insights into their regulation." J Virol 85(2): 996-1010.

Archambault V, Lepine G, Kachaner D. Understanding the Polo Kinase machine. (2015) Oncogene; 34:4799–807. https://doi.org/10.1038/onc.2014.451.

Arnaud L, Pines J, Nigg EA. GFP tagging reveals human Polo-like kinase 1 at the kinetochore/centromere region of mitotic chromosomes. (1998) Chromosoma.; 107:424–9.

Baer R, Bankier AT, Biggin MD, Deininger PL, Farrell PJ, Gibson TJ, et al. (1984) DNA sequence and expression of the B95-8 Epstein-Barr virus genome. Nature –25;310(5974):207–11. pmid:6087149

Bahassi el M, Conn CW, Myer DL, Hennigan RF, McGowan CH, Sanchez Y and Stambrook PJ (2002). Oncogene, 21, 6633–6640.

Bahassi el M (2011) Polo-like kinases and DNA damage checkpoint: Beyond the traditional mitotic functions. Exp Biol Med Maywood; 236(6):648–657

Beria I, Ballinari D, Bertrand JA, Borghi D, Bossi RT, Brasca MG, et al. Identification of 4,5-dihydro-1H-pyrazolo[4,3-h] quinazoline derivatives as a new class of orally and selective polo-like kinase 1 inhibitors. (2010) J Med Chem;53:3532–51.

Bonnet M, Guinebretiere JM, Kremmer E, Grunewald V, Benhamou E, Contesso G, Joab I. (1999); Detection of Epstein-Barr virus in invasive breast cancers. J Natl Cancer Inst. 91(16):1376–1381. doi: 10.1093/jnci/91.16.1376.

Cizmecioglu O, Arnold M, Bahtz R, Settele F, Ehret L, Haselmann-Weiß U, Antony C, Hoffmann I, (2010); Cep152 acts as a scaffold for recruitment of Plk4 and CPAP to the centrosome, The Journal of Cell Biology, 191 (4) 731-739; DOI: 10.1083/jcb.201007107

Cohen JI, Kieff E. (1991) An Epstein-Barr virus nuclear protein 2 domain essential for transformation is a direct transcriptional activator. J Virol.;65(11):5880–5. pmid:1656076

Cohen JI (2000) Epstein-Barr virus infection. New England Journal of Medicine;343:481–492

Cohen JI (2015) Epstein-Barr virus caccines. Clin Transl. Immunology ;4(1):e32. Published 2015 Jan 23. doi:10.1038/cti.2014.27

Cohen, P (2002). Protein phosphatase 1—Targeted in many directions. Journal of cell science. 115. 241-56.

Conn CW, Hennigan RF, Dai W, Sanchez Y and Stambrook PJ. (2000) Cancer Res., 60, 6826–6831.

de Cárcer G, Manning G, Malumbres M (2011) From Plk1 to Plk5: functional evolution of polo-like kinases. Cell Cycle. b;10:2255–2262.

de-Thé G, Geser A, Day NE et al. (1978) Epidemiological evidence for causal relationship between Epstein–Barr virus and Burkitt's lymphoma from Ugandan prospective study. Nature.; 274: 756–761

Dierickx D, Tousseyn T, Gheysens O, (2015). How I treat posttransplant lymphoproliferative disorders. Blood, 126(20), 2274-2283.

Döhner H et al. Phase III randomized tial of volasertib plus low–dose cytarabine (LDAC) versus placebo plus LDAC in patients aged ≥65 years with previously untreated AML, ineligible for intensive therapy. Abstract # S501 presented at the 2016 European Hematology Association Annual Meeting, Copenhagen, Denmark, 9-12 June 2016

Dunleavy K, Little RF., Wilson WH (2016), Update on Burkitt Lymphoma, Hematology/Oncology Clinics of North America, Volume 30, Issue 6, Pages 1333-1343, ISSN 0889-8588

Elgui de Oliveira D, Müller-Coan BG, Pagano JS. (2016) Viral Carcinogenesis Beyond Malignant Transformation: EBV in the Progression of Human Cancers. Trends Microbiol. 2016;24(8):649–664. doi:10.1016/j.tim.03.008

Elia AE, Cantley LC, Yaffe MB (2003) Proteomic screen finds pSer/pThr-binding domain localizing Plk1 to mitotic substrates. Science. a;299:1228–1231.

Elia AE, Rellos P, Haire LF, Chao JW, Ivins FJ, Hoepker K, Mohammad D, Cantley LC, Smerdon SJ, Yaffe MB. (2003) The molecular basis for phosphodependent substrate targeting and regulation of Plks by the Polo-box domain. Cell. 115:83–95.

Epstein MA, Achong BG, and Barr YM (1964) Virus particles in cultured lymphoblasts from Burkitt's lymphoma. Lancet.; 1: 702–703

Fahraeus R, Palmqvist L, Nerdstedt A, Farzad S, Rymo L, and Lain S (1994). Response to cAMP levels of the Epstein-Barr virus EBNA2-inducible LMP1 oncogene and EBNA2 inhibition of a PP1-like activity. Embo J 13, 6041-6051.

Ferry JA. Burkitt's lymphoma: clinicopathologic features and differential diagnosis. Oncologist 2006;11:375–83.

Filipovich AH, Zhang K, Snow AL, Marsh RA, X-linked lymphoproliferative syndromes: brothers or distant cousins?, Blood 2010 116:3398-3408; doi: https://doi.org/10.1182/blood-2010-03-275909

Fischer M, Quaas M, Nickel A & Engeland K (2015) Indirect p53-dependent transcriptional repression of Survivin, CDC25C, and PLK1 genes requires the cyclin-dependent kinase inhibitor p21/CDKN1A and CDE/CHR promoter sites binding the DREAM complex. Oncotarget 6, 41402–41417

Friberg A, Thumann S, Hennig J, Zou P, Nössner E, et al. (2015) The EBNA-2 N-Terminal Transactivation Domain Folds into a Dimeric Structure Required for Target Gene Activation. PLOS Pathogens 11(5): e1004910.

Frost A, Mross K, Steinbild S, Hedbom S, Unger C, Kaiser R, et al. (2012) Phase i study of the Plk1 inhibitor BI 2536 administered intravenously on three consecutive days in advanced solid tumours. Curr Oncol. ;19:e28–35.

García-Alvarez B, de Cárcer G, Ibañez S, Bragado-Nilsson E, Montoya G (2007) Molecular and structural basis of polo-like kinase 1 substrate recognition: implications in centrosomal localisation. Proc. Natl. Acad. Sci. USA.;104:3107–3112.

Gilmartin AG, Bleam MR, Richter MC, Erskine SG, Kruger RG, Madden L, et al. (2009) Distinct concentration-dependent effects of the polo-like kinase 1- specific inhibitor GSK461364A, including differential effect on apoptosis. Cancer Res;69:6969–77.

Gjertsen BT, Schoffski P (2015) Discovery and development of the Polo-like kinase inhibitor volasertib in cancer therapy. Leukemia. ;29:11–9.

Glaser SL, Clarke CA, Gulley ML, et al. (2003) Population-based patterns of human immunodeficiency virus-related Hodgkin lymphoma in the Greater San Francisco Bay Area, 1988-1998. Cancer; 98:300.

Golsteyn RM, Schultz SJ, Bartek J, Ziemiecki A, Ried T, Nigg EA. (1994) Cell cycle analysis and chromosomal localization of human Plk1, a putative homo logue of the mitotic kinases Drosophila polo and Saccharomyces cerevisiae Cdc5. J Cell Sci; 107:1509–17.

Golsteyn RM, Mundt KE, Fry AM & Nigg EA (1995) Cell cycle regulation of the activity and subcellular localization of Plk1, a human protein kinase implicated in mitotic spindle function. J. Cell Biol. 129, 1617–1628

Grabusic K, Maier S, Hartmann A, Mantik A, Hammerschmidt W, Kempkes B (2006) The CR4 region of EBNA2 confers viability of Epstein-Barr virus-

transformed B cells by CBF1-independent signaling. J Gen Virol 87(Pt 11): 3169-3176

Gross H, Barth S, Palermo RD, et al. (2009) Asymmetric Arginine dimethylation of Epstein-Barr virus nuclear antigen 2 promotes DNA targeting. Virology.;397(2):299–310. doi:10.1016/j.virol.2009.11.023

Grywalska E, Rolinski J (2015) Epstein-Barr Virus–Associated Lymphomas, Seminars in Oncology, Volume 42, Issue 2, ISSN 0093-7754

Gumireddy K, Reddy MV, Cosenza SC, Boominathan R, Baker SJ, Papathi N, et al. (2005) ON01910, a non-ATP-competitive small molecule inhibitor of Plk1, is a potent anticancer agent. Cancer Cell ;7:275–86.

Haddow A (1970) Epidemiological evidence suggesting an infective element in the aetiology in Burkitt's Lymphoma. E.&S. Livingstone, Edinburgh; 198–209

Hammerschmidt W, & Sugden B (1989). Genetic analysis of immortalizing functions of Epstein–Barr virus in human B lymphocytes. Nature, 340, 393-397.

Hanisch A, Wehner A, Nigg EA, Sillje H.H. (2006) Different Plk1 functions show distinct dependencies on Polo-Box domain-mediated targeting. Mol. Biol. Cell. ;17:448–459.

Hao Z, Kota VK (2015). Volasertib for AML: Clinical use and patient consideration. OncoTargets and therapy. 8. 1761-71. 10.2147/OTT.S60762.

Helmke C, Becker S, Strebhardt K. (2015) The role of Plk3 in oncogenesis. Oncogene

Henle W, Ho JH, Henle G, Chau JC, and Kwan HC (1977) Nasopharyngeal carcinoma: significance of changes in Epstein–Barr virus-related antibody patterns following therapy. Int. J. Cancer ; 20: 663–672

Hendzel M & W et al. (1997). Mitosis-specific phosphorylation of histone H3 initiates primarily within pericentromeric heterochromatin during G2 and spreads in an ordered fashion coincident with mitotic chromosome condensation. Chromosoma. 106. 348-60. 10.1007/s004120050256.

Herold et al.: Innere Medizin. Eigenverlag 2012, ISBN 978-3-981-46602-7
Hildesheim, A. and Levine, P.H. Etiology of nasopharyngeal carcinoma: a review. Epidemiol. Rev. 1993; 15: 466–485

Ho YS, Duh JS, Jeng JH, Wang YJ, Liang YC, Lin CH, Tseng CJ, Yu CF, Chen RJ and Lin JK (2001). Griseofulvin potentiates antitumorigenesis effects of nocodazole through induction of apoptosis and G2/M cell cycle arrest in human colorectal cancer cells. Int J Cancer 91(3): 393–401.

Holtrich U, et al (1994). Induction and down-regulation of PLK, a human serine/threonine kinase expressed in proliferating cells and tumors. Proc Natl. Acad Sci U S A 91(5), 1736–1740.

Horvath GC, Schubach WH. (1993) Identification of the Epstein-Barr virus nuclear antigen 2 transactivation domain. Biochem Biophys Res Commun. 26;191(1):196–200. pmid:8383488

Hsieh JJ et Hayward SD (1995). Masking of the CBF1/RBPJ kappa transcriptional repression domain by Epstein-Barr virus EBNA2. Science, 268, 560-3.

Hsu J, Glaser SL, (2000) Epstein–Barr virus-associated malignancies: epidemiologic patterns and etiologic implications, Critical Reviews in Oncology/Hematology, Volume 34, Issue 1, Pages 27-53, ISSN 1040-8428

Hummel M, Bentink S et al; (2006) A biologic definition of Burkitt's lymphoma from transcriptional and genomic profiling. N Engl J Med 354 2419-30.

Hunt T, Nasmyth K, Novák B (2011) The cell cycle. Philos Trans R Soc Lond B Biol Sci.;366(1584):3494–3497. doi:10.1098/rstb.2011.0274

Jang YJ, Lin CY, Ma S, Erikson RL , (2002) Functional studies on the role of the C-terminal domain of mammalian polo-like kinase Proc. Natl. Acad. Sci. USA, 99, pp. 1984-1989

Janning M and Fiedler W (2014) Volasertib for the treatment of acute myeloid leukemia: a review of preclinical and clinical development. Future Oncol 10:1157–1165.

Jiang, M., Zhu, J., Guan, Y. S., & Zou, L. Q. (2011). Primary central nervous system burkitt lymphoma with non-immunoglobulin heavy chain translocation in right ventricle: case report. Pediatric hematology and oncology, 28(5), 454–458.

Kang YH, Park JE, Yu LR, Soung NK, Yun SM, Bang JK, Seong YS, Yu H, Veenstra TD, Lee KS (2006) Self-regulation of Plk1 recruitment to the kinetochores is critical for chromosome congression and spindle checkpoint signaling. Mol. Cell.;24:409–422

Kaiser C, Laux G, Eick D, Jochner N, Bornkamm GW, and Kempkes B (1999). The proto-oncogene c-myc is a direct target gene of Epstein-Barr virus nuclear antigen 2. J Virol 73, 4481-4484.

Karrer N (2014) Epstein-Barr-Virus und infektiöse Mononukleose. In: Swiss Medical Forum.

Kempkes B, Pawlita M, Zimber-Strobl U, Eissner G, Laux G and Bornkamm GW (1995). "Epstein-Barr virus nuclear antigen 2-estrogen receptor fusion proteins transactivate viral and cellular genes and interact with RBP-J kappa in a conditional fashion." Virology 214(2): 675-679.

Kempkes B, Spitkovsky D, Jansen-Durr P, Ellwart JW, Kremmer E, Delecluse HJ, Rottenberger C, Bornkamm GW and Hammerschmidt W (1995). "B-cell proliferation and induction of early G1-regulating proteins by Epstein-Barr virus mutants conditional for EBNA2." EMBO J 14(1): 88-96.

Kempkes B (2010) EBNA-2 in Transcription Activation of Viral and Cellular Genes. In Epstein-Barr Virus: Latency and Transformation, Robertson E (ed), pp 61-80. Norfolk, UK: Caister Academic Press

Kempkes B, Robertson ES (2015) Epstein-Barr virus latency: current and future perspectives. Current opinion in virology 14: 138-144

Kempkes B, Ling PD (2015) EBNA2 and Its Coactivator EBNA-LP. Current topics in microbiology and immunology; 391:35–59. pmid:26428371.

Knecht R. et al. (1999) Prognostic significance of polo-like kinase (PLK) expression in squamous cell carcinomas of the head and neck. Cancer Res. 59, 2794–2797

Laichalk LL, Hochberg D, Babcock GJ, Freeman RB, Thorley-Lawson DA (2002) The dispersal of mucosal memory B cells: evidence from persistent EBV infection. Immunity.;16:745–54.

Lane HA, Nigg EA. (1996) Antibody microinjection reveals an essential role for human Polo-like kinase1 (Plk1) in the functional maturation of mitotic centrosomes. J Cell Biol;135(6 Pt 2):1701–1713.

Lee H.W.et al. (2013) Real-time single-molecule co-immunoprecipitation analyses reveal cancer-specific Ras signalling dynamics. *Nat. Commun.* **4**, 1505

Lee KS, Grenfell TZ, Yarm FR, Erikson RL. (1998) Mutation of the polo-box disrupts localization and mitotic functions of the mammalian polo kinase Plk. Proc Natl Acad Sci USA.; 95:9301–6.

Lee KS, Park JE, Kang YH, Zimmerman W, Soung NK, Seong YS, Kwak SJ, Erikson RL (2008) Mechanisms of mammalian polo-like kinase 1 (Plk1) localization: Self- versus non-self-priming. Cell Cycle;7:141–145.

Lee KS, Park JE, Kang YH, Kim TS, Bang JK. (2014) Mechanisms underlying Plk1 polo-box domain-mediated biological processes and their physiological significance. Mol Cells; 37:286–94. https://doi.org/10.14348/ molcells.2014.0002.

Lenart P. et al. (2007) The small-molecule inhibitor BI 2536 reveals novel insights into mitotic roles of polo-like kinase 1. Curr. Biol.: CB 17, 304–315

Leung GC, Hudson JW, Kozarova A, Davidson A, Dennis JW, Sicheri F (2002) The Sak polo-box comprises a structural domain sufficient for mitotic subcellular localization. Nat Struc Biol. ;9:719–724.

Levine PH, Stemmermann G, Lennette ET, Hildesheim A, Shibata D and Nomura A. (1995) Elevated antibody titers to Epstein–Barr virus prior to the diagnosis of Epstein–Barr-virus-associated gastric adenocarcinoma. Int. J. Cancer; 60: 642–644

Lian G, Li L, Shi Y, Jing C, Liu J, Guo X, Zhang Q, Dai T, Ye F, Wang Y, Chen M "BI2536, a potent and selective inhibitor of polo-like kinase 1, in combination with

cisplatin exerts synergistic effects on gastric cancer cells". International Journal of Oncology 52.3 (2018): 804-814.

Liu Z, Sun Q, Wang X, 2017; PLK1, A potential target for cancer therapy Translational Oncology 10(1):22–32. doi: 10.1016/j.tranon.2016.10.003.
Lowery DM, Lim D and Yaffe MB (2005) Structure and function of Polo-like kinases, Oncogene 24, 248–259, doi:10.1038/sj.onc.1208280

Macurek L et al. (2008) Polo-like kinase-1 is activated by aurora A to promote checkpoint recovery. Nature 455, 119–123

Mertens J, Lubbert M, Fiedler W, et al. Phase I/II Study of Volasertib (BI 6727), an Intravenous Polo-Like Kinase (Plk) Inhibitor, in Patients with Acute Myeloid Leukemia (AML): Results From the Randomized Phase II Part for Volasertib in Combination with Low-Dose Cytarabine (LDAC) Versus LDAC Monotherapy in Patients with Previously Untreated AML Ineligible for Intensive Treatment. Blood (ASH Annual Meeting Abstracts). 2012; 120(21):Abstr #411.

Maier S, Staffler G, Hartmann A, Hock J, Henning K, Grabusic K, et al. (2006) Cellular target genes of Epstein-Barr virus nuclear antigen 2. Journal of virology ;80(19):9761–71. pmid:16973580.

McClain KL, Leach CT, Jenson HB et al. (1995) Association of Epstein–Barr virus with leiomyosarcomas in children with AIDS. New Engl. J. Med.; 332: 12–18

McKinley KL & Cheeseman (2014) I. M. Polo-like kinase 1 licenses CENP-A deposition at centromeres. Cell 158, 397–411

Mito K et al. (2005) Expression of Polo-like kinase (PLK1) in non-Hodgkin's lymphomas. Leuk. Lymphoma 46, 225–231

Moison, Céline et al "Complex karyotype AML displays G2/M signature and hypersensitivity to PLK1 inhibition." Blood Advances 3.4 (2019): 552-563. Web. 09 Aug. 2019.

Mondal SK, Bera H, Mondal S, Samanta TK. Primary bilateral ovarian Burkitt's lymphoma in a six-year-old child: report of a rare malignancy. J Can Res Ther. 2014;10:755–7.

Morra M, Howie D, Grande MS, Sayos J, Wang N, Wu C, Engel P, and Terhorst C (2001) X-linked lymphoproliferative disease: a progressive immunodeficiency. Annu Rev Immunol 19:657-82.

Mross K, Dittrich C, Aulitzky WE, Strumberg D, Schutte J, Schmid RM, et al. (2012) A randomised phase II trial of the Polo-like kinase inhibitor BI 2536 in chemonaive patients with unresectable exocrine adenocarcinoma of the pancreas – a study within the Central European Society Anticancer Drug Research collaborative network. Br J Cancer; 107:280–6.

Mueller N, Evans A, Harris NL et al. (1989) Hodgkin's disease and Epstein–Barr virus. Altered antibody pattern before diagnosis. New Engl. J. Med.; 320: 689–695

Nakajima H, Toyoshima-Morimoto F, Taniguchi E, Nishida E (2003) Identification of a consensus motif for Plk (Polo-like kinase) phosphorylation reveals Myt1 as a Plk1 substrate. J Biol Chem 278: 25277–25280

Neef R et al. (2003) Phosphorylation of mitotic kinesin-like protein 2 by polo-like kinase 1 is required for cytokinesis. J. Cell Biol. 162, 863–875

Park JE, Soung NK, Johmura Y, Kang YH, Liao C, Lee KH, Park CH, Nicklaus MC, Lee KS (2010) Polo-box domain: a versatile mediator of polo-like kinase function. Cell. Mol. Life Sci.;67:1957–1970.

Petronczki M, Lenart P, Peters JM. (2008) Polo on the rise-from mitotic entry to cytokinesis with Plk1. Dev Cell; 14:646-59; PMID:18477449;

PhosphoSitePlus®, Development of A Protein Phosphorylation Site Database

Reindl W, Yuan J, Kramer A, Strebhardt K, Berg T. (2008) Inhibition of polo-like kinase 1 by blocking polo-box domain-dependent protein-protein inter- actions. Chem Biol;15:459–66.

Renner AG, Dos Santos C, Recher C, et al. (2009) Polo-like kinase 1 is overexpressed in acute myeloid leukemia and its inhibition preferentially targets the proliferation of leukemic cells. Blood.; 114(3):659–662. [PubMed: 19458358]

Richardson AK, Cox B, McCredie MR, Dite GS, Chang JH, Gertig DM, et al. (2004) Cytomegalovirus, Epstein-Barr virus and risk of breast cancer before age 40 years: a case-control study. Br J Cancer.;90(11):2149–52. PubMed PMID: . Pubmed Central PMCID: 2409506. Epub 2004/05/20. eng.

Rickinson AB and Kieff (1996) E. Epstein–Barr virus. in: B.N. Fields, D.M. Knipe, P.M. How-ley, R.M. Chanock, J.L. Melnick, T.P. Monath, B. Roizman, S.E. Straus (Eds.) Field's Vi-rology. Lippincott-Raven, Philadelphia, PA: 2397–2446

Rickinson AB and Moss DJ (1997). Human cytotoxic T lymphocyte responses to Epstein-Barr virus infection. Annu Rev Immunol 15:405-31.

Rooney C, Howe JG, Speck SH, and Miller G (1989). Influence of Burkitt's lymphoma and primary B cells on latent gene expression by the nonimmortalizing P3J-HR-1 strain of Epstein-Barr virus. J Virol 63, 1531-1539.

Rudolph D, Steegmaier M, Hoffmann M, et al. (2009) BI 6727, a Polo-like kinase inhibitor with improved pharmacokinetic profile and broad antitumor activity. Clin Cancer Res.; 15(9):3094–3102. [PubMed: 19383823]

Saha A, Robertson ES (2011), Epstein-Barr virus-associated B-cell lymphomas: pathogenesis and clinical outcomes Clin Cancer Res, 17 pp. 3056-3063

Scharow A, Raab M, Saxena K, Sreeramulu S, Kudlinzki D, Gande S, et al. (2015) Optimized Plk1 PBD inhibitors based on poloxin induce mitotic arrest and apoptosis in tumor cells. ACS Chem Biol;10:2570–9.

Schmucker S, Sumara I. (2014) Molecular dynamics of PLK1 during mitosis. Mol Cell Oncol. ;1(2):e954507. doi:10.1080/23723548.2014.954507

Schöffski P, Awada A, Dumez H, et al (2012): A phase I, dose-escalation study of the novel Polo-like kinase inhibitor volasertib (BI 6727) in patients with advanced solid tumours. Eur J Cancer 48:179-186

Seki A., Coppinger JA, Jang CY, Yates JR & Fang G. (2008) Bora and the kinase Aurora a cooperatively activate the kinase Plk1 and control mitotic entry. Science 320, 1655–1658

Seong YS, Kamijo K, Lee JS, Fernandez E, Kuriyama R, Miki T, Lee KS (2002) A spindle checkpoint arrest and a cytokinesis failure by the dominant-negative polo-box domain of Plk1 in U-2 OS cells. J. Biol. Chem.; 277:32282–32293.

Spankuch-Schmitt B, Bereiter-Hahn J, Kaufmann M. & Strebhardt K. (2002) Effect of RNA silencing of polo-like kinase-1 (PLK1) on apoptosis and spindle formation in human cancer cells. J. Natl Cancer Inst. 94, 1863–1877

Strebhardt K (2010) Multifaceted polo-like kinases: drug targets and antitargets for cancer therapy. Nat. Rev. Drug Discov.; 9:643–660.

Strebhardt K, Ullrich A. (2006) Targeting polo-like kinase 1 for cancer therapy. Nat Rev Cancer.; 6(4):321–330. [PubMed: 16557283]

Steegmaier M, Hoffmann M, Baum A, Lénárt P, Petronczki M, Krssák M, Gürtler U, Garin-Chesa P, Lieb S, Quant J, et al. (2007) BI 2536, a potent and selective inhibitor of polo-like kinase 1, inhibits tumor growth in vivo. Curr Biol 17:316–322.

Sumara I et al. (2002) The dissociation of cohesin from chromosomes in prophase is regulated by Polo-like kinase. Mol. Cell 9, 515–525

Sugawara Y et al. (1999) Detection of Epstein–Barr Virus (EBV) in Hepatocellular Carcinoma Tissue: A Novel EBV Latency Characterized by the Absence of EBV-Encoded Small RNA Expression, Virology, Volume 256, Issue 2,Pages 196-202, ISSN 0042-6822,

Swallow CJ, Ko MA, Siddiqui NU, Hudson JW, Dennis JW. (2005) Sak/Plk4 and mitotic fidelity. Oncogene.;24:306–312.

Takai N, Hamanaka R, Yoshimatsu J, and Miyakawa I (2005) Polo-like kinases (Plks) and cancer. Oncogene 24:287–291.

Thorley-Lawson DA & Gross A (2004) Persistence of the Epstein-Barr virus and the origins of associated lymphomas. N. Engl. J. Med. 350, 1328–1337

Tokumitsu Y et al. (1999) Prognostic significance of polo-like kinase expression in esophageal carcinoma. Int. J. Oncol. 15, 687–692

Weichert W et al. (2005) Polo-like kinase isoforms in breast cancer: expression patterns and prognostic implications. Virchows Arch. 446, 442–450

Weichert W, Ullrich A, Schmidt M, et al. (2006) Expression patterns of polo-like kinase 1 in human gastric cancer. Cancer Sci.; 97(4):271–276. [PubMed: 16630118]

Weiß L, Efferth T (2012): Polo-like kinase 1 as target for cancer therapy. Exp Hematol Oncol 1:38

Whitley RJ (1996). Baron S; et al. (eds.). Herpesviruses. in: Baron's Medical Microbiology (4th ed.). Univ of Texas Medical Branch. ISBN 0-9631172-1-1.

Xiao D et al. (2016) Polo-like kinase-1 regulates Myc stabilization and activates a feedforward circuit promoting tumor cell survival. Mol Cell ;64(3):493–506.

Young LS, Murray PG. (2003) Epstein-Barr virus and oncogenesis: from latent genes to tumours. Oncogene; 22: 5108-5121

Young LS, Dawson CW. (2014) Epstein-Barr virus and nasopharyngeal carcinoma Chin J Cancer ;33(12):581–590. doi:10.5732/cjc.014.10197

Yuan J, Sanhaji M, Kraemer A, Reindl W, Hofmann M, Kreis N-N, et al. (2011) Polo- Box domain inhibitor poloxin activates the spindle assembly checkpoint and inhibits tumor growth in vivo. Am J Pathol ;179:2091–9.

Yue W, Gershburg E, Pagano JS. (2005) Hyperphosphorylation of EBNA2 by Epstein-Barr virus protein kinase suppresses transactivation of the LMP1 promoter. J Virol.;79(9):5880-5.

Zhao B, Zou J, Wang H, Johannsen E, Peng CW, Quackenbush J, et al. (2011) Epstein-Barr virus exploits intrinsic B-lymphocyte transcription programs to achieve immortal cell growth. Proceedings of the National Academy of Sciences of the USA ;108(36):14902–7. pmid:21746931.

Zhou H, Schmidt SC, Jiang S, Willox B, Bernhardt K, Liang J, et al. (2015) Epstein-Barr virus oncoprotein super-enhancers control B cell growth. Cell host & microbe.;17(2):205–16. pmid:25639793.

Zitouni S, Nabais C, Jana SC, Guerrero A, Bettencourt-Dias M. (2014) Polo-like kinases: Structural variations lead to multiple functions. Nat Rev Mol Cell Biol ;15(7):433–452.